The Role of SEL1L-HRD1 Endoplasmic Reticulum-Associated Degradation in Hypothalamic Regulation of Metabolism and Beyond

by

Hancheng Mao

A dissertation submitted in partial fulfillment
of the requirements for the degree of
Doctor of Philosophy
(Molecular and Integrative Physiology)
in the University of Michigan
2024

Doctoral Committee:

Professor Peter Arvan, Co-chair
Professor Ling Qi, Co-chair
Professor Carol Elias
Professor Daniel Klionsky

Hancheng Mao

hancheng@umich.edu

ORCID iD: 0000-0003-2546-6774

Acknowledgements

One of the best choices I've ever made is accept the admission to University of Michigan – Ann Arbor. The entire community is always welcoming, embracing and vibrant throughout my years here. Wherever I am, my heart will always go blue.

To my primary mentor, Dr. Ling Qi, I really appreciate for your rigorous training not only on my research and scientific literacy, but more importantly, on inspiring me to establish positive attitude, courage, resilience and perseverance that prepare me for facing any difficulty and challenge. I'm glad you have included me in this collaborative lab you built with supportive team members.

To my co-mentor and committee member, Dr. Peter Arvan, I am very grateful for your support that ensures my research and life in the University of Michigan. It's always a pleasure talking to you and I benefit greatly from all the practical suggestions from you. I'm lucky to have the support from you and your lab.

To the lab members in Qi lab, Arvan lab and Reinert lab, thank you all for having me as a member of such warm and harmonious group. I'd like to thank previous Qi lab member Dr. Hyang Kim for training the basic techniques I adopted to finish my dissertation. I'm also very grateful to Dennis who provided detailed guidance and instructions to maintain such a well-organized research environment.

To the staff and faculty of the MIP department and University of Michigan. I really appreciate your dedication to maintaining such a humanizing environment with various supportive systems. To Michele Boggs, you're the best administrative coordinator I've

ever met and thank you for all the help and support. To my committee members, Dr. Carol Elias and Dr. Daniel Klionsky, I'm very grateful for your time and effort in helping navigate me through the difficulties and challenges and encouraging me to keep pushing my research progress. To Dr. Steve Lentz, thank you for your patience and training in all of my immunofluorescent imaging and data analysis. To Dr. Daniel Michele, I really appreciate your dedication and commitment to the development of the MIP department as well as research and life of the MIP graduate students. It's my honor to work here with all the great people, and I'll always proudly be the Umich MIP alumni.

To my family, my mom Jingyi Zhang and my dad Weiping Mao. You're always my strongest backing with your endless unconditional love. I love you.

To Can, thank you for seeing and hearing me. I cherish all the moments with you, bitter or sweet, that inspire me to the better me. Teaming up with you motivates me hustle all day and get things done. Hope you will become the best rapstar and engineer.

Finally, to my cats, Orangey, Joey, Damien, Suzie Poo and Dusty Bun, thank you for providing your soft paws, your warm bellies, your innocent eyes and your endless purring, which always soothe my soul.

Table of Contents

List of Figures

Abstract

The endoplasmic reticulum (ER) is a vital organelle responsible for several aspects of cell function and signaling, including protein synthesis, folding, modification, trafficking and quality control; lipid synthesis and transportation; calcium storage and signaling. Upon physiological stimulus and environmental stress, ER protein homeostasis (proteostasis) can be challenged and disturbed where proteins in the ER misfold and even aggregate, leading to proteotoxicity that threatens function and survival of the cells. To maintain ER proteostasis, numerous ER quality control systems have evolved, including unfolded protein response (UPR), ER-associated degradation (ERAD) and autophagy (ER-phagy). In particular, ERAD is a constitutively active machinery that efficiently clears misfolded ER proteins by targeting them for proteasomal degradation. Among multiple identified ERAD complexes, the Suppressor/enhancer of Lin-12 Like-HMG-coA reductase degradation (SEL1L-HRD1) ERAD complex is most conserved across mammals and comprehensively investigated. To date, the pathophysiological importance of SEL1L-HRD1 ERAD has been well demonstrated in a cell type-specific and substrate-dependent manner. However, it remains largely unknown the role of SEL1L-HRD1 in heterogenous cell populations in central nervous system (CNS) and how this complex engages in organismal health and disease via maintaining proteostasis in CNS. This dissertation provides explorations and findings in the role of hypothalamic SEL1L-HRD1 in metabolic regulation, as a good start for filling the knowledge gap.

The ER proteostasis of hypothalamic neurons is indispensable for neuronal activity and function to mediate organismal energy balance in response to altering nutritional status. Interestingly, we observed, upon acute HFD feeding for one week, a transient induction of SEL1L-HRD1 protein abundance in hypothalamic neurons, including pro-opiomelanocortin (POMC) neurons as key regulators of food intake and energy expenditure. Notably, deficiency of SEL1L in POMC neurons significantly predisposed mice to diet-induced obesity (DIO) due to hyperphagia. Mechanistically, the increased food intake was attributed to leptin resistance in POMC neurons deficient in SEL1L-HRD1, independent of UPR. Further investigation provided evidence that SEL1L-HRD1 controls leptin signaling by maintaining maturation and membrane display of leptin receptor long isoform (LepRb). Particularly, SEL1L-HRD1 ensured efficient degradation of misfolded LepRb, and the deficiency of SEL1L-HRD1 rendered accumulation of misfolded LepRb aggregates, interfering with folding and maturation of nascent LepRb. Hence, SEL1L-HRD1 ERAD regulates leptin signaling via LepRb in a substrate dependent manner.

In addition to demonstrating the role of hypothalamic SEL1L-HRD1 in metabolic regulation, we also identified and characterized astrotactin1 (ASTN1) as a bona fide endogenous substrate of SEL1L-HRD1 that mediates neuronal plasticity and contact with glial cells and closely associated with neurodevelopmental disorders. Together, these findings underscore the significance of SEL1L-HRD1 ERAD in CNS, from hypothalamus and beyond.

Chapter 1 Endoplasmic Reticulum Quality Control of Metabolic Regulation in Neurons and Beyond[1]

1.1 Abstract

Hypothalamic neurons of the central nervous system (CNS) are key regulators for energy homeostasis. As endoplasmic reticulum (ER) homeostasis is indispensable for neuronal activity and function including translation, folding and secretion of neurotransmitters and peptides, a variety of quality control machineries have evolved in organisms to maintain ER proteostasis. This review mainly focuses on recent findings in the roles of ER quality control systems, including ER-associated degradation (ERAD), unfolded protein response (UPR) and autophagy (ER-phagy), in the central nervous systems, mainly hypothalamus, in metabolic regulation.

[1] This chapter is adapted from an invited review for ***Journal of Biological Chemistry*** (to be submitted)

1.2 Introduction

The prevalence of obesity and metabolic disorders has been rising for years[1-3]. Studies have been shifted from understanding the pathogenesis in peripheral tissues towards central nervous systems (CNS) as increasing evidence supporting the importance of central regulation of systemic metabolism[4-9]. The hypothalamus is an essential part of the CNS regulating systemic metabolism mainly via production and secretion of neuropeptides from hypothalamic neurons[10]. Among the heterogenous neuronal populations in hypothalamus, anorexigenic POMC and orexigenic AgRP/NPY neurons are two fundamental regulators for food intake and energy expenditure[11-19]. The neuropeptides are first synthesized and folded as entire prohormones inside of endoplasmic reticulum (ER), followed by post-translational modification, cleavage processing along trafficking from ER through Golgi network before transportation to the cell membrane for secretion[20, 21]. Of note, the proper folding inside of ER is prohormone processing and maturation. The translated peptides, first fold to intermediates and then towards native states with proper functions. Occasionally, the intermediates, instead of getting correctly folded, may misfold into oligomers and further aggregates. The accumulation of excessive and misfolded proteins, if not cleared efficiently, will ultimately lead to proteotoxicity, ER stress and even cell death. In order to avoid proteotoxicity, organisms have evolutionarily developed several effective and efficient protein quality control systems in ER. There are mainly three ER protein quality control machineries: Unfolded protein response (UPR), ER-associated degradation (ERAD) and autophagy (ER-phagy) (Figure 1.1).

The physiological relevance of hypothalamic ER quality control machineries, including UPR, autophagy and ERAD, has been highlighted by the correlation between their transcriptional regulation with alterations in nutritional status[22-26]. Upon food deprivation, several UPR related genes are activated, including ER chaperones as well as ERAD components as downstream of XBP1s, ATF4 and ATF6 in specifically in AgRP but not POMC neurons[23]. On the other hand, refeeding boosts the aforementioned UPR-related genes in POMC neurons[25, 26]. Caloric restriction and starvation induces hypothalamic autophagy[22, 24], which can be reversed by refeeding[24]. Such distinction in the transcriptional profiles of these two populations in response to different nutritional stimuli should correlate with their neuronal activities, where AgRP and POMC neurons are activated upon fasting and reeding respectively. Several genetic studies in combination with a variety of diets have highlighted patho-physiological importance of components of UPR[26-33], autophagy[24, 34-37] and ERAD[25, 38] in the hypothalamic control of energy homeostasis. Each machinery has distinct signaling pathways while there are also cross-talks among the systems where compensatory and/or synergistic effect exist. The ubiquitous expression and functionality of those three machineries have been identified in a variety of peripheral tissues and central nervous systems related to metabolic regulations. This review mainly focuses on the roles of ER quality control systems in hypothalamic neurons, mainly POMC and AgRP neurons, in metabolic regulation (Figure 1.2).

1.3 Hypothalamic POMC and AgRP/NPY neurons

Among various neuron populations within the ARC of the hypothalamus, POMC and AgRP/NPY neurons are two primary metabolic regulators for food intake and energy expenditure[11-19]. Both neurons reside close to each other, adjacent to fenestrated capillaries with access to circulating hormones[11-19]. AgRP/NPY neurons can inhibit POMC neurons by direct synaptic release of GABA[16, 39]. POMC neuropeptides that can be further processed into POMC-derived peptides through ER-Golgi trafficking. AgRP/NPY neurons co-express AgRP and NPY neuropeptides. POMC and AgRP/NPY neurons are regulated reciprocally upon activation and exert opposing effect by projecting into downstream targeting regions, and mediate an integrated response to maintain energy homeostasis[40].

1.4 Leptin signaling in central regulation of energy balance

Leptin is one of the key circulating hormones that can stimulate the function of the aforementioned hypothalamic neurons to express neuropeptides[41, 42]. Leptin is a hormone produced and secreted by the adipose tissues into circulation[43]. The amount of leptin is generally in proportion to the overall fat mass and thus is the reflection of the organism nutritional status[44, 45]. Circulating leptin can be sensed by hypothalamic cells, including POMC and AgRP/NPY neurons that expressing leptin receptors (LepR)[42, 46-49]. Particularly, the long form of the LepR (LepRb) is mainly responsible for leptin action in the hypothalamus for maintaining body weight and food intake[49-54]. In basal inactive state, LepRb is displayed on the membrane surface as homodimers[55, 56], associated with Janus kinase2 (JAK2) in the cytosolic domain[54,

56, 57]. Upon activation by the binding of the leptin, the confirmational change of the LepRb results in the activation of JAK2 via auto-phosphorylation[58], which further phosphorylate LepRb at different sites as well as downstream transcription factor Signal Transducer and activator of Transcription 3 (STAT3)[54, 59]. The phosphorylated STAT3 (pSTAT3) can further translocate to the nucleus and mediate a group of target gene expression including the anorexigenic peptide POMC [60-64] suppressing orexigenic peptides AgRp/NPY[65-68]. Besides, leptin signaling cascades modulate hypothalamic neuronal activities, including directly depolarizing POMC neurons and hyperpolarizing AgRP/NPY neurons. The leptin inhibition of AgRP/NPY neurons further diminishes the GABAergic tone onto POMC neurons as an indirect activation of POMC neurons[16]. Therefore, the integrated action of leptin on hypothalamic neurons coordinates an anorexigenic effect.

1.5 Leptin resistance in CNS

At physiological condition, leptin should exert sufficient anorectic effect to maintain organism energy homeostasis. However, studies in genetic and diet-induced obese mice and human patients reported significantly elevated circulating leptin levels in many obese individuals[44, 69]. These striking findings brought up the concept of central leptin resistance under pathological circumstances. As leptin resistance greatly hinders the therapeutic efficacy of leptin administration in clinical trials [70], many studies have been investigating the mechanisms underlying the pathogenesis of leptin resistance[61]. To date, several hypotheses for leptin resistance have been proposed, including impaired leptin transport from circulation to CNS due to alteration in the blood-brain-

barrier (BBB)[71-74]; desensitization of LepRb and/or strong inhibition of leptin signaling by upregulated suppressors due to hyperleptinemia such as SOCS3[75-78] and PTP1B[79-81]; defective leptin signaling cascades attributed to neuroinflammation[82-84] and disturbed ER homeostasis[29, 83, 85]. Despite the interconnections among aforementioned pathways, following sections will mainly demonstrate current evidence linking ER homeostasis in hypothalamic neurons with development of neuronal dysfunction, leptin resistance and overall pathogenesis of obesity.

1.6 ERAD

ERAD is a constitutively active ER proteostasis control machinery that target and degrades the misfolded and excessive unfolded proteins in a substrate-dependent manner. Step by step, the process includes substrate recognition, targeting, retrotranslocation, ubiquitylation and proteasomal degradation[86]. As the most conserved ERAD complex, Sel1L-Hrd1 has been generally characterized in vivo[87], indicating its vital roles in health and disease in a tissue-specific manner [25, 38, 88-96]. Hrd1 is an E3 ubiquitin ligase and retrotranslocon[97, 98] and Se1l1L is its adaptor. Upon recognition, Hrd1 extracts and ubiquitinates the substrates from ER for cytosolic proteasomal degradation. Sel1L is indispensable for maintaining the stability function of Sel1L-Hrd1 complex[99, 100].

Recent studies have revealed patho-physiological importance of hypothalamic SEL1L-HRD1 ERAD[25, 38]. The SEL1L-HRD1 is independent for maturation and secretion of AVP and POMC, which are vital for systemic water homeostasis and food intake respectively[25, 38]. The fundamental underlying mechanism of how ERAD maintains

maturation of those prohormones is that it ensures the systems towards folding and function via constitutively and efficiently degrading misfolding-prone intermediates that accumulate towards oligomers and aggregates in the absence of ERAD. The misfolding intermediates and aggregates further disturb the ER folding capacity and the proper folding of nascent peptides. This theory can be further applied in the context of disease mutants. The autosomal-dominant disease mutants of the AVP and POMC prohormones not only readily aggregate within themselves, but also associate with other nascent wildtype prohormones to form intermolecular oligomerization via disulfide bonding due to aberrant cysteine exposure[25, 38].

1.7 UPR

The UPR is an adaptive response to accumulation of misfolded proteins inside the ER. The UPR, in mammals, is orchestrated by three ER transmembrane sensors: type I transmembrane protein inositol requiring enzyme 1α (IRE1α), protein kinase RNA-activated (PKR)-like ER kinase (PERK); and activating transcription factor 6 (ATF6). The UPR sensors, in the basal state, are repressed by association with the chaperone BiP in the ER lumen[101]. Upon ER stress, the BiP molecules bound to the UPR sensors are recruited to misfolded proteins. The sensors, upon BiP dissociation, mediate different signaling cascades and activate several downstream effectors to increase the degradation and folding capacity as well as decrease the folding demand of the ER.

1.7.1 IRE1α-XBP1

IRE1α a type I transmembrane protein with functional domain consisting of a serine/threonine kinase and endoribonuclease domain. In basal condition with balanced ER proteostasis, IRE1α largely remains in an inactive form monomer with BiP bound to the luminal domain. Upon ER stress-induced activation, the dissociation of BiP mediates IRE1α oligomerization, trans-autophosphorylation of the kinase domain and RNase domain subsequently[102, 103]. The endoribonuclease domain of the activated IRE1α initiates splicing of the mRNA encoding X-box binding protein (XBP1) and generates a frameshift that encodes XBP1s, a transcription factor of a variety of UPR-related genes related to protein folding, trafficking, lipid synthesis and ERAD[104, 105]. The role of hypothalamic IRE1α-XBP1 branch have been investigated by two groups studying mice with deficiency of IRE1α in POMC neurons ($IRE1\alpha^{POMC}$). One study indicated $IRE1\alpha^{POMC}$ mice were predisposed to DIO with impaired the thermogenesis and glucose homeostasis as well as insulin and leptin resistance[27], suggesting the protective role of POMC neuron-specific IRE1α. However, another group observed completely opposing phenotype that $IRE1\alpha^{POMC}$ mice were protected against DIO, liver steatosis as well as leptin and insulin resistance with increased thermogenesis due to elevated α-MSH production[28]. Notably, regardless of the discrepancy in over nutritional status, both studies agreed on that IRE1α is dispensable in POMC neurons in basal conditions where $IRE1\alpha^{POMC}$ mice maintained comparable body weight and metabolism to the littermate controls upon normal chow diet[27, 28].

The neuron-specific XBP1 knockout rendered mice slightly lower body weight upon regular chow diet with normal serum levels of glucose and leptin as well as glucose

tolerance and insulin sensitivity compared to controls. Hypothalamic leptin sensitivity was also preserved[29]. However, upon HFD feeding, panneuronal XBP1 deficiency significantly predisposed mice to DIO and pathogenesis including increased adiposity, reduced oxygen consumption, glucose intolerance and insulin resistance. Also, hypothalamic leptin sensitivity was significantly impaired[29]. The mice with XBP1s deficiency specifically in POMC neurons ($XBP1^{POMC}$) indicated a tendency towards higher body weight gain without significance. Upon HFD feeding, the $XBP1^{POMC}$ mice had increased food intake compensated by increased energy expenditure with elevated fat oxidation[106]. On the other hand, overexpression of XBP1s in POMC neurons was sufficient to protect mice against DIO with improved leptin and insulin sensitivity[26].

1.7.2 PERK-eIF2α-ATF4

Among three branches of UPR, PERK is the only one that mediates adaptive response via modulating protein synthesis. Similar to IRE1α, PERK is a type I transmembrane protein repressed by BiP bound to the luminal domains, and the release of BiP in response to increased unfolded/misfolded proteins facilitates PERK oligomerization and auto-phosphorylation[107]. The activated PERK further phosphorylates eIF2α[107], which represses the translation of most mRNA except for ATF4 that induces CHOP as a critical intermediate step towards apoptosis upon ER stress[108-110].

PERK deficiencty in POMC neurons ($PERK^{POMC}$) mildly protected male mice against diet-induced obesity by reduction of food intake[30]. However, celastrol administration was only able to improve leptin sensitivity so as to control food intake and bodyweight upon HFD in a PERK-dependent manner[30]. This suggested PERK deficiency alone is

not sufficient to prevent DIO, but instead, a crosstalk between PERK signaling and other pathways may be a key regulator in the metabolic control of the neurons. Indeed, $PERK^{POMC}$ mice exhibited upregulation of other UPR-related components including XBP1s as can be protective against DIO[26, 30]. Another insight is that a low level (but not ablation) of PERK signaling is required for maintaining the adaptive capability of the organisms in response to nutritional overload.

As the direct downstream effector of the PERK mediated signaling cascade, eIF2α phosphorylation is increased by fasting in hypothalamic AgRP neurons[31]. The loss-of-function eif2α Ser51Ala mutant has been studied in the context of AgRP neurons[31]. The mice with impaired phosphorylation of eIF2α specifically in AgRP neurons exhibited decreased body weight, food intake and starvation-induced AgRP neuronal activity with increased leptin responses[31]. Further, the acute deletion of ATF4, the downstream of PERK-eIF2α branch, in AgRP neurons in adulthood led to leaner mice with improved insulin/leptin sensitivity and reduced hepatic lipids, which protected mice against DIO and pathogenesis including insulin resistance and liver steatosis with higher thermogenesis[33]. Deletion of ATF4 in POMC neurons reduced fat mass in mice due to increased energy expenditure and protected mice against diet-associated obesity, glucose intolerance and leptin resistance, in a ATG5 dependent manner[32]. Further, hypothalamic overexpression of ATF4 resulted in no significant alteration in body weight, food intake or fat mass[111].

1.7.3 ATF6

ATF6 is a type II transmembrane protein bound to BiP in the inactive state as well. The dissociation of BiP allows ATF6 to translocate to the Golgi complex where the cytoplasmic, N-terminal domain of ATF6 are released by cleavage and the transcriptional activator fragment enters the nucleus for gene expression regulation. Unlike the other two arms of UPR, IRE1α-XBP1 and PERK- eIF2α-ATF4, in hypothalamic neurons, the role of ATF6 signaling in hypothalamus for metabolic regulation appears relatively limited. One study suggested ATF6α is required for AVP neuron to maintain water homeostasis in male mice upon intermittent water deprivation. Mice with AVP neuron-specific deletion of ATF6α had increased urine volumes compared to the counterparts under dehydration[112]. On the other hand, whole-body ATF6β deficient mice exhibit anxiety-like behavior in consistence with increased hypothalamic corticotropin-releasing expression and circulating corticosterone[113]. In vitro studies using primary cell culture further reveal the vital role of ATF6α, but not ATF6β in the transcriptional control in response to ER stress [114, 115].

1.8 Autophagy/ER-phagy

Autophagy is an evolutionarily conserved cellular process involving the breakdown and recycling of intracellular macromolecules, usually damaged or dysfunctional components, by lysosomal pathways[116-118]. Based on the processing mechanisms, three primary types of autophagy have been identified in mammalian cells: macroautophagy[119], microautophagy[120] and chaperone-mediated autophagy[121]. Autophagy can degrade cargo in both nonselective and selective way, where the former

transports the component in bulk to lysosomes and the latter degrades in a substrate-dependent manner[116-118].

Studies in hypothalamic autophagy generally suggest that activation of autophagy promotes neuronal control of energy homeostasis, the deficiency of which will impair neurometabolic regulation. The inhibition of autophagy by shRNA knockdown of Atg7 in the medio-basal hypothalamus led to hypothalamic inflammation via activation of NF-kB pathways, which significantly predisposed mice HFD-associated obesity and pathogenesis[122].

As the shRNA in the aforementioned studies targeted the whole medio-basal hypothalamus, to further decipher the roles of autophagy in specific neuronal populations of the hypothalamus, several groups looked carefully into POMC and AgRP neurons respectively. Serum starvation can effectively induce autophagy in hypothalamic cells via increased uptake of fatty acid, and autophagy mobilizes lipids to generate endogenous fatty acids, which further promotes expression of AgRP[24]. The inhibition of autophagy in vitro promoted neuronal lipid accumulation and the deficiency of Atg7 in AgRP neurons inhibited the starvation-induced upregulation of AgRP, and concomitant suppression of POMC expression due to decreased inhibitory input from AgRP to POMC neurons[24].

More investigations have been performed in POMC neuron-specific autophagy deficiency mouse models ($Atg7^{\Delta POMC}$). Contrary to the lean phenotype in mice deficient of Atg7 in AgRP neurons, loss of $Atg7^{\Delta POMC}$ mice were very susceptible to obesity with hyperphagia, decreased energy expenditure, elevated adiposity[34-36]. The $Atg7^{\Delta POMC}$ mice exhibited higher body weight shortly post weaning upon regular chow diet, with

increased adiposity and glucose intolerance[34]. The defective POMC axonal projections due to abnormal development was attributed to impaired metabolic regulation[34]. Another study indicated increased adiposity, impaired lipolysis and glucose homeostasis in Atg7$^{\Delta POMC}$ mice, both on regular chow and HFD, due to reduction of POMC-derived peptide α-MSH[36]. However, another study indicated Atg7$^{\Delta POMC}$ mice, though exhibiting higher body weight regardless of the diets, were not more prone to DIO compared to the littermates[35]. Atg7$^{\Delta POMC}$ mice, upon HFD, were more susceptible to hyperglycemia and resistant to leptin-induced suppression of the food intake[35].

More recent studies have unraveled the roles of other autophagy components in POMC neurons[37]. Interestingly, despite the essential complex formed by ATG12 and ATG5 during autophagy process, only the deficiency of Atg12, but not Atg5 in POMC neurons induced DIO phenotypes including increased adiposity, glucose intolerance and hyperphagia due to leptin sensitivity[37]. This suggests that some specific autophagy-related components may involve distinct metabolic regulation cascades outside of autophagy.

Notably, recent studies have revealed the diverse mechanisms underlying selective autophagy of the ER (ER-phagy)[117, 123, 124]. The importance of ER-phagy mediated by ER-phagy receptors has been identified in several neurological disease conditions [125-129]. In particular, FAM134B, though ubiquitously expressed, is particularly abundant in central and peripheral nervous systems[130, 131]. Loss-of-function mutation of FAM134B resulted in sensory and autonomic neuropathy while in vitro knockdown of FAM134B led to apoptosis in primary dorsal root ganglion neurons[128,

129]. FAM134B deficient mice exhibited age-dependent reduction of sensory axons with dilated Golgi cisternae while primary neurons from young FAM134B deficient mice had significantly swollen ER[125]. A more recent study revealed the neuroprotective role of FAM134B-mediated ER-phagy on α-synuclein clearance in Parkinson disease models[126]. Although the particular role of ER-phagy in hypothalamic neurons and metabolic regulation has not yet been revealed, the current studies have implied its importance of maintaining balanced presynaptic neurotransmission[127] and ER remodeling during neurogenesis[132].

1.9 Cell-nonautonomous control of hypothalamic proteostasis

Several studies have indicated cell-nonautonomous control of UPR in metabolic regulation in both C. elegans and mice. Studies in C. elegans suggested XBP-1s can regulate stress response, metabolism and longevity in a cell-nonautonomous manner. Neuronal overexpression of XBP-1s is sufficient to induce distal UPR in intestine dependent on endogenous IRE1-XBP1 axis. The nonautonomous inter-tissue signaling was mediated by the release of neurotransmitters[133]. The extended life span by neuronal induction of XBP-1s can be attributed to remodeled lipid metabolism that increases oleic acid, which enhances lysosomal lipases activity and protects organisms against proteotoxicity[134].

Further studies in mice revealed similar roles of hypothalamic neurons in controlling systemic metabolism in a cell nonautonomous manner. The ectopic overexpression of XBP1s in POMC neurons induced XBP1s and XBP1 target genes in liver with improved insulin sensitivity[26]. More recent study suggested food perception by hypothalamic

POMC neurons was able to promote hepatic mTOR signaling and XBP1 splicing via sympathetic nerve activity from POMC to the liver[135]. Another study indicated the role of anterior pituitary IRE1α-XBP1s signaling in protecting against obesity-associated pathogenesis including nonalcoholic fatty liver disease (NAFLD), via induction of adaptive UPR in liver by hormone signaling[136].

Such cell-nonautonomous effects of UPR are not limited to IRE1α-XBP1s. Another study revealed that the activation of ATF4 in the hypothalamus led to hepatic insulin resistance via mTOR/S6K1 signaling and the vagus nerve[111].

Autophagy has also been identified in the hypothalamic regulation of peripheral tissues. In C. elegans, ATG-18 in chemosensory neurons mediate cell non-autonomous signals to intestinal tissues via release of neurotransmitters and neuropeptides, which is necessary for organismal response to longevity pathways stimulated by dietary restriction and reduced insulin growth factor signaling[137]. Other studies in mice indicated that, the activation of autophagy in hypothalamic POMC neuron by cold exposure or rapamycin induces lipophagy and cytosolic lipases in brown fat and liver, suggesting that activation of central autophagy mediates lipolysis in peripheral tissues[138]. A more recent study suggested food perception by hypothalamic POMC neurons was able to promote hepatic mTOR signaling and XBP1 splicing via sympathetic nerve activity from POMC to the liver[135]. Further, upon sensing energy deprivation, AgRP neurons control the activation of hepatic autophagy by release of NPY and activation of hypothalamic-pituitary adrenal axis with glucocorticoid release[139].

1.10 Crosstalk among ER quality control pathways

Crosstalk among UPR, autophagy (ER-phagy) and ERAD have been widely characterized. Activation of PERK and IRE branches of UPR is necessary and sufficient to induce autophagy by transcriptional regulation upon ER stress [140]. ER stress inducer can activate protective autophagy in a PERK-dependent matter while induction of autophagy by rapamycin can inhibit ER stress[141]. The interplay between UPR and autophagy also includea ER-phagy. ER-phagy relies on the signaling mediated by ER-phagy receptors, which has been found to be upregulated by starvation[142]. Moreover, although UPR activation generally induces ER-phagy [143], further study indicated excessive activation of ER-phagy by FAM134B can induce UPR and cell death[144]. Indeed, studies of the effect of palmitate on hypothalamic cells indicated palmitate inhibited starvation-induced UPR by inhibiting FAM134B mediated ER-phagy[145, 146] UPR, especially the IRE arm, controls the transcription of various ERAD components[147]. On the other hand, ERAD regulates UPR by controlling the degradation of UPR sensors including IRE1α and ATF6 [148-150]. ER-phagy has also been identified to clear ERAD-resistant misfolded proteins via an ER to lysosomal associated degradation, namely ‘ERLAD’[151-153].

1.11 Hypothalamic ER proteostasis in age-related pathogenesis

The capacity of cells to activate of UPR for higher folding capacity declines with age in several aspects. The levels of PERK decrease transcriptionally and the organismal ability to activate IRE1 declines with age. Further, the absolute levels as well as the activity of UPR-induced chaperons are limited[154]. During aging, organisms gradually

lose physiological functions along with the declining capacity of stress-induced adaptative response, concomitantly leading to a variety of age-associated metabolic diseases such as obesity due to the decline in basal metabolic rate and energy expenditure. Further, increased abdominal adiposity and decreased lean muscle mass has been correlated to aging. The hypothalamus, as essential brain region bridging the neuroendocrine system with physiological functions, plays a vital role in the aging process. Alterations in the function of particular neuron populations, including AgRP/NPY and POMC as well as AVP neurons aforementioned are fundamental contributors to the age-related decline in the metabolic control. Dysregulation in nutrient sensing, neuronal network and plasticity are mainly driven by collapse of the machinery that maintains proteostasis.

Rising evidence suggest that the age-dependent alterations in the hypothalamic POMC and AgRP neurons, underlie the imbalance of energy homeostasis with aging. The activity of hypothalamic POMC neurons significantly decreases in aged mice, partially due to elevated mTOR signaling[29]. Of note, Atg7 is inhibited by mTOR[155] and the $Atg7^{\Delta POMC}$ neurons indicated reduced axonal-projection to the targeting region PVH[34, 36] as well as increased adiposity, implying that increased mTOR signaling in POMC neurons may reduce the neurite projection and increase adiposity via inhibition of autophagy in aged mice. Further, such age-associated projection loss and weight gain could be ameliorated by inhibition of mTOR by rapamycin administration[29]. Besides, age-associated metabolic alterations, including increased food intake, body weight and adiposity can also be rescued by exogenous delivery of POMC[156]. Another potential contributor to the reduced POMC firing rate in aged male mice is the increased

innervation from AgRP neurons with increased inhibitory postsynaptic currents onto the POMC neurons[157]. On the other hand, the induction of AgRP/NPY in response to fasting is significantly blunted in aged male rats[158], consistent with the observation of attenuated starvation-induced upregulation of AgRP[24].

1.12 Hypothalamic ER homeostasis in diet-associated pathogenesis

Rising prevalence of obesity and diabetes are partially, if not mostly, attributed to the caloric dense diet. Ever since Ozcan et al. initially proposed the close relationship between ER stress and obesity[159], a variety of studies have demonstrated the vital role of ER homeostasis in both peripheral and central tissues for metabolic control[160-164]. Of note, several studies, combining HFD feeding with genetic modification and pharmacological treatment, investigated mechanisms underlying diet-associated pathogenesis specifically in hypothalamus.

To date, one paradigm that has been supported widely is that hypothalamic ER stress is a key contributor to diet-induced obesity and central leptin resistance. HFD can increase excessive free fatty acid in the hypothalamus and further induce lipotoxicity. Such lipotoxicity can disturb ER homeostasis, trigger UPR activation and even apoptosis. Strong correlations between UPR activation and obesity have been observed where significantly elevated PERK phosphorylation could be observed only in obese mice upon HFD, but not in regular chow fed mice or lean mice resistant to DIO. Moreover, induction of ER stress both in vitro and in vivo via intracerebroventricular administration of ER stress inducers – tunicamycin, thapsigargin, DTT and brefeldin A yielded hypothalamic leptin resistance, hyperphagia and body weight gain in control mice,

which became susceptible to DIO[26, 29, 85, 165]. Further, treatment with chemical chaperones such as 4-phenylbutyrate (4-PBA) or tauroursodeoxycholic acid (TUDCA) can effectively alleviate hypothalamic ER stress and protect mice, fed on HFD or with genetic impairment in ER folding capacity, from hypothalamic resistance and obesity[29, 83, 85]. On the other hand, overexpression of XBP1s protected mice against DIO as well as alleviated the leptin resistance induced by ER stressors.

1.13 Conclusion and future perspective

To date, all the studies suggest patho-physiological importance of hypothalamic ER proteostasis in metabolic regulation. However, closer analysis suggests caveats and limitations in the simplified interpretation and conclusions derived from far more complicated systems.

Above all, the hypothalamus consists of heterogenous populations of cells with chemically and functionally distinct neurons as well as glial cells[166]. The “crude” experiments such as stereotaxic injection of AAV or chemical administration are inevitably affecting all types of cells in the regions. Therefore, several caveats will need to be considered, including different susceptibility to the treatment between neurons and glia; lack of consideration for neuron-neuron or neuron-glia interactions; whether the same signaling pathway in different cell types may generate opposing physiological outcomes. Moreover, even within defined classes of neuronal populations, such as AgRP and POMC neurons discussed in the current studies, the further heterogeneity inside “one” population is neglected[167, 168]. Particularly, in the context of leptin-mediated signaling, not all POMC or AgRP neurons express leptin receptors[167-169].

Therefore, interpretation of the current studies may require further dissection of the neuronal subsets.

Apart from the concerns of heterogeneity, another inherent concern in current mouse models is the specificity of the Cre and its effect on neurodevelopment. Of note, significant difference has been reported in the colocalization of POMC–Cre-expressing cells and POMC neurons in adult mice, due to congenital POMC-Cre expression in neuronal precursors differentiating to a variety of hypothalamic neurons[170]. This caveat may be resolved by more studies using conditional knockout that, however, may give rise to other concerns including the efficiency and physiological effects of tamoxifen administration[171-173].

Further, sexual dimorphism exists in most of the reviewed studies as well as in the majority of the DIO studies. Sexual differences exist in the feeding and energy homeostasis in rodents. More importantly sexual dimorphism is likely to determine the metabolic adaptation of rodents in response to altered nutritional status. In particular, upon HFD induced nutritional overload, male mice are more susceptible to DIO and concomitant pathogenesis including glucose intolerance and insulin resistance, compared to female counterparts. On the other hand, many investigations of hypothalamic proteostasis are focused mainly on males[174-180]. Some observations are consistent in both sexes while some phenotypes are more severe in male. Therefore, a lot more investigation in deciphering sexual dimorphism is still needed.

Modulating hypothalamic ER capacity is a promising therapeutic target for obesity, diabetes and many metabolic disorders related to CNS regulation of metabolism. To date, administration of chemical chaperones including taurine-conjugated

ursodeoxycholic acid (TUDCA) and 4-phenylbutyric acid (4-PBA) could effectively increase ER folding capacity and protect against genetic and/or diet-associated obese mice models via restoring leptin signaling and normal feeding behaviors[29, 83, 181, 182]. However, with difficulty in titrating in vivo and lack of evaluation of broad physiological and even pathological effects, there is still a long way to go before any clinical application can be taken.

1.14 Dissertation goals

Despite of a variety of investigation on importance of ER proteostasis in hypothalamic control of energy homeostasis, the majority of the studies emphasized role of UPR and autophagy. However, there is a neglect of the intricate network of ER quality control machineries as the role of hypothalamic ERAD is somehow underestimated and remains largely unknown. The overarching goal of this dissertation was to explore the cellular mechanisms of hypothalamic ER proteostasis that may contribute to organismal metabolic regulation. In particular, we start with evaluating the ER homeostasis in both peripheral tissues and hypothalamus in the context of diet-induced obesity (DIO) and pathogenesis including leptin resistance. Then we further focus on how SEL1L-HRD1 ERAD controls leptin signaling in hypothalamic POMC neurons upon DIO. Lastly, we demonstrated the validation and characterization, both in vitro and in vivo, of a neuron-specific SEL1L-HRD1 ERAD substrate involved in neuron-glia crosstalk. Overall, we aimed to investigate how SEL1L-HRD1 ERAD regulates neuronal proteostasis and function in response to various pathophysiological circumstances, in hypothalamus and beyond.

1.15 References

1. Han, C., et al., *Global prevalence of prediabetes in children and adolescents: A systematic review and meta-analysis.* J Diabetes, 2022. 14(7): p. 434-441.
2. Rooney, M.R., et al., *Global Prevalence of Prediabetes.* Diabetes Care, 2023. 46(7): p. 1388-1394.
3. Malik, V.S., W.C. Willet, and F.B. Hu, *Nearly a decade on - trends, risk factors and policy implications in global obesity.* Nat Rev Endocrinol, 2020. 16(11): p. 615-616.
4. Oussaada, S.M., et al., *The pathogenesis of obesity.* Metabolism, 2019. 92: p. 26-36.
5. Cone, R.D., *The Central Melanocortin System and Energy Homeostasis.* Trends Endocrinol Metab, 1999. 10(6): p. 211-216.
6. van Galen, K.A., et al., *The role of central dopamine and serotonin in human obesity: lessons learned from molecular neuroimaging studies.* Metabolism, 2018. 85: p. 325-339.
7. Schwartz, M.W., et al., *Central nervous system control of food intake.* Nature, 2000. 404(6778): p. 661-71.
8. Ueno, N., et al., *Leptin modulates orexigenic effects of ghrelin and attenuates adiponectin and insulin levels and selectively the dark-phase feeding as revealed by central leptin gene therapy.* Endocrinology, 2004. 145(9): p. 4176-84.
9. Nakazato, M., et al., *A role for ghrelin in the central regulation of feeding.* Nature, 2001. 409(6817): p. 194-8.
10. Timper, K. and J.C. Bruning, *Hypothalamic circuits regulating appetite and energy homeostasis: pathways to obesity.* Dis Model Mech, 2017. 10(6): p. 679-689.
11. Belgardt, B.F., T. Okamura, and J.C. Bruning, *Hormone and glucose signalling in POMC and AgRP neurons.* J Physiol, 2009. 587(Pt 22): p. 5305-14.
12. Vohra, M.S., et al., *AgRP/NPY and POMC neurons in the arcuate nucleus and their potential role in treatment of obesity.* Eur J Pharmacol, 2022. 915: p. 174611.
13. Varela, L. and T.L. Horvath, *Leptin and insulin pathways in POMC and AgRP neurons that modulate energy balance and glucose homeostasis.* EMBO Rep, 2012. 13(12): p. 1079-86.
14. Chen, Y. and Z.A. Knight, *Making sense of the sensory regulation of hunger neurons.* Bioessays, 2016. 38(4): p. 316-24.
15. Aponte, Y., D. Atasoy, and S.M. Sternson, *AGRP neurons are sufficient to orchestrate feeding behavior rapidly and without training.* Nat Neurosci, 2011. 14(3): p. 351-5.
16. Cowley, M.A., et al., *Leptin activates anorexigenic POMC neurons through a neural network in the arcuate nucleus.* Nature, 2001. 411(6836): p. 480-4.
17. Hahn, T.M., et al., *Coexpression of Agrp and NPY in fasting-activated hypothalamic neurons.* Nat Neurosci, 1998. 1(4): p. 271-2.
18. Krashes, M.J., et al., *Rapid, reversible activation of AgRP neurons drives feeding behavior in mice.* J Clin Invest, 2011. 121(4): p. 1424-8.
19. Zhan, C., et al., *Acute and long-term suppression of feeding behavior by POMC neurons in the brainstem and hypothalamus, respectively.* J Neurosci, 2013. 33(8): p. 3624-32.
20. Pritchard, L.E. and A. White, *Neuropeptide processing and its impact on melanocortin pathways.* Endocrinology, 2007. 148(9): p. 4201-7.

21. Wardlaw, S.L., *Hypothalamic proopiomelanocortin processing and the regulation of energy balance.* Eur J Pharmacol, 2011. 660(1): p. 213-9.
22. Aveleira, C.A., et al., *Neuropeptide Y stimulates autophagy in hypothalamic neurons.* Proc Natl Acad Sci U S A, 2015. 112(13): p. E1642-51.
23. Henry, F.E., et al., *Cell type-specific transcriptomics of hypothalamic energy-sensing neuron responses to weight-loss.* Elife, 2015. 4.
24. Kaushik, S., et al., *Autophagy in hypothalamic AgRP neurons regulates food intake and energy balance.* Cell Metab, 2011. 14(2): p. 173-83.
25. Kim, G.H., et al., *Hypothalamic ER-associated degradation regulates POMC maturation, feeding, and age-associated obesity.* J Clin Invest, 2018. 128(3): p. 1125-1140.
26. Williams, K.W., et al., *Xbp1s in Pomc neurons connects ER stress with energy balance and glucose homeostasis.* Cell Metab, 2014. 20(3): p. 471-82.
27. Yao, T., et al., *Ire1alpha in Pomc Neurons Is Required for Thermogenesis and Glycemia.* Diabetes, 2017. 66(3): p. 663-673.
28. Xiao, Y., et al., *Knockout of inositol-requiring enzyme 1alpha in pro-opiomelanocortin neurons decreases fat mass via increasing energy expenditure.* Open Biol, 2016. 6(8).
29. Ozcan, L., et al., *Endoplasmic reticulum stress plays a central role in development of leptin resistance.* Cell Metab, 2009. 9(1): p. 35-51.
30. He, Z., et al., *PERK in POMC neurons connects celastrol with metabolism.* JCI Insight, 2021. 6(18).
31. Kim, K.K., et al., *Bridging Energy Need and Feeding Behavior: The Impact of eIF2alpha Phosphorylation in AgRP Neurons.* Diabetes, 2023. 72(10): p. 1384-1396.
32. Xiao, Y., et al., *ATF4/ATG5 Signaling in Hypothalamic Proopiomelanocortin Neurons Regulates Fat Mass via Affecting Energy Expenditure.* Diabetes, 2017. 66(5): p. 1146-1158.
33. Deng, J., et al., *Deletion of ATF4 in AgRP Neurons Promotes Fat Loss Mainly via Increasing Energy Expenditure.* Diabetes, 2017. 66(3): p. 640-650.
34. Coupe, B., et al., *Loss of autophagy in pro-opiomelanocortin neurons perturbs axon growth and causes metabolic dysregulation.* Cell Metab, 2012. 15(2): p. 247-55.
35. Quan, W., et al., *Role of hypothalamic proopiomelanocortin neuron autophagy in the control of appetite and leptin response.* Endocrinology, 2012. 153(4): p. 1817-26.
36. Kaushik, S., et al., *Loss of autophagy in hypothalamic POMC neurons impairs lipolysis.* EMBO Rep, 2012. 13(3): p. 258-65.
37. Malhotra, R., et al., *Loss of Atg12, but not Atg5, in pro-opiomelanocortin neurons exacerbates diet-induced obesity.* Autophagy, 2015. 11(1): p. 145-54.
38. Shi, G., et al., *ER-associated degradation is required for vasopressin prohormone processing and systemic water homeostasis.* J Clin Invest, 2017. 127(10): p. 3897-3912.
39. Atasoy, D., et al., *Deconstruction of a neural circuit for hunger.* Nature, 2012. 488(7410): p. 172-7.
40. De Solis, A.J., et al., *Reciprocal activity of AgRP and POMC neurons governs coordinated control of feeding and metabolism.* Nat Metab, 2024.

41. Ahima, R.S. and S.M. Hileman, *Postnatal regulation of hypothalamic neuropeptide expression by leptin: implications for energy balance and body weight regulation.* Regul Pept, 2000. 92(1-3): p. 1-7.
42. Ahima, R.S., et al., *Leptin regulation of neuroendocrine systems.* Front Neuroendocrinol, 2000. 21(3): p. 263-307.
43. Ahima, R.S. and J.S. Flier, *Leptin.* Annu Rev Physiol, 2000. 62: p. 413-37.
44. Maffei, M., et al., *Leptin levels in human and rodent: measurement of plasma leptin and ob RNA in obese and weight-reduced subjects.* Nat Med, 1995. 1(11): p. 1155-61.
45. Frederich, R.C., et al., *Leptin levels reflect body lipid content in mice: evidence for diet-induced resistance to leptin action.* Nat Med, 1995. 1(12): p. 1311-4.
46. Casanueva, F.F. and C. Dieguez, *Neuroendocrine regulation and actions of leptin.* Front Neuroendocrinol, 1999. 20(4): p. 317-63.
47. Cheung, C.C., D.K. Clifton, and R.A. Steiner, *Proopiomelanocortin neurons are direct targets for leptin in the hypothalamus.* Endocrinology, 1997. 138(10): p. 4489-92.
48. Elias, C.F., et al., *Leptin differentially regulates NPY and POMC neurons projecting to the lateral hypothalamic area.* Neuron, 1999. 23(4): p. 775-86.
49. Schwartz, M.W., et al., *Identification of targets of leptin action in rat hypothalamus.* J Clin Invest, 1996. 98(5): p. 1101-6.
50. Tartaglia, L.A., et al., *Identification and expression cloning of a leptin receptor, OB-R.* Cell, 1995. 83(7): p. 1263-71.
51. Mercer, J.G., et al., *Localization of leptin receptor mRNA and the long form splice variant (Ob-Rb) in mouse hypothalamus and adjacent brain regions by in situ hybridization.* FEBS Lett, 1996. 387(2-3): p. 113-6.
52. Chen, H., et al., *Evidence that the diabetes gene encodes the leptin receptor: identification of a mutation in the leptin receptor gene in db/db mice.* Cell, 1996. 84(3): p. 491-5.
53. Lee, G.H., et al., *Abnormal splicing of the leptin receptor in diabetic mice.* Nature, 1996. 379(6566): p. 632-5.
54. Ghilardi, N., et al., *Defective STAT signaling by the leptin receptor in diabetic mice.* Proc Natl Acad Sci U S A, 1996. 93(13): p. 6231-5.
55. Devos, R., et al., *Ligand-independent dimerization of the extracellular domain of the leptin receptor and determination of the stoichiometry of leptin binding.* J Biol Chem, 1997. 272(29): p. 18304-10.
56. White, D.W. and L.A. Tartaglia, *Evidence for ligand-independent homo-oligomerization of leptin receptor (OB-R) isoforms: a proposed mechanism permitting productive long-form signaling in the presence of excess short-form expression.* J Cell Biochem, 1999. 73(2): p. 278-88.
57. Baumann, H., et al., *The full-length leptin receptor has signaling capabilities of interleukin 6-type cytokine receptors.* Proc Natl Acad Sci U S A, 1996. 93(16): p. 8374-8.
58. Couturier, C. and R. Jockers, *Activation of the leptin receptor by a ligand-induced conformational change of constitutive receptor dimers.* J Biol Chem, 2003. 278(29): p. 26604-11.
59. Vaisse, C., et al., *Leptin activation of Stat3 in the hypothalamus of wild-type and ob/ob mice but not db/db mice.* Nat Genet, 1996. 14(1): p. 95-7.

60. Fruhbeck, G., *Intracellular signalling pathways activated by leptin.* Biochem J, 2006. 393(Pt 1): p. 7-20.
61. Myers, M.G., M.A. Cowley, and H. Munzberg, *Mechanisms of leptin action and leptin resistance.* Annu Rev Physiol, 2008. 70: p. 537-56.
62. Schwartz, M.W., et al., *Leptin increases hypothalamic pro-opiomelanocortin mRNA expression in the rostral arcuate nucleus.* Diabetes, 1997. 46(12): p. 2119-23.
63. Thornton, J.E., et al., *Regulation of hypothalamic proopiomelanocortin mRNA by leptin in ob/ob mice.* Endocrinology, 1997. 138(11): p. 5063-6.
64. Mizuno, T.M., et al., *Hypothalamic pro-opiomelanocortin mRNA is reduced by fasting and [corrected] in ob/ob and db/db mice, but is stimulated by leptin.* Diabetes, 1998. 47(2): p. 294-7.
65. Stephens, T.W., et al., *The role of neuropeptide Y in the antiobesity action of the obese gene product.* Nature, 1995. 377(6549): p. 530-2.
66. Schwartz, M.W., et al., *Specificity of leptin action on elevated blood glucose levels and hypothalamic neuropeptide Y gene expression in ob/ob mice.* Diabetes, 1996. 45(4): p. 531-5.
67. Mizuno, T.M. and C.V. Mobbs, *Hypothalamic agouti-related protein messenger ribonucleic acid is inhibited by leptin and stimulated by fasting.* Endocrinology, 1999. 140(2): p. 814-7.
68. Kitamura, T., et al., *Forkhead protein FoxO1 mediates Agrp-dependent effects of leptin on food intake.* Nat Med, 2006. 12(5): p. 534-40.
69. Considine, R.V., et al., *Serum immunoreactive-leptin concentrations in normal-weight and obese humans.* N Engl J Med, 1996. 334(5): p. 292-5.
70. Heymsfield, S.B., et al., *Recombinant leptin for weight loss in obese and lean adults: a randomized, controlled, dose-escalation trial.* JAMA, 1999. 282(16): p. 1568-75.
71. Caro, J.F., et al., *Decreased cerebrospinal-fluid/serum leptin ratio in obesity: a possible mechanism for leptin resistance.* Lancet, 1996. 348(9021): p. 159-61.
72. El-Haschimi, K., et al., *Two defects contribute to hypothalamic leptin resistance in mice with diet-induced obesity.* J Clin Invest, 2000. 105(12): p. 1827-32.
73. Schwartz, M.W., et al., *Cerebrospinal fluid leptin levels: relationship to plasma levels and to adiposity in humans.* Nat Med, 1996. 2(5): p. 589-93.
74. Oh, I.S., et al., *Molecular mechanisms associated with leptin resistance: n-3 polyunsaturated fatty acids induce alterations in the tight junction of the brain.* Cell Metab, 2005. 1(5): p. 331-41.
75. Bjorbaek, C., et al., *Identification of SOCS-3 as a potential mediator of central leptin resistance.* Mol Cell, 1998. 1(4): p. 619-25.
76. Howard, J.K., et al., *Enhanced leptin sensitivity and attenuation of diet-induced obesity in mice with haploinsufficiency of Socs3.* Nat Med, 2004. 10(7): p. 734-8.
77. Mori, H., et al., *Socs3 deficiency in the brain elevates leptin sensitivity and confers resistance to diet-induced obesity.* Nat Med, 2004. 10(7): p. 739-43.
78. Banks, A.S., et al., *Activation of downstream signals by the long form of the leptin receptor.* J Biol Chem, 2000. 275(19): p. 14563-72.
79. White, C.L., et al., *HF diets increase hypothalamic PTP1B and induce leptin resistance through both leptin-dependent and -independent mechanisms.* Am J Physiol Endocrinol Metab, 2009. 296(2): p. E291-9.

80. Kaszubska, W., et al., *Protein tyrosine phosphatase 1B negatively regulates leptin signaling in a hypothalamic cell line.* Mol Cell Endocrinol, 2002. 195(1-2): p. 109-18.
81. Bence, K.K., et al., *Neuronal PTP1B regulates body weight, adiposity and leptin action.* Nat Med, 2006. 12(8): p. 917-24.
82. De Souza, C.T., et al., *Consumption of a fat-rich diet activates a proinflammatory response and induces insulin resistance in the hypothalamus.* Endocrinology, 2005. 146(10): p. 4192-9.
83. Zhang, X., et al., *Hypothalamic IKKbeta/NF-kappaB and ER stress link overnutrition to energy imbalance and obesity.* Cell, 2008. 135(1): p. 61-73.
84. Posey, K.A., et al., *Hypothalamic proinflammatory lipid accumulation, inflammation, and insulin resistance in rats fed a high-fat diet.* Am J Physiol Endocrinol Metab, 2009. 296(5): p. E1003-12.
85. Hosoi, T., et al., *Endoplasmic reticulum stress induces leptin resistance.* Mol Pharmacol, 2008. 74(6): p. 1610-9.
86. Hampton, R.Y. and T. Sommer, *Finding the will and the way of ERAD substrate retrotranslocation.* Curr Opin Cell Biol, 2012. 24(4): p. 460-6.
87. Mueller, B., B.N. Lilley, and H.L. Ploegh, *SEL1L, the homologue of yeast Hrd3p, is involved in protein dislocation from the mammalian ER.* J Cell Biol, 2006. 175(2): p. 261-70.
88. Vashistha, N., et al., *Direct and essential function for Hrd3 in ER-associated degradation.* Proc Natl Acad Sci U S A, 2016. 113(21): p. 5934-9.
89. Bhattacharya, A. and L. Qi, *ER-associated degradation in health and disease - from substrate to organism.* J Cell Sci, 2019. 132(23).
90. Bhattacharya, A., et al., *Hepatic Sel1L-Hrd1 ER-associated degradation (ERAD) manages FGF21 levels and systemic metabolism via CREBH.* EMBO J, 2018. 37(22).
91. Bhattacharya, A., et al., *SEL1L-HRD1 ER-associated degradation suppresses hepatocyte hyperproliferation and liver cancer.* iScience, 2022. 25(10): p. 105183.
92. Shrestha, N., et al., *Sel1L-Hrd1 ER-associated degradation maintains beta cell identity via TGF-beta signaling.* J Clin Invest, 2020. 130(7): p. 3499-3510.
93. Shrestha, N., et al., *Integration of ER protein quality control mechanisms defines beta cell function and ER architecture.* J Clin Invest, 2023. 133(1).
94. Sha, H., et al., *The ER-associated degradation adaptor protein Sel1L regulates LPL secretion and lipid metabolism.* Cell Metab, 2014. 20(3): p. 458-70.
95. Zhou, Z., et al., *Endoplasmic reticulum-associated degradation regulates mitochondrial dynamics in brown adipocytes.* Science, 2020. 368(6486): p. 54-60.
96. Yoshida, S., et al., *Endoplasmic reticulum-associated degradation is required for nephrin maturation and kidney glomerular filtration function.* J Clin Invest, 2021. 131(7).
97. Schoebel, S., et al., *Cryo-EM structure of the protein-conducting ERAD channel Hrd1 in complex with Hrd3.* Nature, 2017. 548(7667): p. 352-355.
98. Vasic, V., et al., *Hrd1 forms the retrotranslocation pore regulated by auto-ubiquitination and binding of misfolded proteins.* Nat Cell Biol, 2020. 22(3): p. 274-281.
99. Lin, L.L., et al., *SEL1L-HRD1 interaction is required to form a functional HRD1 ERAD complex.* Nat Commun, 2024. 15(1): p. 1440.

100. Sun, S., et al., *Sel1L is indispensable for mammalian endoplasmic reticulum-associated degradation, endoplasmic reticulum homeostasis, and survival.* Proc Natl Acad Sci U S A, 2014. 111(5): p. E582-91.
101. Bertolotti, A., et al., *Dynamic interaction of BiP and ER stress transducers in the unfolded-protein response.* Nat Cell Biol, 2000. 2(6): p. 326-32.
102. Liu, C.Y., Z. Xu, and R.J. Kaufman, *Structure and intermolecular interactions of the luminal dimerization domain of human IRE1alpha.* J Biol Chem, 2003. 278(20): p. 17680-7.
103. Shamu, C.E. and P. Walter, *Oligomerization and phosphorylation of the Ire1p kinase during intracellular signaling from the endoplasmic reticulum to the nucleus.* EMBO J, 1996. 15(12): p. 3028-39.
104. Acosta-Alvear, D., et al., *XBP1 controls diverse cell type- and condition-specific transcriptional regulatory networks.* Mol Cell, 2007. 27(1): p. 53-66.
105. Cox, J.S. and P. Walter, *A novel mechanism for regulating activity of a transcription factor that controls the unfolded protein response.* Cell, 1996. 87(3): p. 391-404.
106. Cakir, I. and E.A. Nillni, *Endoplasmic Reticulum Stress, the Hypothalamus, and Energy Balance.* Trends Endocrinol Metab, 2019. 30(3): p. 163-176.
107. Ma, K., K.M. Vattem, and R.C. Wek, *Dimerization and release of molecular chaperone inhibition facilitate activation of eukaryotic initiation factor-2 kinase in response to endoplasmic reticulum stress.* J Biol Chem, 2002. 277(21): p. 18728-35.
108. Zinszner, H., et al., *CHOP is implicated in programmed cell death in response to impaired function of the endoplasmic reticulum.* Genes Dev, 1998. 12(7): p. 982-95.
109. Ron, D. and P. Walter, *Signal integration in the endoplasmic reticulum unfolded protein response.* Nat Rev Mol Cell Biol, 2007. 8(7): p. 519-29.
110. Rutkowski, D.T., et al., *Adaptation to ER stress is mediated by differential stabilities of pro-survival and pro-apoptotic mRNAs and proteins.* PLoS Biol, 2006. 4(11): p. e374.
111. Zhang, Q., et al., *Central activating transcription factor 4 (ATF4) regulates hepatic insulin resistance in mice via S6K1 signaling and the vagus nerve.* Diabetes, 2013. 62(7): p. 2230-9.
112. Azuma, Y., et al., *Activating transcription factor 6alpha is required for the vasopressin neuron system to maintain water balance under dehydration in male mice.* Endocrinology, 2014. 155(12): p. 4905-14.
113. Tanaka, T., et al., *ATF6beta Deficiency Elicits Anxiety-like Behavior and Hyperactivity Under Stress Conditions.* Neurochem Res, 2023. 48(7): p. 2175-2186.
114. Lu, W., et al., *Unfolded protein response in hypothalamic cultures of wild-type and ATF6alpha-knockout mice.* Neurosci Lett, 2016. 612: p. 199-203.
115. Adachi, Y., et al., *ATF6 is a transcription factor specializing in the regulation of quality control proteins in the endoplasmic reticulum.* Cell Struct Funct, 2008. 33(1): p. 75-89.
116. Yang, Z. and D.J. Klionsky, *Eaten alive: a history of macroautophagy.* Nat Cell Biol, 2010. 12(9): p. 814-22.
117. Morishita, H. and N. Mizushima, *Diverse Cellular Roles of Autophagy.* Annu Rev Cell Dev Biol, 2019. 35: p. 453-475.

118. Ohsumi, Y., *Historical landmarks of autophagy research.* Cell Res, 2014. 24(1): p. 9-23.
119. Nakatogawa, H., *Mechanisms governing autophagosome biogenesis.* Nat Rev Mol Cell Biol, 2020. 21(8): p. 439-458.
120. Schuck, S., *Microautophagy - distinct molecular mechanisms handle cargoes of many sizes.* J Cell Sci, 2020. 133(17).
121. Kaushik, S. and A.M. Cuervo, *The coming of age of chaperone-mediated autophagy.* Nat Rev Mol Cell Biol, 2018. 19(6): p. 365-381.
122. Meng, Q. and D. Cai, *Defective hypothalamic autophagy directs the central pathogenesis of obesity via the IkappaB kinase beta (IKKbeta)/NF-kappaB pathway.* J Biol Chem, 2011. 286(37): p. 32324-32.
123. Chino, H. and N. Mizushima, *ER-Phagy: Quality Control and Turnover of Endoplasmic Reticulum.* Trends Cell Biol, 2020. 30(5): p. 384-398.
124. Molinari, M., *ER-phagy responses in yeast, plants, and mammalian cells and their crosstalk with UPR and ERAD.* Dev Cell, 2021. 56(7): p. 949-966.
125. Khaminets, A., et al., *Regulation of endoplasmic reticulum turnover by selective autophagy.* Nature, 2015. 522(7556): p. 354-8.
126. Kim, D.Y., et al., *A selective ER-phagy exerts neuroprotective effects via modulation of alpha-synuclein clearance in parkinsonian models.* Proc Natl Acad Sci U S A, 2023. 120(37): p. e2221929120.
127. Kuijpers, M., et al., *Neuronal Autophagy Regulates Presynaptic Neurotransmission by Controlling the Axonal Endoplasmic Reticulum.* Neuron, 2022. 110(4): p. 734.
128. Kurth, I., et al., *Mutations in FAM134B, encoding a newly identified Golgi protein, cause severe sensory and autonomic neuropathy.* Nat Genet, 2009. 41(11): p. 1179-81.
129. Murphy, S.M., et al., *Mutation in FAM134B causing severe hereditary sensory neuropathy.* J Neurol Neurosurg Psychiatry, 2012. 83(1): p. 119-20.
130. Keles, U., et al., *Differential expression of full-length and NH(2) terminally truncated FAM134B isoforms in normal physiology and cancer.* Am J Physiol Gastrointest Liver Physiol, 2020. 319(6): p. G733-G747.
131. Wang, D., et al., *A deep proteome and transcriptome abundance atlas of 29 healthy human tissues.* Mol Syst Biol, 2019. 15(2): p. e8503.
132. Hoyer, M.J., et al., *Combinatorial selective ER-phagy remodels the ER during neurogenesis.* Nat Cell Biol, 2024.
133. Taylor, R.C. and A. Dillin, *XBP-1 is a cell-nonautonomous regulator of stress resistance and longevity.* Cell, 2013. 153(7): p. 1435-47.
134. Imanikia, S., et al., *XBP-1 Remodels Lipid Metabolism to Extend Longevity.* Cell Rep, 2019. 28(3): p. 581-589 e4.
135. Brandt, C., et al., *Food Perception Primes Hepatic ER Homeostasis via Melanocortin-Dependent Control of mTOR Activation.* Cell, 2018. 175(5): p. 1321-1335 e20.
136. Qian, Q., et al., *Obesity Disrupts Pituitary UPR Leading to NAFLD.* bioRxiv, 2022: p. 2022.07. 06.498610.
137. Minnerly, J., et al., *The cell non-autonomous function of ATG-18 is essential for neuroendocrine regulation of Caenorhabditis elegans lifespan.* PLoS Genet, 2017. 13(5): p. e1006764.

138. Martinez-Lopez, N., et al., *Autophagy in the CNS and Periphery Coordinate Lipophagy and Lipolysis in the Brown Adipose Tissue and Liver.* Cell Metab, 2016. 23(1): p. 113-27.
139. Chen, W., et al., *Nutrient-sensing AgRP neurons relay control of liver autophagy during energy deprivation.* Cell Metab, 2023. 35(5): p. 786-806 e13.
140. Deegan, S., et al., *Stress-induced self-cannibalism: on the regulation of autophagy by endoplasmic reticulum stress.* Cell Mol Life Sci, 2013. 70(14): p. 2425-41.
141. Zheng, W., et al., *ATG5 and ATG7 induced autophagy interplays with UPR via PERK signaling.* Cell Commun Signal, 2019. 17(1): p. 42.
142. Kohno, S., et al., *An N-terminal-truncated isoform of FAM134B (FAM134B-2) regulates starvation-induced hepatic selective ER-phagy.* Life Sci Alliance, 2019. 2(3).
143. Song, S., et al., *Crosstalk of ER stress-mediated autophagy and ER-phagy: Involvement of UPR and the core autophagy machinery.* J Cell Physiol, 2018. 233(5): p. 3867-3874.
144. Liao, Y., et al., *Excessive ER-phagy mediated by the autophagy receptor FAM134B results in ER stress, the unfolded protein response, and cell death in HeLa cells.* J Biol Chem, 2019. 294(52): p. 20009-20023.
145. Lim, Y., S. Kim, and E.K. Kim, *Palmitate reduces starvation-induced ER stress by inhibiting ER-phagy in hypothalamic cells.* Mol Brain, 2021. 14(1): p. 65.
146. Park, S., et al., *The endoplasmic reticulum stress-autophagy pathway controls hypothalamic development and energy balance regulation in leptin-deficient neonates.* Nat Commun, 2020. 11(1): p. 1914.
147. Hetz, C., E. Chevet, and S.A. Oakes, *Proteostasis control by the unfolded protein response.* Nat Cell Biol, 2015. 17(7): p. 829-38.
148. Sugimoto, T., et al., *SEL1L-dependent Substrates Require Derlin2/3 and Herp1/2 for Endoplasmic Reticulum-associated Degradation.* Cell Struct Funct, 2017. 42(2): p. 81-94.
149. Horimoto, S., et al., *The unfolded protein response transducer ATF6 represents a novel transmembrane-type endoplasmic reticulum-associated degradation substrate requiring both mannose trimming and SEL1L protein.* J Biol Chem, 2013. 288(44): p. 31517-27.
150. Sun, S., et al., *IRE1alpha is an endogenous substrate of endoplasmic-reticulum-associated degradation.* Nat Cell Biol, 2015. 17(12): p. 1546-55.
151. Fregno, I. and M. Molinari, *Proteasomal and lysosomal clearance of faulty secretory proteins: ER-associated degradation (ERAD) and ER-to-lysosome-associated degradation (ERLAD) pathways.* Crit Rev Biochem Mol Biol, 2019. 54(2): p. 153-163.
152. Fregno, I., et al., *ER-to-lysosome-associated degradation of proteasome-resistant ATZ polymers occurs via receptor-mediated vesicular transport.* EMBO J, 2018. 37(17).
153. Fregno, I., et al., *N-glycan processing selects ERAD-resistant misfolded proteins for ER-to-lysosome-associated degradation.* EMBO J, 2021. 40(15): p. e107240.
154. Taylor, R.C., *Aging and the UPR(ER).* Brain Res, 2016. 1648(Pt B): p. 588-593.
155. Kim, Y.C. and K.L. Guan, *mTOR: a pharmacologic target for autophagy regulation.* J Clin Invest, 2015. 125(1): p. 25-32.
156. Li, G., et al., *Hypothalamic pro-opiomelanocortin gene delivery ameliorates obesity and glucose intolerance in aged rats.* Diabetologia, 2005. 48(11): p. 2376-85.

157. Newton, A.J., et al., *AgRP innervation onto POMC neurons increases with age and is accelerated with chronic high-fat feeding in male mice.* Endocrinology, 2013. 154(1): p. 172-83.
158. Wolden-Hanson, T., B.T. Marck, and A.M. Matsumoto, *Blunted hypothalamic neuropeptide gene expression in response to fasting, but preservation of feeding responses to AgRP in aging male Brown Norway rats.* Am J Physiol Regul Integr Comp Physiol, 2004. 287(1): p. R138-46.
159. Ozcan, U., et al., *Endoplasmic reticulum stress links obesity, insulin action, and type 2 diabetes.* Science, 2004. 306(5695): p. 457-61.
160. Bravo, R., et al., *Endoplasmic reticulum: ER stress regulates mitochondrial bioenergetics.* Int J Biochem Cell Biol, 2012. 44(1): p. 16-20.
161. Cnop, M., F. Foufelle, and L.A. Velloso, *Endoplasmic reticulum stress, obesity and diabetes.* Trends Mol Med, 2012. 18(1): p. 59-68.
162. Lee, J. and U. Ozcan, *Unfolded protein response signaling and metabolic diseases.* J Biol Chem, 2014. 289(3): p. 1203-11.
163. Ajoolabady, A., et al., *ER stress and inflammation crosstalk in obesity.* Med Res Rev, 2023. 43(1): p. 5-30.
164. Ajoolabady, A., et al., *ER stress in obesity pathogenesis and management.* Trends Pharmacol Sci, 2022. 43(2): p. 97-109.
165. Won, J.C., et al., *Central administration of an endoplasmic reticulum stress inducer inhibits the anorexigenic effects of leptin and insulin.* Obesity (Silver Spring), 2009. 17(10): p. 1861-5.
166. Siletti, K., et al., *Transcriptomic diversity of cell types across the adult human brain.* Science, 2023. 382(6667): p. eadd7046.
167. Lam, B.Y.H., et al., *Heterogeneity of hypothalamic pro-opiomelanocortin-expressing neurons revealed by single-cell RNA sequencing.* Mol Metab, 2017. 6(5): p. 383-392.
168. Biglari, N., et al., *Functionally distinct POMC-expressing neuron subpopulations in hypothalamus revealed by intersectional targeting.* Nat Neurosci, 2021. 24(7): p. 913-929.
169. Steuernagel, L., et al., *HypoMap-a unified single-cell gene expression atlas of the murine hypothalamus.* Nat Metab, 2022. 4(10): p. 1402-1419.
170. Padilla, S.L., J.S. Carmody, and L.M. Zeltser, *Pomc-expressing progenitors give rise to antagonistic neuronal populations in hypothalamic feeding circuits.* Nat Med, 2010. 16(4): p. 403-5.
171. Yuan, Y., et al., *Postnatal Tamoxifen Exposure Induces Long-Lasting Changes to Adipose Tissue in Adult Mice.* Mol Biotechnol, 2023.
172. Wade, G.N. and H.W. Heller, *Tamoxifen mimics the effects of estradiol on food intake, body weight, and body composition in rats.* Am J Physiol, 1993. 264(6 Pt 2): p. R1219-23.
173. Valny, M., et al., *Tamoxifen in the Mouse Brain: Implications for Fate-Mapping Studies Using the Tamoxifen-Inducible Cre-loxP System.* Front Cell Neurosci, 2016. 10: p. 243.
174. Shi, H., R.J. Seeley, and D.J. Clegg, *Sexual differences in the control of energy homeostasis.* Front Neuroendocrinol, 2009. 30(3): p. 396-404.

175. Morselli, E., et al., *A sexually dimorphic hypothalamic response to chronic high-fat diet consumption.* Int J Obes (Lond), 2016. 40(2): p. 206-9.
176. Sugiyama, M.G. and L.B. Agellon, *Sex differences in lipid metabolism and metabolic disease risk.* Biochem Cell Biol, 2012. 90(2): p. 124-41.
177. Grove, K.L., et al., *A microarray analysis of sexual dimorphism of adipose tissues in high-fat-diet-induced obese mice.* Int J Obes (Lond), 2010. 34(6): p. 989-1000.
178. Benz, V., et al., *Sexual dimorphic regulation of body weight dynamics and adipose tissue lipolysis.* PLoS One, 2012. 7(5): p. e37794.
179. Stubbins, R.E., et al., *Estrogen modulates abdominal adiposity and protects female mice from obesity and impaired glucose tolerance.* Eur J Nutr, 2012. 51(7): p. 861-70.
180. Yang, Y., et al., *Variations in body weight, food intake and body composition after long-term high-fat diet feeding in C57BL/6J mice.* Obesity (Silver Spring), 2014. 22(10): p. 2147-55.
181. Cakir, I., et al., *Obesity induces hypothalamic endoplasmic reticulum stress and impairs proopiomelanocortin (POMC) post-translational processing.* J Biol Chem, 2013. 288(24): p. 17675-88.
182. Schneeberger, M., et al., *Mitofusin 2 in POMC neurons connects ER stress with leptin resistance and energy imbalance.* Cell, 2013. 155(1): p. 172-87.

1.16 Figures and figure legends

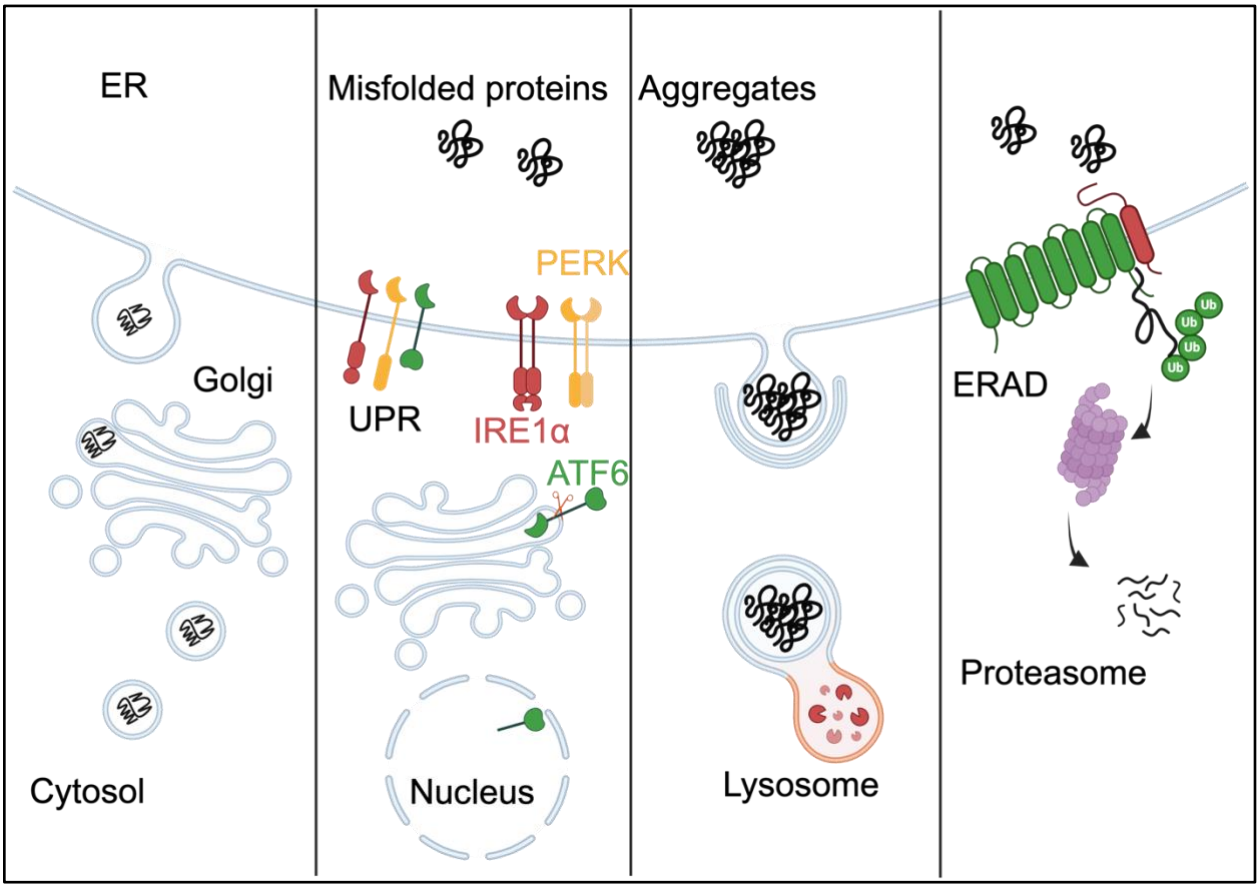

Figure 1.1 ER protein quality control pathways.

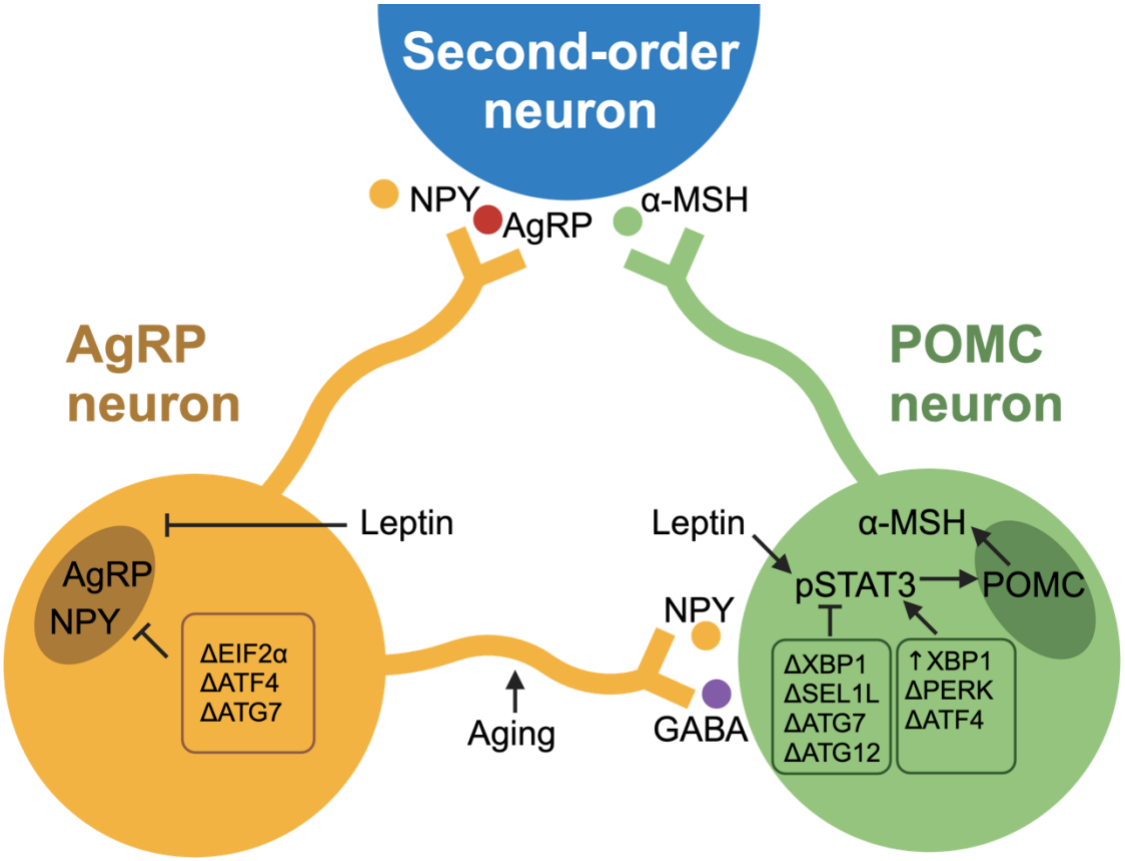

Figure 1.2 Schematic diagram of ER protein quality control machineries regulation in hypothalamic neurons.

POMC and AgRP/NPY neurons project to second-order neurons for the regulation of energy balance including food intake and energy expenditure with opposing effects, where POMC neurons and derived peptides such as α-MSH decreases food intake while AgRP neurons and its neuropeptides increase appetite. AgRP neurons can also inhibit the activity of POMC neurons via GABAergic synapses, which are enhanced during aging. Leptin can increase activity of POMC neurons as well as upregulate POMC transcription via pSTAT3 to induce satiety. On the hand, leptin can inhibit activity of AgRP neurons, and thus inhibit appetite. Hence, the integrative external metabolic effect of leptin on hypothalamic neurons is inhibition of food intake.

1.17 Summary of mouse models of UPR, autophagy, and ERAD in hypothalamic neurons

Gene	Model	Phenotype	Ref
UPR			
Ern1 (IRE1α)	POMC-Cre	Accelerated DIO; decreased thermogenesis; leptin and insulin resistance in POMC neurons; increased food intake; impaired systemic insulin sensitivity and glycemia	[27]
Ern1 (IRE1α)	POMC-Cre	Lean and resistant to DIO; Increased thermogenesis in brown adipose tissue; increased α-MSH	[28]
XBP1s	Induction by POMC-Cre	Protected against DIO; improved leptin and insulin sensitivity; activated hepative XBP1s axis; improved hepatic insulin sensitivity	[26]
XBP1	NESTIN-Cre	No significant effect on body weight or metabolic parameters upon normal chow; susceptible to DIO and leptin resistance	[29]
Eif2αk3 (PERK)	POMC-Cre	Decreased food intake and body weight in male mice; attenuated celastrol-induced improvements in leptin sensitivity and decreased food intake in DIO	[30]
Eif2α	Ser51Ala in AgRP neurons	Impaired eIF2α phosphorylation; decreased starvation-induced AgRP neuronal activity, food intake and body weight; increased leptin sensitivity in ARC	[31]

Atf4	POMC-Cre	Resistant to DIO, glucose intolerance and leptin resistance	[32]
Atf4	AgRP-Cre^{ER}	Lean; improved insulin and leptin sensitivity; decreased hepatic lipid accumulation; decreased food intake and increased energy expenditure; resistant to DIO	[33]
Autophagy			
Atg7	POMC-Cre	Higher postweaning body weight; increased adiposity and glucose intolerance; sexual dimorphism	[34]
Atg7	POMC-Cre	Increased body weight with increased food intake and decreased energy expenditure; susceptible to hyperglycemia upon HFD; sexual dimorphism	[35]
Atg7	POMC-Cre	Increased adiposity; impaired lipolysis and glucose tolerance; male mice only	[36]
Atg7	AgRP-Cre	Decreased body weight and adiposity; less food intake upon fasting-refeeding; decreased AgRP and increased POMC expression; neuronal lipid accumulation	[24]
Atg5	POMC-Cre	Comparable body weight gain, adiposity or reduced energy expenditure to the littermates upon HFD; comparable leptin sensitivity and POMC expression to the littermates upon HFD	[37]
Atg12	POMC-Cre	Increased body weight gain, adiposity and reduced energy expenditure upon HFD; impaired leptin sensitivity and POMC expression upon HFD	[37]

ERAD			
Sel1l	AVP-Cre ER-Cre	Polyuria and polydipsia; Impaired maturation of AVP prohormone due to misfolding, aggregation and ER retention	[38]
Sel1l	POMC-Cre	Age-dependent obesity; hyperphagia; Impaired maturation of POMC prohormone due to misfolding, aggregation and ER retention	[25]

HFD: high fat diet; DIO: diet-induced obesity

Chapter 2 Revisiting Unfolded Protein Response in Diet-induced Obesity[2]

Hancheng Mao[1], Geun Hyang Kim[1,3], Ling Qi[2*]

[1]Department of Molecular & Integrative Physiology, University of Michigan Medical School, Ann Arbor, MI 48105, USA

[2] Department of Molecular Physiology and Biological Physics, University of Virginia, School of Medicine, Charlottesville, VA 22903, USA

[3] Present address: Regeneron Pharmaceuticals, Inc., 777 Old Saw Mill River Road, Tarrytown, New York 10591, USA

[*]Correspondence: xvr2hm@virginia.edu

The authors have declared that no conflict of interest exists.

Short title: Revisiting UPR in diet-induced obesity

Summary: This study re-investigates the UPR in both peripheral tissues and central nervous systems covering multiple time scales of HFD feeding, and provides evidence uncoupling UPR from diet-associated pathogenesis.

Keywords: diet-induced obesity, ER homeostasis, unfolded protein response (UPR), ER-associated degradation (ERAD), SEL1L-HRD1, leptin resistance

[2] This chapter is in preparation to be submitted for publication: Mao, H., Kim, GH. and Qi, L. (2024) “Revisiting unfolded protein response in diet-induced obesity” In preparation

2.1 Abstract

Endoplasmic reticulum (ER) stress in peripheral tissues and the central nervous system have been suggested as contributors to the development of diet-induced obesity. In particular, hypothalamic ER stress and inflammation has been proposed to causally link HFD to hypothalamic resistance. However, the molecular evidence for this hypothesis remains circumstantial. Here, we show that, PERK and IRE1α arms of the UPR respond differently to nutritional overload in a tissue specific manner. HFD feeding progressively induces bodyweight gain along with hypothalamic leptin resistance and liver steatosis and increased adiposity. However, HFD does not overtly activate ER stress or unfolded protein response (UPR) in all tissues despite the progression of the pathogenesis. Mechanistically, we show that ER stress/UPR activation does not necessarily impair leptin-pSTAT3 signaling mediated by leptin receptor long isoforms (LepRb). Instead, depending on distinct mechanisms, different ER stress inducers may or may not affect leptin signaling due to direct effects on the LepRb while UPR activation is more likely to be auxiliary phenotype.

2.2 Introduction

The prevalence of obesity and diabetes has dramatically increased in the past decade[1-4]. From a variety of studies to understand the mechanisms underlying the obesity and metabolic disorders, close relationships between ER homeostasis and disease pathogenesis have been widely investigated in both peripheral tissues and central nervous systems[5-10]. Considering the fat-enriched caloric dense diet as one major contributor to the increased risk of obesity and metabolic disorders, here, we revisit the UPR closely and comprehensively, testing the phosphorylation of the sensors and downstream effectors in both peripheral and central organs, at both initiation and processing stage of diet-associated pathogenesis. In contrary to the current belief, UPR is not significantly activated during both acute (1-week) and chronic (8-week) HFD feeding in hypothalamus and liver, with only evident induction in PERK-eIF2α in adipose tissues upon chronic HFD. Notably, an induction of SEL1L-HRD1 expression has been observed in both hypothalamus and liver but not in adipose tissue, indicating potential tissue-specific organismal regulation of ERAD machinery. However, the absence of UPR activation suggests such induction of the ERAD component may not necessarily be through the UPR.

Moreover, it has been proposed that ER stress/UPR activation due in the hypothalamus plays a causal role in leptin resistance in diet-induced obesity (DIO) and type-2 diabetes [11-17]. To date, several studies in genetic or diet-associated obesity models suggested that hypothalamic ER stress/UPR activation is a major contributor to obesity pathogenesis[16, 18-23]. However, the molecular evidence for a direct and causal link between UPR and diet-induced obesity remains incomplete, in part due to the over-

reliance on pharmacological ER stress inducers and chemical chaperones[16, 18, 21, 24-26], or inaccurate or incomplete assessment of ER stress *in vivo*. Notably, this study provides evidence suggesting UPR activation per se may not be a direct contributor to leptin resistance. Of note, the distinct working mechanisms of different ER stress inducers can better explain the correlation, instead of causation, between UPR activation and leptin resistance upon various stress induction.

2.3 Results

HFD induces pathogenesis in peripheral and CNS.

The mice gained body weight progressively during HFD feeding (Figure 2.1A) with progressive liver steatosis (Figure 2.1B) and adiposity (Figure 2.6A). Meanwhile, the mice exhibited glucose intolerance (Figure 2.1C) upon 8w-HFD with maintained insulin sensitivity (Figure 2.1D). Moreover, chronic HFD significantly increased the serum level of leptin (Figure 2.1E), suggesting hyperleptinemia and potential leptin resistance in mice. Then, to further delineate the leptin sensitivity in CNS upon HFD feeding, we performed fasting-leptin administration in the mice fed on normal chow diet or HFD for 1 week or 8 weeks. Immunohistochemical staining was performed to evaluate the response of hypothalamic neurons to the leptin, indicated by pSTAT3 signaling (Figure 2.1F). Leptin sensitivity in the arcuate nucleus (ARC) of the hypothalamus was slightly decreased by 1-week HFD and significantly impaired by 8-week HFD (Figure 2.1F). Thus, upon 8-week HFD feeding, mice developed significant bodyweight gain, glucose intolerance as well as hypothalamic leptin resistance.

No evident UPR activation upon acute or chronic HFD in liver.

We then wondered whether there could be ER stress in the liver with evident pathogenesis. The mRNA levels of UPR sensors Perk and Atf6 as well as downstream effectors including Chop, chaperones Bip, ERAD component Hrd1 and Erdj4 were decreased upon high fat diet feeding (Figure 2.7A). On the contrary, western blotting for protein abundance and phosphorylation indicated no significant alteration in PERK-eIF2α (Figure 2.2A) or IRE1α-xbp1s (Figure 2.2B and C) signaling arms of the UPR. Interestingly, upon acute HFD, the protein abundance of HRD1 significantly increased (Figure 2.2D and E) and meanwhile, there was also a trend of transient increased chaperones BiP and PDI protein levels (Figure 2.2D and E). The transient induction of hepatic HRD1 protein level is coincidentally consistent with the previous finding of acute induction of hypothalamic HRD1. Besides, no significant phosphorylation of Akt or JNK was observed in the liver upon HFD (Figure 2.2F and G).

PERK-eIF2α, but not IRE1α-Xbp1s was activated in adipose tissue upon HFD.

We evaluated the UPR and inflammation in adipose tissues upon HFD feeding. No evident alteration in mRNA levels of UPR sensors or downstream effectors including chaperones and ERAD components (Figure 2.8A). However, we observed a significant eIF2α phosphorylation upon chronic, but not acute HFD feeding (Figure 2.3A). This activated p-eIF2α can be partially attributed to the increased of PERK signaling cascades (Figure 2.3A). On the contrary, the IRE1α-xbp1s arm of the UPR is not significantly activated (Figure 2.3B and C). Intriguingly, acute HFD feeding significantly increased SEL1L protein abundance in gWAT (Figure 2.3D and E) and there was also a

trend of transient increased HRD1 levels (Figure 2.3D and E), indicating similarity to findings in liver (Figure 2.2D and E). Besides, AKT and JNK phosphorylation is not significantly altered upon chronic HFD feeding (Figure 2.3F and G).

UPR can be uncoupled from HFD-induced hypothalamic leptin resistance.

We next asked whether HFD feeding triggers UPR activation in the hypothalamic region with observed leptin resistance. Much to our surprise, we failed to detect any signs of UPR, including phosphorylation of UPR sensors IRE1α and PERK, as well as the downstream effector XBP1 mRNA splicing and phosphorylation of eIF2α (Figure 2.4A-C). Moreover, the 8-week HFD feeding significantly elevated mRNA (Figure 2.9A), but not protein levels (Figure 2.4D and E) of key ER chaperon BiP in the ARC. Quantitative PCR analysis suggests no significant effects of HFD on the transcriptional levels of UPR sensors (Figure 2.9A). Thus, we concluded that HFD feeding, acute or chronic, does not trigger overt UPR in the hypothalamus. Further, there's an increase of astrocytes observed at DMH regions of the hypothalamus upon 1w-, but not 8w-HFD, suggesting a mild hypothalamic astrogliosis upon chronic HFD feeding.

The ER stress inducers may affect leptin signaling differently despite of UPR activation.

Our data suggested ER stress and UPR activation were absent in both 1w- and 8w-HFD in hypothalamus where leptin resistance was clearly established, suggesting UPR can be uncoupled from HFD-associated central leptin resistance. We then tested whether ER stress can necessarily impair the leptin signaling. We used both

thapsigargin and tunicamycin to induce ER stress in 293T cells with LepRb expression. Both ER stress inducers effectively triggered the UPR activation including PERK phosphorylation as well as IRE1α phosphorylation (Figure 2.5A and C). Notably, Tg treatment, didn't alter leptin-induced pSTAT3 signaling while TM treatment can significantly inhibit leptin-induced pSTAT3 in a dose dependent manner. This is likely due to the intrinsic difference in their working mechanisms, where Tg disturbs calcium balance inside of ER with maintained and even induced abundance of glycosylated full-length LepRb (Figure 2.5B and Figure 2.10A), while Tm disrupts all N-linked glycosylation, as indicated by significant reduction of the fully glycosylated mature LepRb with increased smaller size LepRb bands likely due to defective glycosylation (Figure 2.5C and Figure 2.10A).

2.4 Discussion

Previous studies have proposed that hypothalamic ER stress, UPR activation, links HFD feeding to leptin resistance and concomitant pathogenesis. However, a distinguish between causation and correlation is difficult, the administration of various UPR inducers/inhibitors may not be representative of physiological situations, and the conclusions are controversial between different studies[19, 20]. More importantly, previous studies lacked a comprehensive analysis of the complex machineries maintaining ER homeostasis. Thus, our study revisits carefully the UPR in DIO and provides extensive evidence suggesting that hypothalamic UPR can be uncoupled from HFD induced leptin resistance.

Interestingly, we found transient induction of SEL1L-HRD1 protein levels upon 1w-HFD in various tissues. Due to absence of UPR activation, such increase of protein abundance may be uncoupled from UPR known as canonical cascade for ERAD components upregulation. It is reported that androgen could upregulate HRD1 in an IRE1α independent manner[27]. However, much further investigation is needed to elucidate any potential non-canonical signaling pathways that mediate SEL1L-HRD1 expression in both CNS and peripheral tissues upon HFD.

Another intriguing observance is that the acute upregulation of SEL1L-HRD1 in liver and gWAT, along with hypothalamus[28], somehow showed up simultaneously. It has been reported that proteostasis and its regulators, including UPR and autophagy, in CNS may regulate proteostasis in peripheral tissues accordingly in a cell non-autonomous manner[18, 29-35]. Therefore, the outstanding question is whether SEL1L-HRD1 may also possess this feature, which if addressed, may provide groundbreaking insights of the field.

With a more comprehensive analysis, revisiting hypothalamic UPR during DIO provides strong evidence suggesting that UPR can be absent, and thus not required for HFD-induced pathogenesis including leptin resistance. Further, we have provided evidence that the presence of UPR activation doesn't necessarily lead to leptin resistance. Instead, different ER stressors may or may not impair leptin signaling depending on their working mechanisms[36-42] and distinct effects on LepRb maturation regardless of induction of ER stress/UPR. Our study, therefore, calls for caution when interpreting UPR as primary causal link to metabolic diseases where it is likely to be secondary effects of adaptation or maladaptation of the organisms under various patho-

phosiological conditions. The risk of attributing pathogenesis to UPR is that such generalization may lose the comprehensive insights towards intricate regulation of ER homeostasis and proteostasis. Moreover, this study questions the value of targeting ER stress as a therapeutic approach, e.g., the use of chemical chaperones to reduce ER stress [43], for the treatment of diet-induced obesity and type-2 diabetes.

2.5 Methods

Mice. WT B6 mice were purchased from JAX and bred in our mouse facility. Mice were fed a chow diet (13% fat, 57% carbohydrate and 30% protein, PicoLab Rodent Diet 5L0D) and placed on a high-fat diet (HFD, calories provided by 60% fat, 20% carbohydrate and 20% protein, Research Diet D12492) from 5 or 12 weeks of age for 8 weeks or 1 week. All mice were housed in a temperature-controlled room with a 12-hour light/12-hour dark cycle.

Glucose (GTT) and insulin tolerance test (ITT). As described [44], male mice were fasted for 16 or 6 hours for GTT and ITT respectively, followed by i.p. injection with glucose (2 g/kg body weight) or insulin (1 unit/kg body weight). At indicated time points, blood glucose was monitored using AimStrip ™ Plus Blood Glucose Testing System.

Leptin ELISA. Mouse serum samples were stored at -80°C. The samples were defrosted on ice and used for leptin measurement by Mouse/Rat Leptin Quantikine ELISA Kit (R&D Systems; catalog MOB00B).

Leptin treatment in mice. For phosphorylated STAT3 staining, leptin (2 mg/kg body weight, R&D systems; catalog 498-OB-05M) were intraperitoneally (i.p.) injected to thirteen-week-old mice, followed by overnight fasting. PBS was used as control. Mice were anesthetized by isoflurane for fixation-perfusion 30 min after injection.

Tissue and blood collection. These procedures were carried out as previously described[44]. Briefly, blood was collected from anesthetized mice via cardiac puncture, transferred to 1.5ml microcentrifuge tubes, kept at room temperature for 30 minutes prior to centrifugation at 2,000 *g* for 15 minutes. Serum was aliquoted and stored at -80°C until analysis. For brain microdissection, Adult Mouse Brain Slicer Matrix (BSMAA001-1, Zivic Instruments) was used to collect coronal brain slices containing ARC region with further microdissection to obtain ARC-enriched region. All tissues were snap-frozen in liquid nitrogen and stored at -80°C before use.

Preparation of brain sections. Mice were anesthetized with isoflurane, perfused with PBS followed by 4% paraformaldehyde (PFA) (Electron Microscopy Sciences; catalog 19210) for fixation. Brains were then postfixed in 4% PFA for overnight at 4°C, dehydrated in 15% sucrose and then 30% sucrose consecutively overnights at 4°C, and sectioned (30 μm) on a cryostat (Microm HM550 Cryostat, Thermo Fisher Scientific). The sections were stored in DEPC-containing anti-freezing media (50% 0.05 M sodium phosphate pH 7.3, 30% ethylene glycol, 20% glycerol) at −20°C. Different brain regions were identified using the Paxinos and Franklin atlas. Counted as distance from bregma,

the following coordinates were used: PVN (–0.82 mm to –0.94 mm) and ARC (–1.58 mm to –1.7 mm).

Western blot and antibodies. Frozen tissue or cells were homogenized by sonication in lysis buffer [150mM NaCl, 50mM Tris pH 7.5, 10 mM EDTA, 1% Triton X-100] with freshly added protease inhibitors (Sigma; catalog P8340), phosphatase inhibitors (Sigma; catalog P5726) and 10 mM N-ethylmaleimide (Thermo Scientific; catalog 23030). Lysates were incubated on ice for 30 min followed by centrifugation (13,000 g, 10 min at 4 °C). Supernatants were collected and analyzed for protein concentration using Bradford assay (Bio-Rad; catalog 5000006). For denaturing SDS-PAGE, samples were further suppled with 1mM DTT and denatured at 95°C for 5 min in 5x SDS sample buffer (250 mM Tris-HCl pH 6.8, 10% sodium dodecyl sulfate, 0.05% Bromophenol blue, 50% glycerol, and 1.44 M β-mercaptoethanol). For phostag gel analysis based on phos-tag system as described[45, 46], SDS-PAGE gel was supplemented by 50μM MnCl2 (Sigma) and 25μM phostag reagent (NARD Institute; catalog AAL-107) and must be protected from light until finishing running. Protein isolated from the liver of mice treated with tunicamycin (TM, 1 mg/kg, i.p.) for 24 hours was used as a positive control to indicate the position of phosphorylated PERK and IRE1a.

All samples were incubated in 65°C for 10min and run with 15-30 μg total lysate on SDS-PAGE gel for separation followed by electrophoretic transfer to PVDF membrane (0.45μm, Millipore; catalog IPFL00010). The blots were incubated in 2% BSA/Tri-buffered saline tween-20 (TBST) with primary antibodies overnight at 4°C, washed with TBST followed by 1hr incubation with goat anti-rabbit or mouse IgG HRP at room

temperature. Band density was quantitated using the Image Lab software on the ChemiDOC XRS+ system (Bio-Rad).

Antibodies for Western blot were as follows: SEL1L (rabbit, 1:8000, Abclonal; catalog E112049), HRD1 (rabbit, 1:2000, ABclonal; catalog E15102), GRP78 BiP (rabbit, 1:5000, Abcam; catalog ab21685), HSP90 (rabbit, 1:5,000, Santa Cruz Biotechnology Inc.; catalog sc-7947), FLAG (mouse, 1:2000, Sigma-Aldrich; catalog F-1804), IRE1α (rabbit, 1:2,000, Cell Signaling Technology; catalog 3294), p-eIF2α (rabbit, 1:2000, Cell Signaling Technology; catalog 3597), eIF2α (rabbit, 1:2000, Cell Signaling Technology; catalog 9722), p-JNK (mouse, 1:2000, Cell Signaling Technology; catalog 9255), JNK (rabbit, 1:1000, Cell Signaling Technology; catalog 9252), PERK (Rabbit, 1:1000, Cell Signaling Technology; catalog 3192), pSTAT3 (Tyr705) (rabbit, 1:1000, catalog 9131, Cell Signaling Technology), STAT3 (rabbit, 1:1000, Cell Signaling Technology; catalog 9132), pJAK2 (Tyr1007/1008) (rabbit, 1:1000, Cell Signaling Technology; catalog 3771), JAK2 (rabbit, 1:1000, ABclonal; catalog A19629), Tubulin (mouse, 1:5000, Santa Cruz Biotechnology Inc.; catalog sc-5286).

Secondary antibodies for Western blot were goat anti-rabbit IgG HRP and goat anti-mouse IgG HRP at 1:5,000, both from Bio-Rad.

Immunostaining and antibodies. For fluorescent immunostaining in free-floating brain sections, samples were picked out of anti-freezing buffer followed by 3 washes with PBS. Free-floating sections were simultaneously incubated with primary antibodies in blocking buffer (0.3% donkey serum and 0.25% Triton X-100 in 0.1 M PBS) overnight at 4°C. Following 3 washes with PBS, sections were incubated with secondary antibodies

for 2 hours at room temperature. Brain sections were then mounted on gelatin-coated slides (Southern Biotech; catalog SLD01-CS). Counterstaining and mounting were performed with mounting medium containing DAPI (Vector Laboratories; catalog H-1200) and Fisherfinest Premium Cover Glasses (Fisher Scientific; catalog 12-548-5P). To quantify immunoreactivity, identical acquisition settings were used for imaging each brain section from all groups within an experiment. The numbers of immunoreactivity-positive soma analysis and intensity of immunoreaction were quantified in 3D stack volumes after uniform background subtraction using the NIS Elements AR software (Nikon) and FIJI (National Institute of Health, USA).

Antibodies for immunostaining were as follows: GRP78 BiP (rabbit, 1:500, Abcam; catalog ab21685), p-Y705 STAT3 (rabbit, 1:200, Cell Signaling Technology; catalog 9145), GFAP (rabbit, 1:500, Agilent; Z033429-2).

Secondary antibodies for fluorescent immunostaining (all 1:500) were as follows: Anti-rabbit IgG Alexa Fluor 647; anti-goat IgG Alexa Fluor 488 & 647; anti-sheep IgG Cy5 were from Jackson ImmunoResearch. Donkey anti-mouse IgG Alexa flour 555 was from Invitrogen (catalog A32773) and goat anti-chicken IgY FITC was from Aves Labs (catalog F-1005).

Plasmids. Mouse LepRb cDNA was provided by Dr. Martin Myer at University of Michigan Medical School. The *LepRb* coding region was amplified by PCR using a primer set containing HindIII and XbaI restriction site at 5' and 3' respectively.

F: 5′- CCG AAGCTT ATGATGTGTCAGAAATTCTATGTGGTT-3′

R: 5′- TGC TCTAGA CACAGTTAAGTCACACATCTTATT-3′

Both PCR products and the backbone vector p3xFLAG-CMV14 were digested using HindIII and XbaI restriction enzymes in the double digestion system from New England BioLabs. For construction of LepRb point mutants, quick change mutagenesis was performed using PFU DNA polymerase (600140, Agilent). The following primers were used for mutagenesis to construct LepRb-C602S:

F: 5'- CCTGCTGGTGTCAGACCTCAGTGCAGTCTATG-3'

R: 5'- CATAGACTGCACTGAGGTCTGACACCAGCAGG-3'

RNA isolation, RT-PCR and qRCR. Microdissected brain tissues were homogenized in Trizol reagent (Invitrogen; catalog 15596-018). The RNA was further extracted using BCP phase separation reagent (Molecular Research Center; catalog TR 118) and isopropanol precipitation. cDNA was synthesized with SuperScript™ III Reverse Transcriptase (Invitrogen; catalog 18080044). mRNA extraction and cDNA synthesis from liver and ARC of mice treated with tunicamycin (TM, 1 mg/kg, i.p.) for 24 hours were used as positive controls to indicate the position of spliced *Xbp1*.

The ratio of *Xbp1s* to total *Xbp1* (*Xbp1u* + *Xbp1s*) levels was quantified by Image Lab (Bio-Rad) software. For RT-PCR analysis the following primer sequences were used:

mXbp1-F: 5'-ACGAGGTTCCAGAGGTGGAG-3'

R: 5'-AAGAGGCAACAGTGTCAGAG-3'

mL32- F: 5'-GAGCAACAAGAAAACCAAGCA-3'R:

5'-TGCACACAAGCCATCTACTCA-3'

Gene expression was analyzed using ABI (QuantStudio 5). Primers were used for this study:

mHrd1-F: 5’- CTGGGTATCCTGGACTTCCT -3’

R: 5’- ATTCTGATGACCATGGTGCT -3’

mSel1L-F: 5’- AGCCCAGATGCACAAGTACC -3’

R: 5’- ACACAGAATATCCAGGCAGC -3’

mPerk-F: 5’- TCAAGTTTCCTCTACTGTTCACTCA -3’

R: 5’- CCATGAGTTCATCTGGAACAAA -3’

mIRE1α-F: 5’- ATCTGCGCAAATTCAGAACC -3’

R: 5’- ACACCTACCAAGCCATGGAG -3’

mAtf6-F: 5’- ATTCTCAGCTGATGGCTGTC -3’

R: 5’- TTACCAAGGCTTCTTTGACG -3’

mChop-F: 5’- TTACCAAGGCTTCTTTGACG -3’

R: 5’- AAACAGAGTGGTCAGTGCCC -3’

mBip- F: 5’- TGTGGTACCCACCAAGAAGTC -3’

R: 5’- ATTCTCCGAGTGACAGCTGAA -3’

mErdj4-F: 5’- CTTAGGTGTGCCAAAGTCTGC -3’

R: 5’- TATGAAACACTCTCGGATGCC -3’

mEro1l-F: 5’- CGGACCAAGTTATGAGTTCCA -3’

R: 5’- TGAAGGGCAGAATCTCTCTGA -3’

H&E staining. Peripheral tissues were collected from mice and fixed in 10% formalin for overnight at 4 °C, washed with PBS and stored in 70% ethanol at 4 °C until dehydration for paraffin-embedding. Sectioning and H&E staining were performed on a fee-for- service basis by the Michigan Histology Core Facilities.

Cell lines and transfection. HEK293T cells (ATCC) were cultured in DMEM (Corning; catalog 10-013-CV) with 1% Penicillin-Streptomycin (Gibco; catalog 15140122) and heat inactivated 10% FBS (ThermoFisher; catalog FB12999102), respectively. Cells were transfected within 24 hours at 60-80% confluency after plating using polyethylenimine (PEI). Cells were treated and harvested within 48 hours after transfection.

Thapsigargin, tunicamycin and leptin treatment in vitro. HEK293T cells transfected with LepRb-3xFLAG were serum depraved for 6hrs followed by leptin (100nM, R&D systems; catalog 498-OB-05M) treatment for 30min and harvested by snap-frozen in liquid nitrogen. For thapsigargin treatment, indicated dose of thapsigargin (Millipore; catalog T9033-1MG) will be added into cells after 2h-serum deprivation followed by leptin treatment after another 4 hours. For tunicamycin treatment, indicated dose of tunicamycin will be added into cells after 2h-serum deprivation followed by leptin treatment after another 4 hours.

Statistics. Results are expressed as the mean ± SEM unless otherwise stated. Statistical analyses were performed in GraphPad Prism version 8.0 (GraphPad Software Inc.). Comparisons between the groups were made by unpaired two-tailed Student's t test for two groups, or one-way ANOVA or two-way ANOVA followed by multiple comparisons test for more than two groups. P value < 0.05 was considered as

statistically significant. All experiments were repeated at least twice and/or performed with several independent biological samples, and representative data are shown.

Study Approval. All experiments performed with mice were in compliance with University of Michigan (Ann Arbor, MI) Institutional Animal Care and Use Committee (#PRO00006888) guidelines.

Data and material availability. The materials and reagents used are either commercially available or available upon the request, with detailed information included in Methods.

Author Contribution

H.M. designed the most of experiments and H.M., with the help of G.H.K., performed most of the experiments and data analysis. H.M., with the help of G.H.K., wrote the methods and figure legends. L.Q. and H.M. wrote the manuscript. All authors have approved the manuscript.

Acknowledgement

We thank Drs. Peter Arvan, Carol Elias and Daniel Klionsky for critical comments and suggestions, and members of the Qi and Arvan laboratories for comments and technical assistance. This work was supported by NIH grants 1R01DK11174 (to P.A. and L.Q.), 1R01DK105393, 1R01DK120047, and American Diabetes Association (ADA) 1-19-IBS-235 (to L.Q.).

2.6 References

1. Ampofo, A.G. and E.B. Boateng, *Beyond 2020: Modelling obesity and diabetes prevalence.* Diabetes Res Clin Pract, 2020. 167: p. 108362.
2. Han, C., et al., *Global prevalence of prediabetes in children and adolescents: A systematic review and meta-analysis.* J Diabetes, 2022. 14(7): p. 434-441.
3. Malik, V.S., W.C. Willet, and F.B. Hu, *Nearly a decade on - trends, risk factors and policy implications in global obesity.* Nat Rev Endocrinol, 2020. 16(11): p. 615-616.
4. Rooney, M.R., et al., *Global Prevalence of Prediabetes.* Diabetes Care, 2023. 46(7): p. 1388-1394.
5. Ozcan, U., et al., *Endoplasmic reticulum stress links obesity, insulin action, and type 2 diabetes.* Science, 2004. 306(5695): p. 457-61.
6. Cnop, M., F. Foufelle, and L.A. Velloso, *Endoplasmic reticulum stress, obesity and diabetes.* Trends Mol Med, 2012. 18(1): p. 59-68.
7. Lee, J. and U. Ozcan, *Unfolded protein response signaling and metabolic diseases.* J Biol Chem, 2014. 289(3): p. 1203-11.
8. Pagliassotti, M.J., et al., *Endoplasmic reticulum stress in obesity and obesity-related disorders: An expanded view.* Metabolism, 2016. 65(9): p. 1238-46.
9. Ajoolabady, A., et al., *ER stress and inflammation crosstalk in obesity.* Med Res Rev, 2023. 43(1): p. 5-30.
10. Ajoolabady, A., et al., *ER stress in obesity pathogenesis and management.* Trends Pharmacol Sci, 2022. 43(2): p. 97-109.
11. Ozcan, L., et al., *Endoplasmic reticulum stress plays a central role in development of leptin resistance.* Cell Metab., 2009. 9(1): p. 35-51.
12. Schneeberger, M., et al., *Mitofusin 2 in POMC neurons connects ER stress with leptin resistance and energy imbalance.* Cell, 2013. 155(1): p. 172-87.
13. Ye, Z., et al., *Hypothalamic endoplasmic reticulum stress as a key mediator of obesity-induced leptin resistance.* Obes Rev, 2018. 19(6): p. 770-785.
14. Sun, S., et al., *Mechanisms of inflammatory responses in obese adipose tissue.* Annu Rev Nutr, 2012. 32: p. 261-86.
15. Ramirez, S. and M. Claret, *Hypothalamic ER stress: A bridge between leptin resistance and obesity.* FEBS Lett, 2015. 589(14): p. 1678-87.
16. Zhang, X., et al., *Hypothalamic IKKbeta/NF-kappaB and ER stress link overnutrition to energy imbalance and obesity.* Cell, 2008. 135(1): p. 61-73.
17. Purkayastha, S., et al., *Neural dysregulation of peripheral insulin action and blood pressure by brain endoplasmic reticulum stress.* Proc Natl Acad Sci U S A, 2011. 108(7): p. 2939-44.
18. Williams, K.W., et al., *Xbp1s in Pomc neurons connects ER stress with energy balance and glucose homeostasis.* Cell Metab, 2014. 20(3): p. 471-82.
19. Yao, T., et al., *Ire1alpha in Pomc Neurons Is Required for Thermogenesis and Glycemia.* Diabetes, 2017. 66(3): p. 663-673.
20. Xiao, Y., et al., *Knockout of inositol-requiring enzyme 1alpha in pro-opiomelanocortin neurons decreases fat mass via increasing energy expenditure.* Open Biol, 2016. 6(8).
21. Ozcan, L., et al., *Endoplasmic reticulum stress plays a central role in development of leptin resistance.* Cell Metab, 2009. 9(1): p. 35-51.

22. He, Z., et al., *PERK in POMC neurons connects celastrol with metabolism.* JCI Insight, 2021. 6(18).
23. Deng, J., et al., *Deletion of ATF4 in AgRP Neurons Promotes Fat Loss Mainly via Increasing Energy Expenditure.* Diabetes, 2017. 66(3): p. 640-650.
24. Hosoi, T., et al., *Endoplasmic reticulum stress induces leptin resistance.* Mol Pharmacol, 2008. 74(6): p. 1610-9.
25. Won, J.C., et al., *Central administration of an endoplasmic reticulum stress inducer inhibits the anorexigenic effects of leptin and insulin.* Obesity (Silver Spring), 2009. 17(10): p. 1861-5.
26. Bull, V.H. and B. Thiede, *Proteome analysis of tunicamycin-induced ER stress.* Electrophoresis, 2012. 33(12): p. 1814-23.
27. Erzurumlu, Y. and P. Ballar, *Androgen Mediated Regulation of Endoplasmic Reticulum-Associated Degradation and its Effects on Prostate Cancer.* Sci Rep, 2017. 7: p. 40719.
28. Mao, H., G.H. Kim, and L. Qi, *SEL1L-HRD1 ER-associated degradation regulates leptin receptor maturation and signaling in POMC neurons in diet-induced obesity.* Res Sq, 2024.
29. Zhang, Q., et al., *Central activating transcription factor 4 (ATF4) regulates hepatic insulin resistance in mice via S6K1 signaling and the vagus nerve.* Diabetes, 2013. 62(7): p. 2230-9.
30. Imanikia, S., et al., *XBP-1 Remodels Lipid Metabolism to Extend Longevity.* Cell Rep, 2019. 28(3): p. 581-589 e4.
31. Brandt, C., et al., *Food Perception Primes Hepatic ER Homeostasis via Melanocortin-Dependent Control of mTOR Activation.* Cell, 2018. 175(5): p. 1321-1335 e20.
32. Qian, Q., et al., *Obesity Disrupts Pituitary UPR Leading to NAFLD.* bioRxiv, 2022: p. 2022.07. 06.498610.
33. Minnerly, J., et al., *The cell non-autonomous function of ATG-18 is essential for neuroendocrine regulation of Caenorhabditis elegans lifespan.* PLoS Genet, 2017. 13(5): p. e1006764.
34. Martinez-Lopez, N., et al., *Autophagy in the CNS and Periphery Coordinate Lipophagy and Lipolysis in the Brown Adipose Tissue and Liver.* Cell Metab, 2016. 23(1): p. 113-27.
35. Chen, W., et al., *Nutrient-sensing AgRP neurons relay control of liver autophagy during energy deprivation.* Cell Metab, 2023. 35(5): p. 786-806 e13.
36. Kuo, S.C. and J.O. Lampen, *Tunicamycin--an inhibitor of yeast glycoprotein synthesis.* Biochem Biophys Res Commun, 1974. 58(1): p. 287-95.
37. Takatsuki, A., K. Arima, and G. Tamura, *Tunicamycin, a new antibiotic. I. Isolation and characterization of tunicamycin.* J Antibiot (Tokyo), 1971. 24(4): p. 215-23.
38. Yoo, J., et al., *GlcNAc-1-P-transferase-tunicamycin complex structure reveals basis for inhibition of N-glycosylation.* Nat Struct Mol Biol, 2018. 25(3): p. 217-224.
39. Heifetz, A., R.W. Keenan, and A.D. Elbein, *Mechanism of action of tunicamycin on the UDP-GlcNAc:dolichyl-phosphate Glc-NAc-1-phosphate transferase.* Biochemistry, 1979. 18(11): p. 2186-92.

40. Thastrup, O., et al., *Thapsigargin, a tumor promoter, discharges intracellular Ca2+ stores by specific inhibition of the endoplasmic reticulum Ca2(+)-ATPase.* Proc Natl Acad Sci U S A, 1990. 87(7): p. 2466-70.
41. Lytton, J., M. Westlin, and M.R. Hanley, *Thapsigargin inhibits the sarcoplasmic or endoplasmic reticulum Ca-ATPase family of calcium pumps.* J Biol Chem, 1991. 266(26): p. 17067-71.
42. Treiman, M., C. Caspersen, and S.B. Christensen, *A tool coming of age: thapsigargin as an inhibitor of sarco-endoplasmic reticulum Ca(2+)-ATPases.* Trends Pharmacol Sci, 1998. 19(4): p. 131-5.
43. Noack, J., G. Brambilla Pisoni, and M. Molinari, *Proteostasis: bad news and good news from the endoplasmic reticulum.* Swiss Med Wkly, 2014. 144: p. w14001.
44. Kim, G.H., et al., *Hypothalamic ER-associated degradation regulates POMC maturation, feeding, and age-associated obesity.* J Clin Invest, 2018. 128(3): p. 1125-1140.
45. Qi, L., L. Yang, and H. Chen, *Detecting and quantitating physiological endoplasmic reticulum stress.* Methods Enzymol, 2011. 490: p. 137-46.
46. Yang, L., et al., *A Phos-tag-based approach reveals the extent of physiological endoplasmic reticulum stress.* PLoS One, 2010. 5(7): p. e11621.

2.7 Figures and figure legends

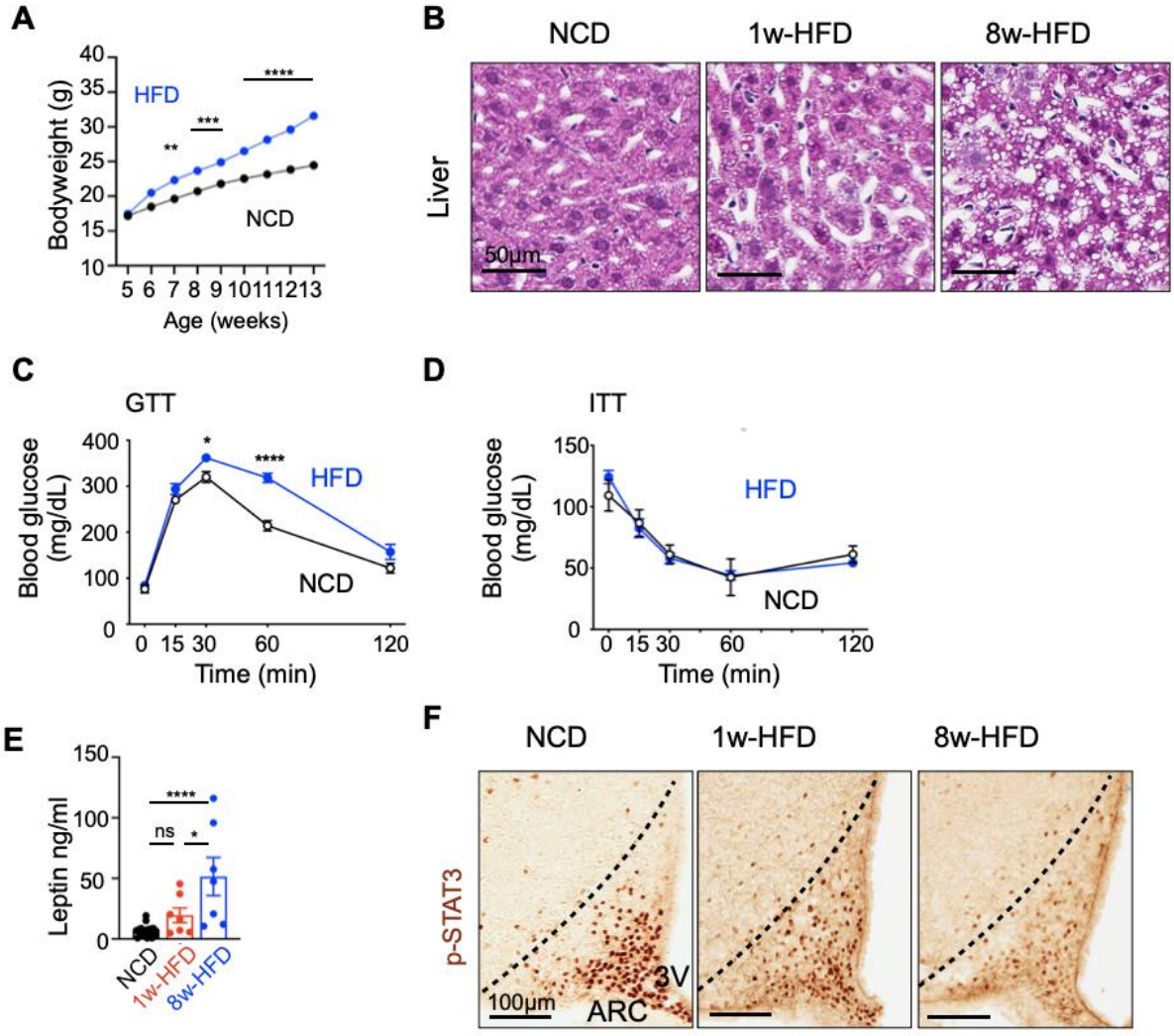

Figure 2.1 High fat diet-associated pathogenesis in peripheral tissues.
(A) Growth curve of C57BL/6J male mice on normal chow diet (NCD) or 60% fat diet (HFD) (n>20 in each group).
(B) Representative images of H&E staining in the liver of the male mice fed on NCD and 8w-HFD.
(C) GTT in male mice fed NCD or HFD for 8 weeks. Mice were fasted for 16 hours prior to glucose (2 g/kg body weight). (n=7 for NCD group, n=8 for HFD group)
(D) ITT in male mice fed NCD or HFD for 8 weeks. Mice were fasted for 16 hours prior to glucose (2 g/kg body weight). (n=7 for NCD group, n=8 for HFD group)
(E) Serum leptin levels at mice fed on NCD, 1w- and 8w-HFD (n=6-13 mice per group)
(F) Representative immunohistochemical (IHC) staining of pSTAT3 in C57BL/6J male mice at NCD, 1w- and 8w-HFD. Mice were fasted for overnight (16hrs) and administrated with leptin (i.p., 2 mg/kg body weight) followed by perfusion 30 minutes after injection (n=2 mice per group)

NCD for normal chow diet; 1w-HFD for 1-week; 8w-HFD for 8-week; ARC, arcuate nucleus; 3V, third ventricle. Values, mean ± SEM. n.s., not significant; *p<0.05, **p<0.01, ***p<0.001 and ****p<0.0001 by two-way ANOVA followed by Tukey's multiple comparison tests (A, C, D) or one-way ANOVA followed by Tukey's multiple comparison tests (E)

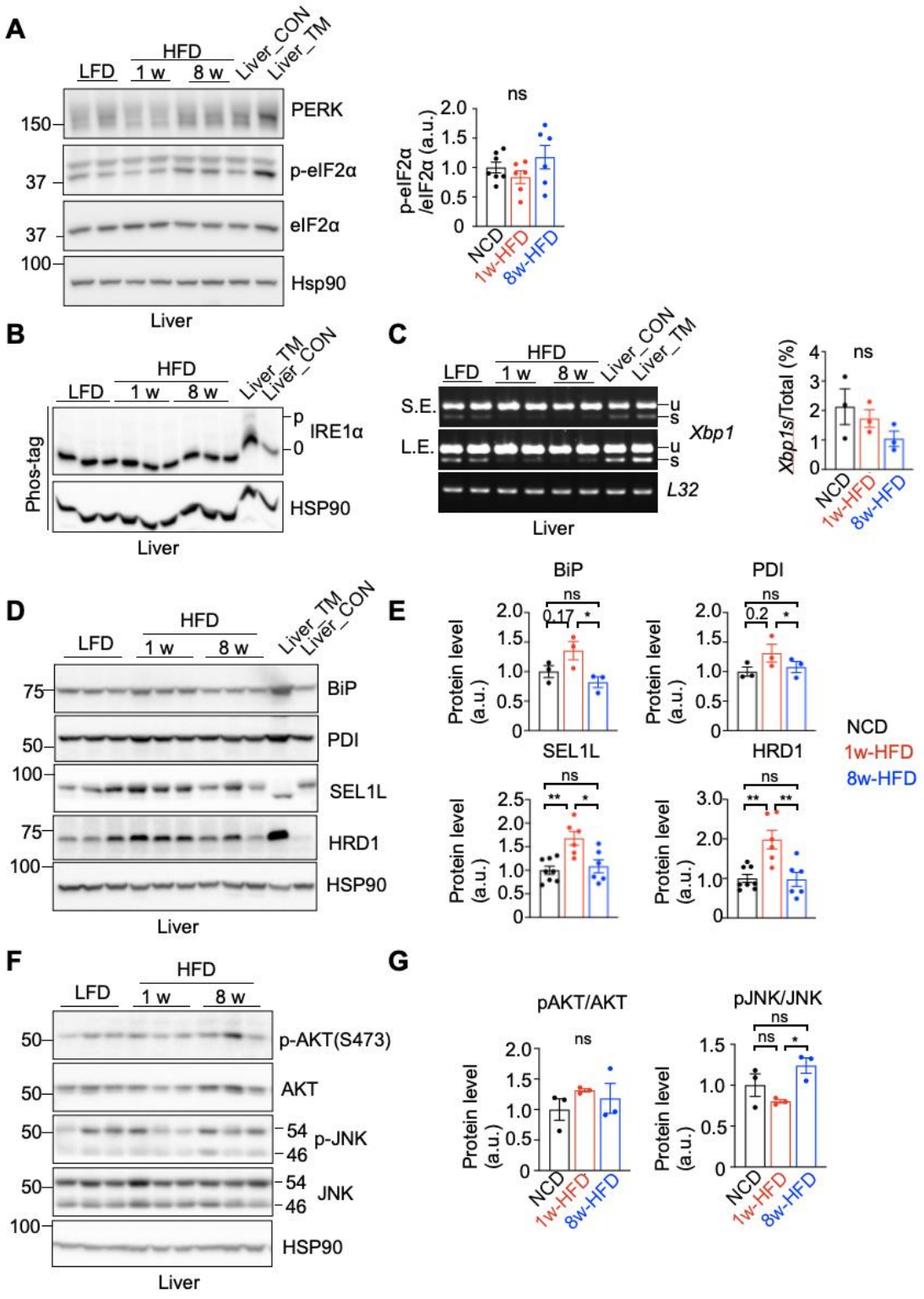

Figure 2.2 UPR can be uncoupled from hepatic pathogenesis upon HFD.
(A) Representative images and quantitation of western blot for PERK-eIF2α analysis in the liver of the male mice fed on NCD, 1w- and 8w-HFD. (n=6-7 mice each group)

(B) Representative images of phostag-gel (P-T) for IRE1α phosphorylation analysis in the liver of the male mice fed on NCD, 1w- and 8w-HFD. Protein isolated from the liver of mice treated with tunicamycin (1 mg/kg, i.p.) for 24 hours was used as a positive control to indicate the position of phosphorylated IRE1a shipped up on the phostag-gel. HSP 90 is used as a protein loading control.
(C) Representative images and quantification of reverse transcriptase PCR (RT-PCR) analysis of *Xbp1* mRNA splicing (u, unspliced; s, spliced) in liver. *L32* is used as a house keeping gene control.
(D-E) Representative images (D) and quantitation (E) of western blot for chaperones (BiP and PDI) and ERAD (SEL1L and HRD1) analysis in the liver of the male mice fed on NCD, 1w- and 8w-HFD. (n=3-5 each group)
(F-G) Representative images (F) and quantitation (G) of western blot for phosphorylation of Akt and JNK analysis in the liver of the male mice fed on NCD, 1w- and 8w-HFD. (n=3 each group)
NCD for normal chow diet; 1w-HFD for 1-week; 8w-HFD for 8-week. Values, mean ± SEM. n.s., not significant; *p<0.05, **p<0.01, ***p<0.001 and ****p<0.0001 by one-way ANOVA followed by Tukey's multiple comparison tests (A, C, E, G)

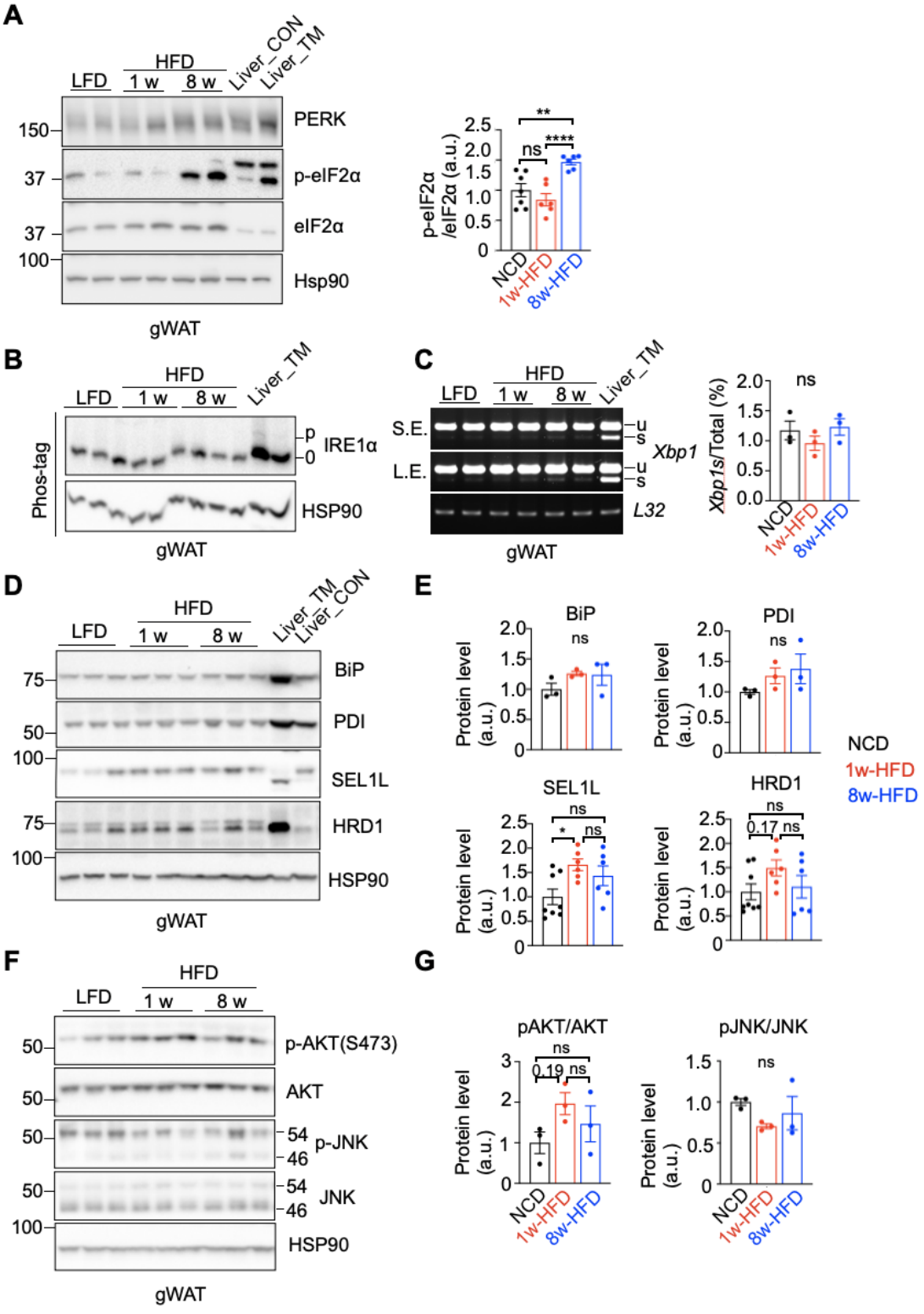
A
LFD
HFD
1 w
8 w
Liver_CON
Liver_TM
150
37
37
100
PERK
p-eIF2α
eIF2α
Hsp90
gWAT
p-eIF2α /eIF2α (a.u.)
2.5
2.0
1.5
1.0
0.5
0
**
ns
****
NCD
1w-HFD
8w-HFD
B
Phos-tag
p
0
IRE1α
HSP90
gWAT
C
S.E.
L.E.
u
s
Xbp1
L32
gWAT
Xbp1s/Total (%)
2.0
1.5
1.0
0.5
0.0
ns
D
75
50
100
75
100
BiP
PDI
SEL1L
HRD1
HSP90
gWAT
E
BiP
PDI
SEL1L
HRD1
Protein level (a.u.)
ns
*
0.17
NCD
1w-HFD
8w-HFD
F
50
50
50
50
100
p-AKT(S473)
AKT
54
46
p-JNK
54
46
JNK
HSP90
gWAT
G
pAKT/AKT
pJNK/JNK
Protein level (a.u.)
0.19
ns
NCD
1w-HFD
8w-HFD

Figure 2.3 Upregulated PERK-eIF2α, but not IRE1α-Xbp1s are detected in adipose tissue upon HFD feeding.
(A) Representative images and quantitation of western blot for PERK-eIF2α analysis in the gWAT of the male mice fed on NCD, 1w- and 8w-HFD. (n=6-7 mice each group)
(B) Representative images of phostag-gel (P-T) for IRE1α phosphorylation analysis in the gWAT of the male mice fed on NCD, 1w- and 8w-HFD. Protein isolated from the liver of mice treated with tunicamycin (1 mg/kg, i.p.) for 24 hours was used as a positive control to indicate the position of phosphorylated IRE1a shipped up on the phostag-gel. HSP 90 is used as a protein loading control.
(C) Representative images and quantification of reverse transcriptase PCR (RT-PCR) analysis of *Xbp1* mRNA splicing (u, unspliced; s, spliced) in gWAT. *L32* is used as a house keeping gene control.
(D-E) Representative images (D) and quantitation (E) of western blot for chaperones (BiP and PDI) and ERAD (SEL1L and HRD1) analysis in the gWAT of the male mice fed on NCD, 1w- and 8w-HFD. (n=3-5 each group)
(F-G) Representative images (F) and quantitation (G) of western blot for phosphorylation of Akt and JNK analysis in the gWAT of the male mice fed on NCD, 1w- and 8w-HFD. (n=3 each group)
NCD for normal chow diet; 1w-HFD for 1-week; 8w-HFD for 8-week; gWAT, gonadal white adipose tissue.Values, mean ± SEM. n.s., not significant; *p<0.05, **p<0.01, ***p<0.001 and ****p<0.0001 by one-way ANOVA followed by Tukey's multiple comparison tests (A, C, E, G)

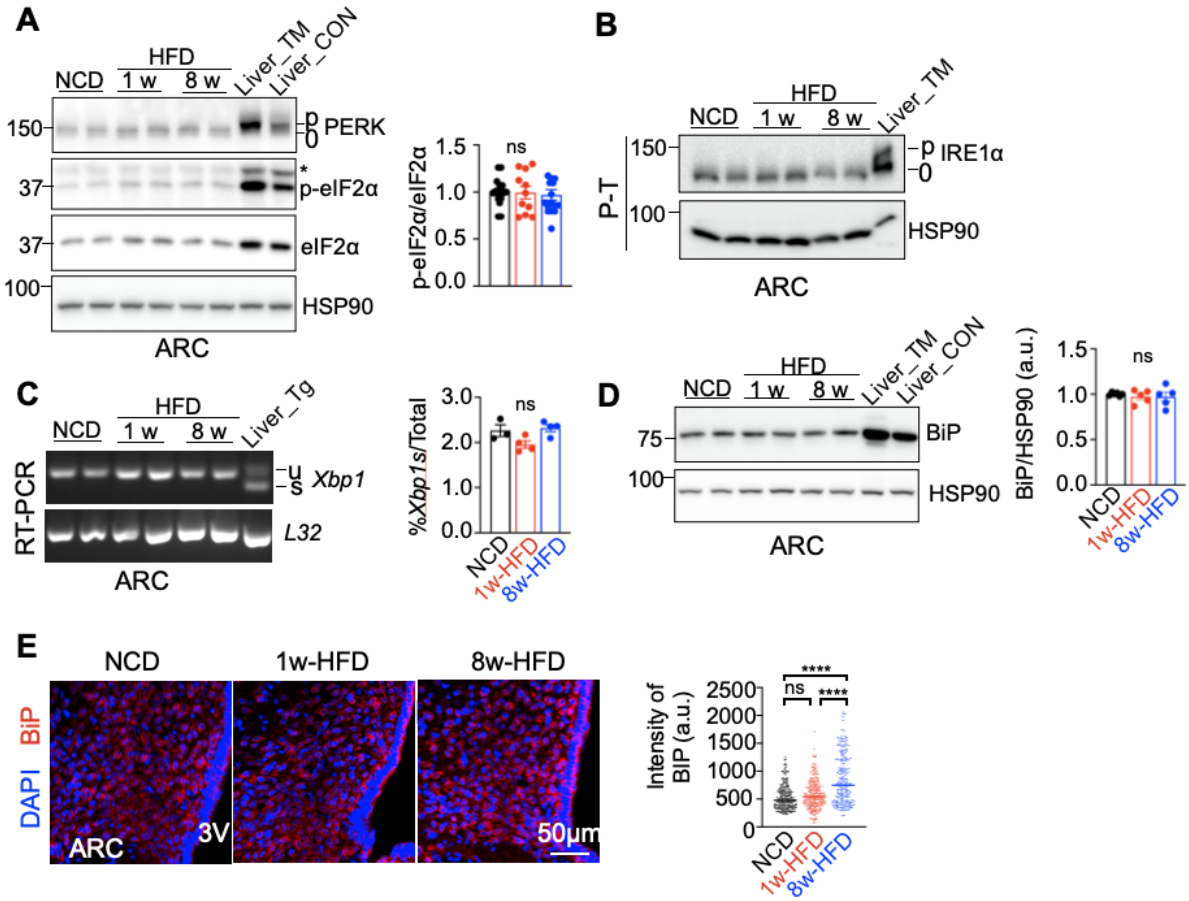

Figure 2.4 UPR can be uncoupled from high fat diet associated leptin resistance in the CNS.

(A) Representative images and quantitation of western blot for PERK-eIF2α analysis in the ARC of the male mice fed on NCD, 1w- and 8w-HFD.

(B) Representative images of phostag-gel (P-T) for IRE1α phosphorylation analysis in the ARC of the male mice fed on NCD, 1w- and 8w-HFD. Protein isolated from the liver of mice treated with tunicamycin (1 mg/kg, i.p.) for 24 hours was used as a positive control to indicate the position of phosphorylated IRE1a shipped up on the phostag-gel. HSP 90 is used as a protein loading control.

(C) Representative images and quantification of reverse transcriptase PCR (RT-PCR) analysis of *Xbp1* mRNA splicing (u, unspliced; s, spliced) in ARC. *L32* is used as a house keeping gene control.

(D) Representative images and quantitation of western blot for BiP analysis in the ARC of the male mice fed on NCD, 1w- and 8w-HFD. (n=5 each group)

(E) Representative images shown IF staining of BiP in the ARC of C57BL/6J male mice fed on NCD, 1w- and 8w-HFD. (n=2 mice per group, 90-130 cells per mice).

NCD for normal chow diet; 1w-HFD for 1-week; 8w-HFD for 8-week; ARC, arcuate nucleus; 3V, third ventricle. Values, mean ± SEM. n.s., not significant; *p<0.05, **p<0.01, ***p<0.001 and ****p<0.0001 by one-way ANOVA followed by Tukey's multiple comparison tests (A, C, D, E)

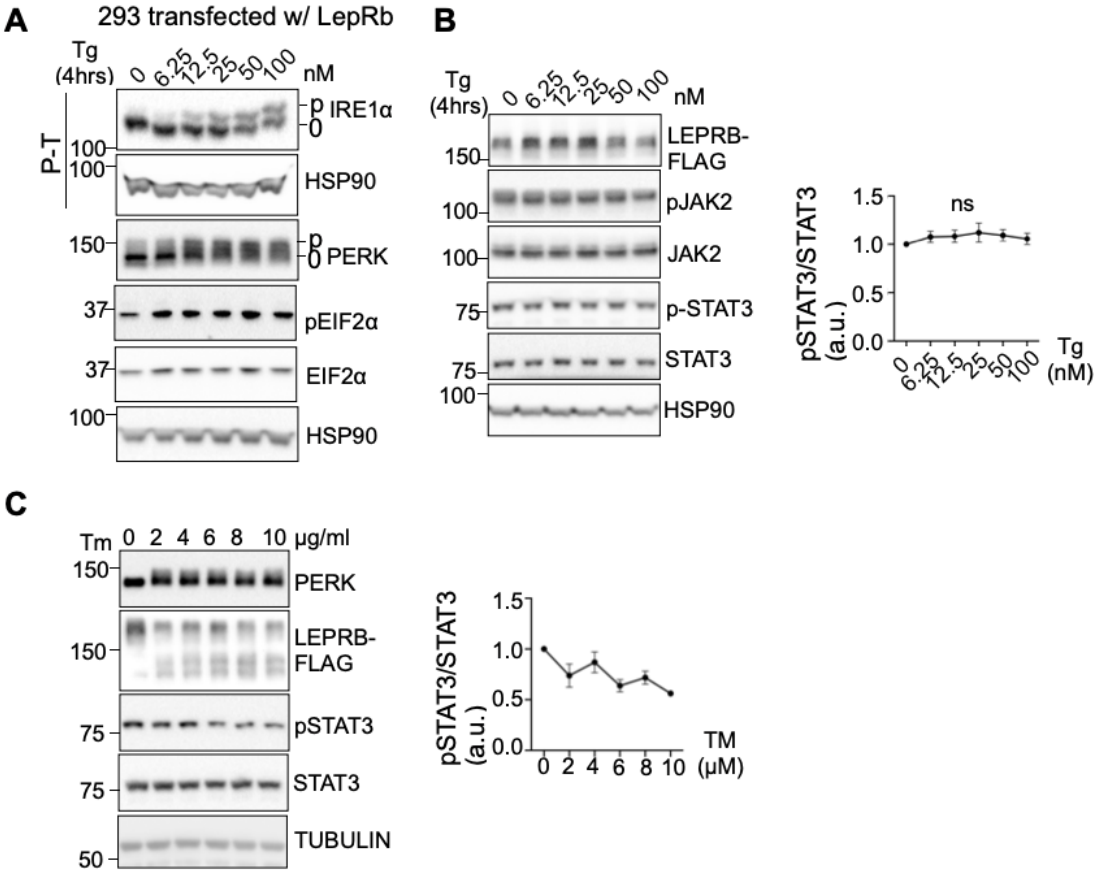

Figure 2.5 Activation of UPR induced by distinct ER stressors may differentially affect leptin sensitivity.
(A) Representative images of UPR in HEK293T transfected with LepRb treated with leptin after fasted in Thapsigargin (Tg)-containing serum free DMEM.
(B) Representative images and quantitation of leptin signaling analysis in HEK293T transfected with LepRb treated with leptin after fasted in Thapsigargin (Tg)-containing serum free DMEM.
(C) Representative images of UPR and leptin signaling analysis in HEK293T transfected with LepRb treated with leptin after fasted in Tunicamycin (Tm)-containing serum free DMEM.

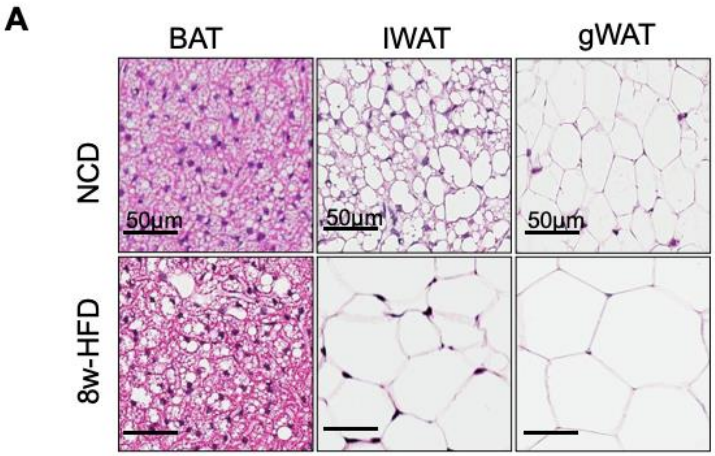

Figure 2.6 HFD-associated pathogenesis in peripheral tissues.
(A) Representative images of H&E staining in the BAT, IWAT and gWAT of the mice fed on NCD and 8w-HFD.
NCD for normal chow diet; 8w-HFD for 8-week; BAT, brown adipose tissue; IWAT, inguinal white adipose tissue; gWAT, gonadal white adipose tissue.

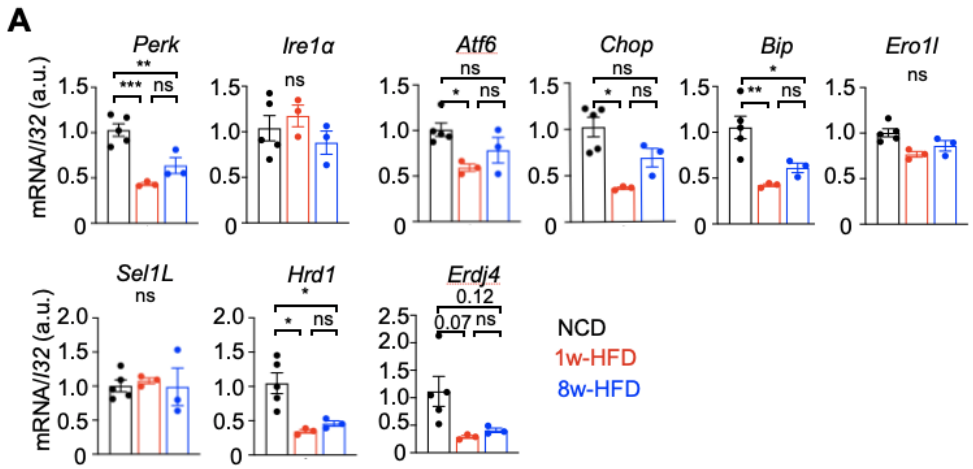

Figure 2.7 Transcriptional analysis of UPR in liver upon HFD feeding.
(A) Quantitative PCR (qPCR) analysis of UPR and ERAD in the liver of C57BL/6J male mice fed on NCD, 1w- and 8w-HFD. (n=3-5 mice per group)
NCD for normal chow diet; 1w-HFD for 1-week; 8w-HFD for 8-week. Values, mean ± SEM. n.s., not significant; *p<0.05, **p<0.01, ***p<0.001 and ****p<0.0001 by one-way ANOVA followed by Tukey's multiple comparison tests (A)

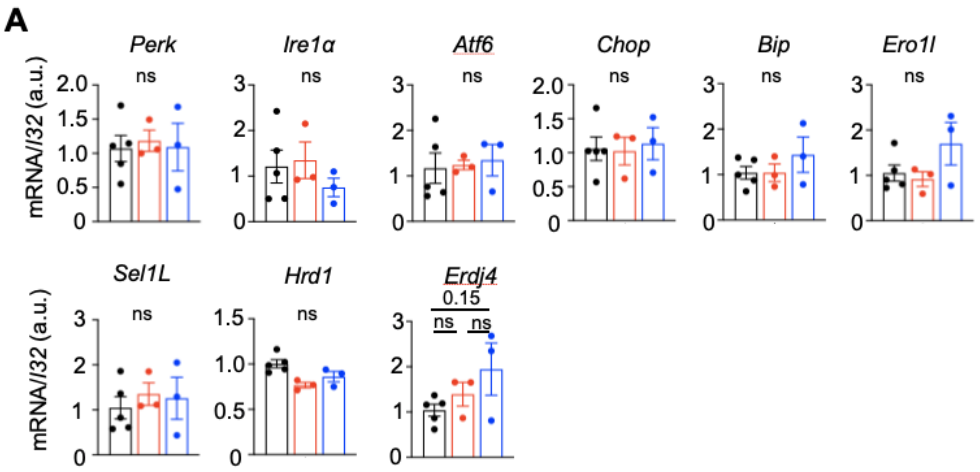

Figure 2.8 Transcriptional analysis of UPR in gWAT upon HFD feeding.
(A) Quantitative PCR (qPCR) analysis of UPR and ERAD in the gWAT of C57BL/6J male mice fed on NCD, 1w- and 8w-HFD. (n=3-5 mice per group)
NCD for normal chow diet; 1w-HFD for 1-week; 8w-HFD for 8-week; gWAT, gonadal white adipose tissue. Values, mean ± SEM. n.s., not significant; *p<0.05, **p<0.01, ***p<0.001 and ****p<0.0001 by one-way ANOVA followed by Tukey's multiple comparison tests (A)

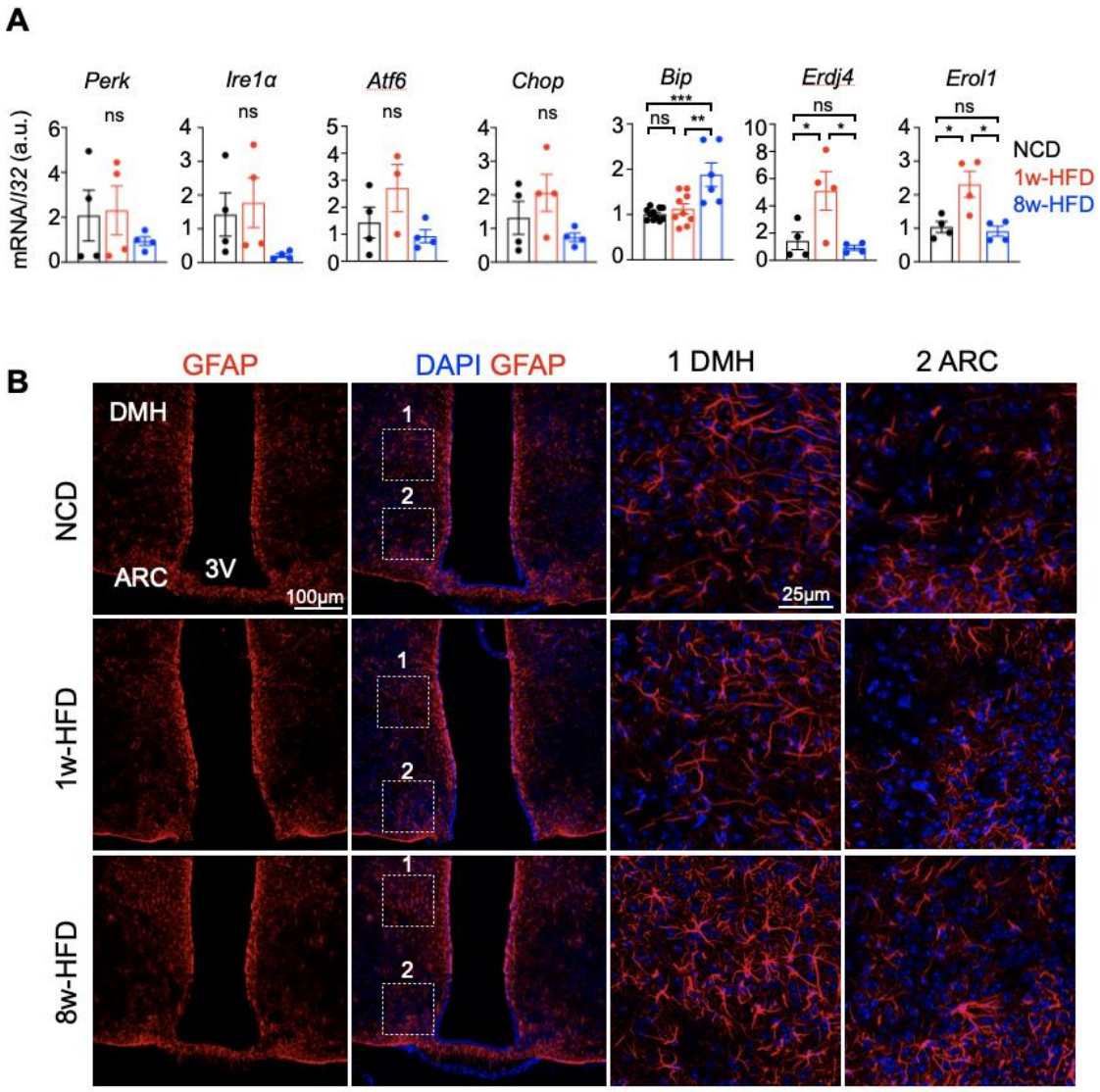

Figure 2.9 Transcriptional analysis of UPR and inflammatory analysis for astrogliosis in ARC upon HFD feeding.

(A) Quantitative PCR (qPCR) analysis of UPR in the ARC of C57BL/6J male mice fed on NCD, 1w- and 8w-HFD. (n=4 mice per group).

(B) Representative images shown IF staining of GFAP in the hypothalamic ARC and DMH of C57BL/6J male mice fed on NCD, 1w- and 8w-HFD. (n=3 mice per group). NCD for normal chow diet; 1w-HFD for 1-week; 8w-HFD for 8-week; ARC, arcuate nucleus; DMH, dorsomedial hypothalamus; 3V, third ventricle. Values, mean ± SEM. n.s., not significant; *p<0.05, **p<0.01, ***p<0.001 and ****p<0.0001 by one-way ANOVA followed by Tukey's multiple comparison tests (A)

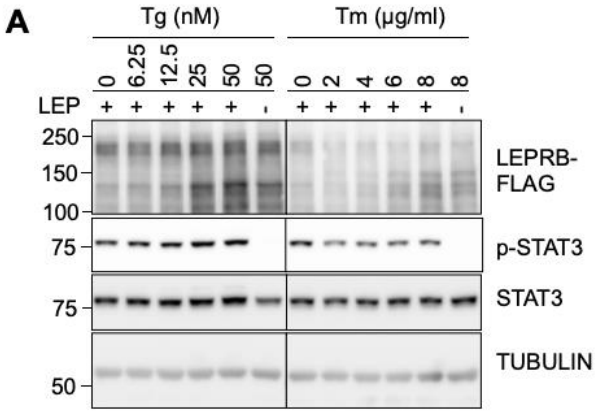

Figure 2.10 Tm, but not Tg, impaired leptin signaling by disrupting glycosylation of LepRb.
(A) Representative images and quantitation of leptin signaling analysis in HEK293T transfected with LepRb treated with leptin after fasted in Tg-or Tm- containing serum free DMEM.

Chapter 3 SEL1L-HRD1 ER-associated Degradation Regulates Leptin Receptor Maturation and Signaling in POMC Neurons in Diet-induced Obesity[3]

Hancheng Mao[1], Geun Hyang Kim[1,3], Ling Qi[2*]

[1]Department of Molecular & Integrative Physiology, University of Michigan Medical School, Ann Arbor, MI 48105, USA

[2] Department of Molecular Physiology and Biological Physics, University of Virginia, School of Medicine, Charlottesville, VA 22903, USA

[3] Present address: Regeneron Pharmaceuticals, Inc., 777 Old Saw Mill River Road, Tarrytown, New York 10591, USA

[*]Correspondence: xvr2hm@virginia.edu

The authors have declared that no conflict of interest exists.

Short title: Regulation of leptin receptor maturation and signaling by SEL1L-HRD1 ERAD

Summary: Here we report that POMC-specific SEL1L-HRD1 ER-associated degradation is indispensable for leptin signaling in diet-induced obesity by controlling the turnover and maturation of nascent leptin receptor in the ER.

Keywords: SEL1L-HRD1 ERAD, POMC, diet-induced obesity, leptin signaling, LepRb

[3] This chapter is adapted from: Mao, H., G.H. Kim, and L. Qi. (2024) "SEL1L-HRD1 ER-associated degradation regulates leptin receptor maturation and signaling in POMC neurons in diet-induced obesity." *Nature Communications*. Under revision.

3.1 Abstract

Endoplasmic reticulum (ER) homeostasis in the hypothalamus has been implicated in the pathogenesis of certain patho-physiological conditions such as diet-induced obesity (DIO) and type 2 diabetes; however, the significance of ER quality control mechanism(s) and its underlying mechanism remain largely unclear and highly controversial in some cases. Moreover, how the biogenesis of nascent leptin receptor in the ER is regulated remains largely unexplored. Here we report that the SEL1L-HRD1 protein complex of the highly conserved ER-associated protein degradation (ERAD) machinery in POMC neurons is indispensable for leptin signaling in diet-induced obesity. SEL1L-HRD1 ERAD is constitutively expressed in hypothalamic POMC neurons. Loss of SEL1L in POMC neurons attenuates leptin signaling and predisposes mice to HFD-associated pathologies including leptin resistance. Mechanistically, newly synthesized leptin receptors, both wildtype and disease-associated human mutant Cys604Ser (Cys602Ser in mice), are misfolding prone and bona fide substrates of SEL1L-HRD1 ERAD. Indeed, defects in SEL1L-HRD1 ERAD markedly impair the maturation of these receptors and causes their ER retention. This study not only uncovers a new role of SEL1L-HRD1 ERAD in the pathogenesis of diet-induced obesity and central leptin resistance, but a new regulatory mechanism for leptin signaling.

3.2 Introduction

Hypothalamic neurons play important roles in the adaptation and mal-adaptation to pathophysiological conditions such as diet-induced obesity (DIO) and type-2 diabetes [1-7]. Homeostasis in the endoplasmic reticulum (ER) regulates many physiological processes such as systemic inflammation, inter-organellar crosstalk and mitochondrial dynamics [8-14]. It has been proposed that hypothalamic ER stress or unfolded protein response (UPR) may play a causal role in inflammation and leptin resistance in DIO and type-2 diabetes [15-21]. However, others have reported a protective role of UPR in similar experimental settings [22, 23]. Hence, the significance of ER quality control pathways and its underlying mechanisms remain controversial.

In addition to UPR that responds to misfolded proteins in the ER, ER-associated protein degradation (ERAD) is a constitutively active and highly conserved process responsible for recruiting unfolded or misfolded proteins in the ER for cytosolic proteasomal degradation [24-31]. Among over a dozen of putative ERAD complexes, the SEL1L-HRD1 protein complex represents the most evolutionarily conserved ERAD branch where SEL1L/Hrd3p is an obligatory cofactor for the E3 ligase HRD1 [28-30, 32-34]. Recent studies using cell type-specific SEL1L or HRD1 knockout mouse models have revealed the patho-physiological importance of SEL1L-HRD1 ERAD in a substrate-specific manner [35-42]. Particularly relevant to this study, SEL1L-HRD1 ERAD has been reported as indispensable for AVP and POMC neurons to control water balance and food intake via the maturation of prohormones, proAVP and POMC, respectively [39, 40]. POMC neuron-specific *Sel1L* deletion leads to hyperphagia and age-

associated obesity starting around 13 weeks of age when fed a low-fat chow diet [39]. Given the importance of POMC neurons in maintaining energy homeostasis under various nutritional status, one outstanding question is the relevance and significance of SEL1L-HRD1 ERAD in POMC neurons under pathophysiological conditions, including DIO.

Here, we show that SEL1L-HRD1 ERAD in POMC neurons at the arcuate nucleus (ARC) of the hypothalamus, a key group of metabolic neurons that control food intake and energy expenditure [43], controls DIO pathogenesis and leptin sensitivity via the regulation of leptin receptor biogenesis and signaling. Soon after weaning, POMC-specific *Sel1L* deficient (*Sel1L*^{POMC}) mice are hypersensitive to DIO. Much to our surprise, SEL1L-HRD1 ERAD is indispensable for the maturation of nascent leptin receptor to reach to the cell surface. Hence, SEL1L-HRD1 ERAD is a critical regulator of the maturation of leptin receptor in the ER and thereby leptin signaling in POMC neurons.

3.3 Results

Transient upregulation of SEL1L-HRD1 ERAD expression in the hypothalamus in response to high fat diet (HFD) feeding.

We previously showed that the SEL1L-HRD1 protein complex is constitutively expressed in the ARC of the hypothalamus [39]. Here we first asked whether its expression in the ARC region is regulated in response to overnutrition by placing the mice on 60% HFD (60% calories derived from fat) for 1 or 8 weeks. HFD feeding

expectedly reduced the expression of *Pomc, Npy* and *Agrp* (Figure 3.10A), while enhancing the protein levels of POMC derivatives β-Endorphin and α-MSH (Figure 3.10B-E). Moreover, HFD feeding enhanced neuronal activity in the PVH region as measured by nuclear c-FOS following both 1- and 8-week HFD (Figure 3.10D and E). One-week HFD significantly induced *Hrd1* mRNA level, but not *Sel1L* mRNA level, while 8-week HFD feeding had no such effect (Figure 3.1A). At the protein level, both SEL1L and HRD1 proteins, were elevated at 1-week HFD, and returned to basal levels after 8-week HFD (Figure 3.1B and C), pointing to transient response of SEL1L-HRD1 expression in the hypothalamus in response to HFD challenge. We next performed confocal microscopy to visualize SEL1L-HRD1 expression in the ARC regions in response to HFD. To visualize POMC neurons, we used POMC-eGFP transgenic mice where eGFP is under the control of POMC promoter [39, 44]. SEL1L protein level was increased specifically in POMC neurons upon 1-week HFD, and returned to the basal level with prolonged HFD feeding (Figure 3.1D and E). Similar observation was obtained for HRD1 protein levels in POMC neurons, but unlike SEL1L, HRD1 protein level was transiently upregulated in non POMC neurons as well (Figure 3.1F and G). Hence, SEL1L-HRD1 expression in POMC neurons are responsive to acute, but not chronic, nutrient overload.

Hypothalamic POMC-specific ERAD deficiency leads to early-onset DIO and its pathologies.

To delineate the significance of hypothalamic ERAD in DIO, we next characterized the phenotypes of $Sel1L^{POMC}$ mice, generated by crossing $Sel1L^{f/f}$ with the Pomc-Cre

mouse line [39], following 8-week HFD feeding from 5 weeks of age. In line with our previous report, *Sel1L*^{POMC} mice appeared comparably to WT littermates in terms of body weight on chow diet for the first 13 weeks of age [39] (Figure 3.2A), *Sel1L*^{POMC} mice, both sexes, gained significantly more body weight soon after HFD feeding (Figure 3.2A). Body composition analysis showed that fat content was significantly increased in *Sel1L*^{POMC} mice, reaching over 50% of body mass after 8-week HFD (Figure 3.2B and Figure 3.11A) with more lipid deposition in the liver, as well as both white and brown adipose tissues (WAT and BAT) (Figure 3.2C). *Sel1L*^{POMC} mice became highly glucose intolerant and insulin resistant following 8-week HFD (Figure 3.2D and E), with elevated ad libitum and fasting blood glucose (Figure 3.2F) and ad libitum insulin levels (Figure 3.2G). In addition, glucagon and corticosterone levels were elevated in *Sel1L*^{POMC} mice (Figure 3.11B and C), while rectal temperature in *Sel1L*^{POMC} mice was decreased by 2 degrees compared to that of WT littermates (Figure 3.11D). Hence, we concluded that mice with POMC-specific ERAD defects exhibit early onset DIO and its pathologies including glucose intolerance and insulin resistance.

Hypothalamic ERAD deficiency triggers hyperphagia and leptin resistance.

We next explored the possible mechanism underlying the susceptibility to DIO in *Sel1L*^{POMC} mice. *Sel1L*^{POMC} mice consumed ~ 40% more food daily, i.e., hyperphagia, upon both 1- and 8-week HFD feeding (Figure 3.3A). To directly demonstrate the direct causal link between food intake and weight gain, we performed pair feeding (giving the same amount of the food as WT littermates consume) following 8-week ad libitum HFD feeding. *Sel1L*^{POMC} mice gained weight quite rapidly under *ad libitum* feeding of HFD;

however, their weight gain was significantly slowed following pair-feeding and recovered when placed on ad libitum HFD feeding again (Figure 3.3B). Indeed, weight gain of *Sel1L*^{POMC} mice was comparable to that of WT littermates if pair-feeding was performed at the beginning of HFD feeding (Figure 3.3C). We then tested whether hyperphagia of *Sel1L*^{POMC} mice is caused by leptin resistance (Figure 3.3D). Leptin injection was expected to induce body weight loss in WT mice, but not *Sel1L*^{POMC} mice. Indeed, unlike WT mice, *Sel1L*^{POMC} mice continued to gain body weight following leptin injection (Figure 3.3D and E). This difference in body weight gain was likely due to the differences in food intake in response to leptin injection (Figure 3.3F), pointing to a significant leptin resistance in *Sel1L*^{POMC} mice. *Sel1L*^{POMC} mice exhibited progressively marked hyperleptinemia with HFD feeding (Figure 3.3G). Hence, we concluded that hypothalamic POMC neurons-specific ERAD deficiency triggers hyperphagia and leptin resistance.

The effect of hypothalamic SEL1L-HRD1 ERAD in DIO is mediated by leptin resistance.

To further establish the effect of leptin resistance in ERAD deficiency-associated DIO, we next performed parabiosis between two littermates to allow the sharing of the circulation (Figure 3.4A). Following two weeks of recovery on chow diet, the parabionts *WT*: *Sel1L*^{POMC} (Group III) were placed on HFD for 8 weeks (Figure 3.4A). Two control parabionts, *WT: WT* (Group I) and *Sel1L*^{POMC}:*Sel1L*^{POMC} (Group II), gained weight as expected with the latter pair becoming obese (Figure 3.4B). However, in *WT*: *Sel1L*^{POMC} (Group III) parabionts, body weight gain for WT mice was attenuated compared to WT

mice in *WT: WT* (Group I) control parabionts (P=0.08), while body weight gain for *Sel1L*^{POMC} mice was comparable to that of *Sel1L*^{POMC}:*Sel1L*^{POMC} parabionts (Group II) (Figure 3.4B). Body compositions (i.e., lean vs. fat) in parabionts were not affected by the partner (Figure 3.4C). Moreover, serum leptin and insulin levels were highly elevated in the *Sel1L*^{POMC} mice, but unaltered in WT mice regardless of the partners (Figure 3.4D and E). Hence, these data suggested that hypothalamic SEL1L-HRD1 ERAD controls DIO pathogenesis via hyperleptinemia.

Hypothalamic SEL1L-HRD1 ERAD deficiency impairs leptin-pSTAT3 signaling.

We next asked how POMC-specific SEL1L-HRD1 ERAD regulates leptin sensitivity. As leptin signaling induces phosphorylation of STAT3 (pSTAT3), we next examined the levels of pSTAT3 in POMC neurons following leptin challenge. To visualize POMC neurons, we generated *Sel1L*^{POMC} mice on the POMC-eGFP background (*Sel1L*^{POMC};POMC-eGFP) [39, 44]. HFD feeding progressively blunted leptin-induced pSTAT3 in the POMC neurons of the ARC region of WT mice, but to a much greater extent, in *Sel1L*^{POMC} mice (Figure 3.5A-D and Figure 3.12). In keeping with the notion that pSTAT3 is a critical transcription factor for the *Pomc* gene [45], hypothalamic *Pomc* mRNA expression was markedly decreased in *Sel1L*^{POMC} mice with HFD (Figure 3.5E). Moreover, Western blot analysis of pSTAT3 of the ARC region also showed a greater reduction of the percent of STAT3 being phosphorylated following HFD feeding (Figure 3.5F and G). Thus, our data suggested that SEL1L-HRD1 ERAD in POMC neurons is vital for maintaining central leptin sensitivity during DIO pathogenesis.

The effect of POMC-specific ERAD in DIO is likely uncoupled from UPR or inflammation.

As ERAD deficiency expectedly causes the accumulation of unfolded/misfolded proteins in the ER that can potentially trigger UPR and given the reported role of UPR in DIO pathogenesis, we next tested whether ERAD deficiency activates UPR and if so, to what extent. There was no detectable activation of the PERK pathway as measured by phosphorylation of PERK and its downstream phosphorylation of eIF2α (Figure 3.6A and Figure 13A). Phosphorylation of IRE1α, on the other hand, was moderately elevated in the ARC of *Sel1L*^{POMC} mice, so was the splicing of *Xbp1* mRNA (a downstream effector of IRE1α) (Figure 3.6B and C, Figure 3.13B and C). Consistently, ER chaperon BiP (an XBP1 target) was mildly elevated in the ARC of *Sel1L*^{POMC} mice (Figure 3.6A and Figure 3.13A and D). In vitro, treatment with an ER stress inducer thapsigargin (Tg) induced strong ER stress, but failed to affect leptin signaling in WT HEK293T cells transfected with long isoform of mouse Leptin receptors (mLepRb) (Figure 3.6D and Figure 3.13E), indicating that UPR is not sufficient to induce leptin resistance. Importantly, we found no significant POMC neuronal loss in the ARC of *Sel1L*^{POMC};POMC-eGFP mice (Figure 3.6E). Inflammatory markers were largely comparable in the ARC of *Sel1L*^{POMC} mice compared to those in WT littermates as measured by phosphorylation and protein levels of c-Jun N-terminal Kinase (JNK) as well as protein levels of I kappa B alpha (IκBα) (Figure 3.6F and G). Chronic HFD feeding mildly increased astrogliosis in the ARC regions of both *Sel1L*^{POMC} and *Sel1L*^{POMC} mice as measured by both Western blot and immunofluorescence staining of astrocyte marker Glial Fibrillary acidic protein (GFAP) and/or microglia marker Ionized

calcium-binding adaptor molecule 1 (IBA1) (Figure 3.6F-H and Figure 3.13F). Taken together, these data demonstrate that *Sel1L* deficiency in POMC neurons triggers leptin resistance, independently of UPR, neuronal cell death and inflammation.

SEL1L-HRD1 is required for the maturation of nascent leptin receptor (LepR).

The forementioned data suggested that SEL1L-HRD1 ERAD regulates leptin sensitivity upstream of STAT3. To further explore the underlying mechanism, we generated leptin-responsive HEK293T cell system expressing the long isoform of LepR (LepRb) responsible for leptin-induced JAK2-STAT3 signaling [46-49]. Indeed, in line with decreased leptin sensitivity in vivo, mLepRb-positive *HRD1*$^{-/-}$ HEK293T cells exhibited impaired phosphorylation of JAK2 and STAT3 compared to those in transfected *WT* cells in response to leptin stimulation (Figure 3.7A and B). Surprisingly, the protein level of mLepRb was significantly higher in *HRD1*$^{-/-}$ HEK293T cells compared to that of WT cells, under both serum-deprived and -supplemented conditions (Figure 3.7B and C). Moreover, SEL1L interaction with in LepRb-transfected cells was markedly enhanced in *HRD1*$^{-/-}$ cells where substrate-SEL1L interaction is known to be stabilized [29, 50, 51] (Figure 3.7D and E). LepRb was ubiquitinated in an HRD1-dependent manner (Figure 3.7F) and was significantly stabilized in *HRD1*$^{-/-}$ cells compared to that in *WT* cells (Figure 3.7G).

We next assessed the consequence of ERAD deficiency on LepRb maturation in the ER. Endoglycosidase H (EndoH) digestion, which cleaves asparagine-linked high mannose or hybrid glycans of the immature glycoproteins predominantly in ER [52], revealed a significantly lower fraction of EndoH resistant LepRb (i.e., the form able to

exit the ER for complete maturation) in *HRD1*$^{-/-}$ HEK293T cells (Fig. 7H). This was further confirmed by surface biotinylation assay followed by immunoprecipitation with streptavidin-beads, which indicated reduced proportion of surface LepRb in *HRD1*$^{-/-}$ cells (Figure 3.7I and Figure 3.14A). Moreover, confocal microscopy following immunofluorescence staining further demonstrated an altered distribution of LepRb with increased intracellular, but decreased surface, expression in ERAD-deficient cells (Figure 3.7J and Figure 3.14B). In the absence of SEL1L-HRD1, LepRb protein was prone to form high molecular weight aggregates via disulfide bonds (Figure 3.7K) Taken together, our data show that SEL1L-HRD1 ERAD is required for the maturation of LepRb by targeting the misfolding-prone or misfolded LepRb for proteasomal degradation.

SEL1L-HRD1 ERAD degrades and limits the pathogenicity of human LepRb Cys604Ser (C604S) mutant.

To demonstrate the clinical relevance of our findings, we asked whether human LepRb (hLepRb) mutants [53, 54] are SEL1L-HRD1 ERAD substrates. Here, we focused on hLepRb mutant C604S, a recessive point mutation due to missense homozygous substitution T > A at position 1810, identified in two brothers at 1- and 5-years old with severely early onset obesity [54, 55]. C604-C674 forms a disulfide bond in human LepRb corresponding to C602-C672 in mouse LepRb (Figure 3.8A and B) [56-58]. This mutation has been predicted as loss-of-function likely due to defects in folding [54, 56-58]. C602S mLepRb significantly impaired leptin response compared to WT mLepRb in *WT* cells, which was further diminished in *HRD1*$^{-/-}$ cells (Figure 3.8C). Similar to WT

mLepRb, C602S mLepRb was stabilized in the absence of HRD1 (Figure 3.8D). Notably, C602S mLepRb readily formed HMW aggregates in *WT* HEK293T cells, and to much greater extent, in *HRD1*$^{-/-}$ cells (Figure 3.8E). Such aggregates likely formed in the ER as demonstrated by their colocalization with the ER chaperone BiP based on immunostaining (Figure 3.8F-I). Hence, SEL1L-HRD1 ERAD is indispensable for the degradation of nascent WT and, at least a subset of, disease mutant LepRb, which ensures the maturation, trafficking and membrane display of functional LepRb.

3.4 Discussion

This study not only identifies a novel regulatory mechanism for leptin receptor and signaling, but also reports a key role of hypothalamic ERAD in maintaining energy homeostasis under nutrient overload conditions. SEL1L-HRD1 ERAD defects in POMC neurons predispose mice to DIO and its pathologies, due to hyperphagia and hypothalamic leptin resistance. Our mechanistic studies establish LepRb as a bona fide endogenous substrate of SEL1L-HRD1 ERAD. Pointing to the clinical relevance of our findings, human recessive LepRb C604S variant is trapped in the ER and degraded by SEL1L-HRD1 ERAD (Figure 3.9). In the absence of SEL1L-HRD1 ERAD, both WT and C604S LepRb are trapped in the ER in the form of HMW aggregates, with attenuated cell surface expression (Fig. 8E-I and Fig. 9). While this reported effect of ERAD in POMC neurons is in keeping with recent studies demonstrating the profound physiological importance of SEL1L-HRD1 ERAD in vivo [39, 40], it uncovers a novel function of SEL1L-HRD1 ERAD in leptin signaling and a novel regulatory mechanism for leptin biology.

Our data show that hypothalamic SEL1L deficiency markedly increases the progression and pathogenesis of DIO in mice. *Sel1L*-deficient POMC neurons exhibit mild alterations in ER homeostasis including elevated activation of the IRE1α -XBP1 pathway and expression of ER chaperones, but without any detectable cell death. As previous studies have shown that deficiency of *Ire1a* or *Xbp1* in POMC neurons predispose mice to DIO [21], while gain-of-function of XBP1s in POMC neurons had an opposite effect [23], we conclude that the effect of SEL1L-HRD1 ERAD is uncoupled from IRE1α -XBP1 pathway of the UPR and cell death, which is in line with many recent studies of various tissue-specific *Sel1L*- or *Hrd1*-deficient models [37, 39-42, 59]. These findings point to cellular adaption in response to ERAD deficiency [25]. Such mild UPR activation and chaperone expression are potentially cyto-protective in response to the accumulation of misfolding proteins in the ER.

Previous reports have suggested that UPR may play a causal role in leptin resistance due to impaired leptin signaling [15, 17, 60]. These studies were performed via the administration of ER stress inducers tunicamycin and thapsigargin which can be fraught with artefacts. Indeed, tunicamycin can inhibit glycosylation of the glycoproteins[61] including LepRb, and thus the impaired leptin signaling can be directly due to defective glycosylation and concomitant functionality of LepRb instead of UPR activation as a general outcome of numerous dysregulation of glycoproteins. Further, high dosage of ER stress inducers included in previous studies may fall far from any physiological relevance[15, 17, 60]. In our study, thapsigargin treatment induced a range of ER stress

response in a dose dependent manner, but failed to alter leptin signaling in *WT* HEK293T cells transfected with mLepRb even at a high level of UPR. Hence, collective evidence suggests that UPR is likely uncoupled from leptin signaling. The reason for these discrepancies remains unknown. Careful future studies are needed to validate either model.

This study demonstrates an important role of SEL1L-HRD1 ERAD in leptin signaling, at least in part via the regulation of the maturation of nascent LepRb protein. We previously showed that SEL1L-HRD1 ERAD is required for the posttranslational maturation of POMC prohormone in mice on chow diet and that *Sel1L* deficiency in POMC neurons cause age-associate obesity in mice on chow diet due to the ER retention of POMC prohormone [39]. In DIO mouse models, we found defects in *Sel1L*^{POMC} mice occurring upstream of POMC transcription as leptin-induced STAT3 phosphorylation is impaired in the absence of SEL1L-HRD1 ERAD [45-49]. Further mechanistic studies identify partial loss-of-function of LepRb resulted from attenuated ER exit of nascent LepRb in SEL1L-HRD1 ERAD deficient cells. This study suggests that nascent LepRb protein is likely misfolding prone in the ER, likely due to multiple glycosylation and the formation of disulfide bonds, and hence relies on SEL1L-HRD1 ERAD to generate an ER environment conducive for the proper folding and conformation of bystander LepRb.

Several human mutants have also been identified as SEL1L-HRD1 ERAD substrates that readily form aggregates and become resistant to and bypass the quality control

mediated by ERAD, leading to loss-of-function disease phenotype. These misfolded substrates with highly reactive cysteine thiols accumulate and promote the formation of inter- or intra-molecular disulfide-bonded aggregates [39-41]. Hence, SEL1L-HRD1 ERAD-mediated degradation of nascent unfolded and misfolded substrates, including LepRb in this study, may effectively prevent protein aggregation and maintain the folding environment in the ER. Efforts to target SEL1L-HRD1 ERAD function may represent a viable means for the treatment of certain diseases caused by a dominant-negative disease allele or a general collapse of the folding environment in the ER.

3.5 Methods

Mice. As described previously [39], POMC-specific *Sel1L*-deficient mice (*Sel1L*^{POMC}) and control littermates (*Sel1L*$^{f/f}$) were generated. The mice were further crossed with Pomc-eGFP reporter mice to generate *Sel1L*^{POMC};POMC-eGFP and control littermates *Sel1L*$^{f/f}$;POMC-eGFP. WT B6 mice were purchased from JAX and bred in our mouse facility. Mice were fed a chow diet (13% fat, 57% carbohydrate and 30% protein, PicoLab Rodent Diet 5L0D) and placed on a high-fat diet (HFD, calories provided by 60% fat, 20% carbohydrate and 20% protein, Research Diet D12492) from 5 weeks of age for 1 week or 8 weeks. All mice were housed in a temperature-controlled room with a 12-hour light/12-hour dark cycle.

Food intake measurement and pair-feeding. Food intake were measured as previously described [39]. Briefly, to perform daily food intake measurement, mice were first acclimatized to single housing 24 hours before the experiment. Daily food intake

was measured 1 hour before the onset of the dark cycle each day. For the pair-feeding at later stage of HFD feeding, *Sel1L*^{POMC} and WT littermates had continuous free access to HFD for eight weeks and were then single housed and fed ~2.5 g, which was determined by the average of daily food intake of WT littermates, at the start of the dark cycle. For the pair-feeding at early stage of HFD feeding, 5-week-old *Sel1L*^{POMC} mice were split into two groups: One group of *Sel1L*^{POMC} and WT littermates had continuous free access to food; the other group of *Sel1L*^{POMC} mice (pair-fed) was fed ~2.5 g at the start of dark hours. Weekly bodyweight gains were monitored.

Leptin treatment in mice. Twelve-week-old mice were intraperitoneally (i.p.) injected PBS followed by leptin (2 mg/kg body weight, R&D systems; catalog 498-OB-05M) 1 hour before the onset of dark cycle for three consecutive days as described [39]. Body weight and food intake were monitored daily during the treatment period. For phosphorylated STAT3 staining, 2 mg/kg leptin were i.p. injected to mice, followed by overnight fasting. Mice were anesthetized by isoflurane for fixation-perfusion 30 min after injection.

Tissue and blood collection. These procedures were carried out as previously described[39]. Briefly, blood was collected from anesthetized mice via cardiac puncture, transferred to 1.5ml microcentrifuge tubes, kept at room temperature for 30 minutes prior to centrifugation at 2,000 *g* for 15 minutes. Serum was aliquoted and stored at -80°C until analysis. For brain microdissection, Adult Mouse Brain Slicer Matrix (BSMAA001-1, Zivic Instruments) was used to collect coronal brain slices containing

ARC region with further microdissection to obtain ARC-enriched region. All tissues were snap-frozen in liquid nitrogen and stored at -80°C before use.

Preparation of brain sections. Mice were anesthetized with isoflurane, perfused with PBS followed by 4% paraformaldehyde (PFA) (Electron Microscopy Sciences; catalog 19210) for fixation. Brains were then postfixed in 4% PFA for overnight at 4°C, dehydrated in 15% sucrose and then 30% sucrose consecutively overnights at 4°C, and sectioned (30 µm) on a cryostat (Microm HM550 Cryostat, Thermo Fisher Scientific). The sections were stored in DEPC-containing anti-freezing media (50% 0.05 M sodium phosphate pH 7.3, 30% ethylene glycol, 20% glycerol) at −20°C. Different brain regions were identified using the Paxinos and Franklin atlas. Counted as distance from bregma, the following coordinates were used: PVN (–0.82 mm to –0.94 mm) and ARC (–1.58 mm to –1.7 mm).

Western blot and antibodies. Frozen tissue or cells were homogenized by sonication in lysis buffer [150mM NaCl, 50mM Tris pH 7.5, 10 mM EDTA, 1% Triton X-100] with freshly added protease inhibitors (Sigma; catalog P8340), phosphatase inhibitors (Sigma; catalog P5726) and 10 mM N-ethylmaleimide (Thermo Scientific; catalog 23030). Lysates were incubated on ice for 30 min followed by centrifugation (13,000 g, 10 min at 4 °C). Supernatants were collected and analyzed for protein concentration using Bradford assay (Bio-Rad; catalog 5000006). For denaturing SDS-PAGE, samples were further suppled with 1mM DTT and denatured at 95°C for 5 min in 5x SDS sample buffer (250 mM Tris-HCl pH 6.8, 10% sodium dodecyl sulfate, 0.05% Bromophenol

blue, 50% glycerol, and 1.44 M β-mercaptoethanol). For non-reducing SDA-PAGE, samples were prepared in 5x non-denaturing sample buffer (250 mM Tris-HCl pH 6.8, 10% sodium dodecyl sulfate, 0.05% bromophenol blue, 50% glycerol). For phostag gel analysis based on phos-tag system as described[62, 63], SDS-PAGE gel was supplemented by 50μM MnCl2 (Sigma) and 25μM phostag reagent (NARD Institute; catalog AAL-107) and must be protected from light until finishing running. Protein isolated from the liver of mice treated with tunicamycin (TM, 1 mg/kg, i.p.) for 24 hours was used as a positive control to indicate the position of phosphorylated PERK and IRE1a. For phosphatase treatment, 100 μg tissue lysates were incubated with 1 μl lambda phosphatase (λPPase, New England BioLabs; catalog P0753S) in 1× PMP buffer (New England BioLabs; catalog B0761S) with 1 mM $MnCl_2$ (New England BioLabs; catalog B1761S) at 30°C for 30 min. Reaction was stopped by adding 5× SDS sample buffer and incubated at 90°C for 5 min.

All samples were incubated in 65°C for 10min and run with 15-30 μg total lysate on SDS-PAGE gel for separation followed by electrophoretic transfer to PVDF membrane (0.45μm, Millipore; catalog IPFL00010). The blots were incubated in 2% BSA/Tri-buffered saline tween-20 (TBST) with primary antibodies overnight at 4°C, washed with TBST followed by 1hr incubation with goat anti-rabbit or mouse IgG HRP at room temperature. Band density was quantitated using the Image Lab software on the ChemiDOC XRS+ system (Bio-Rad).

Antibodies for Western blot were as follows: SEL1L (rabbit, 1:8000, Abclonal; catalog E112049), HRD1 (rabbit, 1:2000, ABclonal; catalog E15102), GRP78 BiP (rabbit, 1:5000, Abcam; catalog ab21685), HSP90 (rabbit, 1:5,000, Santa Cruz Biotechnology

Inc.; catalog sc-7947), FLAG (mouse, 1:2000, Sigma-Aldrich; catalog F-1804), IRE1α (rabbit, 1:2,000, Cell Signaling Technology; catalog 3294), p-eIF2α (rabbit, 1:2000, Cell Signaling Technology; catalog 3597), eIF2α (rabbit, 1:2000, Cell Signaling Technology; catalog 9722), p-JNK (mouse, 1:2000, Cell Signaling Technology; catalog 9255), JNK (rabbit, 1:1000, Cell Signaling Technology; catalog 9252), PERK (Rabbit, 1:1000, Cell Signaling Technology; catalog 3192), pSTAT3 (Tyr705) (rabbit, 1:1000, catalog 9131, Cell Signaling Technology), STAT3 (rabbit, 1:1000, Cell Signaling Technology; catalog 9132), pJAK2 (Tyr1007/1008) (rabbit, 1:1000, Cell Signaling Technology; catalog 3771), JAK2 (rabbit, 1:1000, ABclonal; catalog A19629), Tubulin (mouse, 1:5000, Santa Cruz Biotechnology Inc.; catalog sc-5286), IκBα (rabbit, 1:1000, Cell Signaling Technology; catalog 9242) and IBA1 (rabbit, 1:1000, Proteintech; catalog 10904-1-AP)
Secondary antibodies for Western blot were goat anti-rabbit IgG HRP and goat anti-mouse IgG HRP at 1:5,000, both from Bio-Rad.

Immunostaining and antibodies. For fluorescent immunostaining in free-floating brain sections, samples were picked out of anti-freezing buffer followed by 3 washes with PBS. Free-floating sections were simultaneously incubated with primary antibodies in blocking buffer (0.3% donkey serum and 0.25% Triton X-100 in 0.1 M PBS) overnight at 4°C. Following 3 washes with PBS, sections were incubated with secondary antibodies for 2 hours at room temperature. Brain sections were then mounted on gelatin-coated slides (Southern Biotech; catalog SLD01-CS). Counterstaining and mounting were performed with mounting medium containing DAPI (Vector Laboratories; catalog H-1200) and Fisherfinest Premium Cover Glasses (Fisher Scientific; catalog 12-548-5P).

For immunostaining in cells, 24 hours after transfection of LepRb-3xFLAG constructs, cells were placed on Poly-L-Lysine (Advanced Biomatrix; catalog 5048) coated Millicell EZ SLIDE 8-well glasses (Millipore; catalog PEZGS0816) for 24 hours before treatment and fixation. For staining surface bound leptin, samples were washed by ice cold PBS for 5 times and fixed by 4% formaldehyde (VWR; catalog 89370-094) for 15 minutes on ice followed by 3 washes with PBS. No permeabilization reagents were involved. For staining other markers, permeabilization was included and the overall process were the same as described above. To quantify immunoreactivity, identical acquisition settings were used for imaging each brain section from all groups within an experiment. The numbers of immunoreactivity-positive soma analysis and intensity of immunoreaction were quantified in 3D stack volumes after uniform background subtraction using the NIS Elements AR software (Nikon) and FIJI (National Institute of Health, USA).

Antibodies for immunostaining were as follows: HRD1 (rabbit, 1:500, homemade), GRP78 BiP (rabbit, 1:500, Abcam; catalog ab21685), α-MSH (sheep, 1:2,000, Millipore; catalog AB5087), β-endorphin (rabbit, 1:2,000, Phoenix Pharmaceuticals; catalog H-022-33, provided by Carol Elisa), and GFP (chicken IgY, 1:300, Abcam; catalog ab13970), p-Y705 STAT3 (rabbit, 1:200, Cell Signaling Technology; catalog 9145), GFAP (rabbit, 1:500, Agilent; Z033429-2), FLAG (mouse, 1:500, Sigma-Aldrich; catalog F-1804), KDEL (rabbit, 1:500, Novus Biologicals; catalog NBP2-75549), eIF3η (goat, 1:500, Santa Cruz Biotechnology; catalog sc-16377).
Secondary antibodies for fluorescent immunostaining (all 1:500) were as follows: Anti-rabbit IgG Alexa Fluor 647; anti-goat IgG Alexa Fluor 488 & 647; anti-sheep IgG Cy5

were from Jackson ImmunoResearch. Donkey anti-mouse IgG Alexa flour 555 was from Invitrogen (catalog A32773) and goat anti-chicken IgY FITC was from Aves Labs (catalog F-1005).

Plasmids. Mouse LepRb cDNA was provided by Dr. Martin Myer at University of Michigan Medical School. The *LepRb* coding region was amplified by PCR using a primer set containing HindIII and XbaI restriction site at 5' and 3' respectively.
F: 5′- CCG AAGCTT ATGATGTGTCAGAAATTCTATGTGGTT-3′
R: 5′- TGC TCTAGA CACAGTTAAGTCACACATCTTATT-3′
Both PCR products and the backbone vector p3xFLAG-CMV14 were digested using HindIII and XbaI restriction enzymes in the double digestion system from New England BioLabs. For construction of LepRb point mutants, quick change mutagenesis was performed using PFU DNA polymerase (600140, Agilent). The following primers were used for mutagenesis to construct LepRb-C602S:
F: 5'- CCTGCTGGTGTCAGACCTCAGTGCAGTCTATG-3'
R: 5'- CATAGACTGCACTGAGGTCTGACACCAGCAGG-3'

CRISPR/Cas9-based knockout (KO) in HEK293T cells. HEK293T cells were cultured at 37°C with 5% CO_2 in DMEM with 10% fetal bovine serum (Fisher Scientific). To generate HRD1-deficient HEK293T cells, sgRNA oligonucleotides designed for human *HRD1* (5'-GGACAAAGGCCTGGATGTAC-3') was inserted into lentiCRISPR v2 (plasmid 52961, Addgene). Cells transfected with empty plasmids without sgRNA were used as wild type control. Cells grown in 10 cm petri dishes were transfected with

indicated plasmids using 5µl 1 mg/ml polyethylenimine (PEI, Sigma) per 1µg of plasmids for HEK293T cells. Cells were cultured 24 hours after transfection in medium containing 2 µg/ml puromycin for 48 hours and then in normal growth media.

Glucose (GTT) and insulin tolerance test (ITT). As described [39], male mice were fasted for 16 or 6 hours for GTT and ITT respectively, followed by i.p. injection with glucose (2 g/kg body weight) or insulin (1 unit/kg body weight). At indicated time points, blood glucose was monitored using AimStrip ™ Plus Blood Glucose Testing System.

Body composition. Mice were anesthetized and scanned using DEXA as described **[39]**. (PIXImus, GE Medical Systems Lunar).

Parabiosis. Parabiosis surgery was performed in the mice at 7 weeks of age followed by two weeks of recovery as previously described[64]. After recovery, mice were fed on HFD for eight weeks. Body weights were recorded before and after parabiosis.

Leptin ELISA. Mouse serum samples were stored at -80°C. The samples were defrosted on ice and used for leptin measurement by Mouse/Rat Leptin Quantikine ELISA Kit (R&D Systems; catalog MOB00B).

RNA isolation, RT-PCR and qRCR. Microdissected brain tissues were homogenized in Trizol reagent (Invitrogen; catalog 15596-018). The RNA was further extracted using BCP phase separation reagent (Molecular Research Center; catalog TR 118) and

isopropanol precipitation. cDNA was synthesized with SuperScript™ III Reverse Transcriptase (Invitrogen; catalog 18080044). mRNA extraction and cDNA synthesis from liver and ARC of mice treated with tunicamycin (TM, 1 mg/kg, i.p.) for 24 hours were used as positive controls to indicate the position of spliced *Xbp1*.

The ratio of *Xbp1s* to total *Xbp1* (*Xbp1u* + *Xbp1s*) levels was quantified by Image Lab (Bio-Rad) software. For RT-PCR analysis the following primer sequences were used:

mXbp1-F: 5'-ACGAGGTTCCAGAGGTGGAG-3'

R: 5'-AAGAGGCAACAGTGTCAGAG-3'

mL32- F: 5'-GAGCAACAAGAAAACCAAGCA-3'

R: 5'-TGCACACAAGCCATCTACTCA-3'

hXbp1-F: 5'-GAATGAAGTGAGGCCAGTGG-3'

R: 5'-ACTGGGTCCTTCTGGGTAGA-3'

hL32- F: 5'-AGTTCCTGGTCCACAACGTC-3'

R: 5'-TTGGGGTTGGTGACTCTGAT-3'

Gene expression was analyzed using ABI (QuantStudio 5). Primers were used for this study:

mHrd1-F: 5'-AGCTACTTCAGTGAACCCCACT-3'

R: 5'-CTCCTCTACAATGCCCACTGAC-3'

mSel1L-F: 5’-TGGGTTTTCTCTCTCTCCTCTG-3’

R: 5’-CCTTTGTTCCGGTTACTTCTTG-3’

mPomc-F: 5’-AACGTTGCTGAGAACGAGTC-3’

R: 5’-ACCTGCTCCAAGCCTAATG-3’

mCart-F: 5’-GCCTGGCTTTAGCAACAATA-3’

R: 5’-AGGCATTCTCCTTCACACAA-3’

mAgRP-F: 5’-GAATGGCCTCAAGAAGACAA-3’

R: 5’-CGGTTCTGTGGATCTAGCAC-3’

mNpy-F: 5’- CGCTCTATCTCTGCTCGTGT-3’

R: 5’-GTATCTGGCCATGTCCTCTG-3’

mBdnf-F: 5’-AAGTAAACGTCCACGGACAA-3’

R: 5’-TCAAAAGTGTCAGCCAGTGA-3’

H&E staining. Peripheral tissues were collected from mice and fixed in 10% formalin for overnight at 4 °C, washed with PBS and stored in 70% ethanol at 4 °C until dehydration for paraffin-embedding. Sectioning and H&E staining were performed on a fee-for- service basis by the Michigan Histology Core Facilities.

Cell lines and transfection. HEK293T cells (ATCC) were cultured in DMEM (Corning; catalog 10-013-CV) with 1% Penicillin-Streptomycin (Gibco; catalog 15140122) and

heat inactivated 10% FBS (ThermoFisher; catalog FB12999102), respectively. Cells were transfected within 24 hours at 60-80% confluency after plating using polyethylenimine (PEI). Cells were treated and harvested within 48 hours after transfection.

Cycloheximide (CHX) and Brefeldin A (BFA) treatment in vitro. To study protein degradation, cycloheximide (CHX) chase experiments were performed where (transfected) HEK293T cells were cultured in DMEM w/ 10%FBS with 1h pretreatment of BFA (1µg/ml), followed by treatment with CHX (50 µg/ml) for the indicated times and harvested by snap-frozen in liquid nitrogen.

Leptin and thapsigargin treatment in vitro. HEK293T cells transfected with LepRb-3xFLAG were serum depraved for 6hrs followed by leptin (100nM, R&D systems; catalog 498-OB-05M) treatment for 30min and harvested by snap-frozen in liquid nitrogen. For thapsigargin treatment, indicated dose of thapsigargin (Millipore; catalog T9033-1MG) will be added into cells after 2h-serum deprivation followed by leptin treatment after another 4 hours.

Immunoprecipitation. Cells were lysed in IP lysis buffer [150 mM NaCl, 0.2% Nonidet P-40 (NP40), 0.1% Triton X-100, 25 mM Tris-HCl pH 7.5] supplemented with protease inhibitors, protein phosphatase inhibitors, and 10 mM N ethylmaleimide for anti-LepRb-FLAG and SEL1L IP. A total of 2 mg protein lysate was incubated with 20 µl anti-FLAG agarose (Sigma; catalog A2220), or 1µl anti-SEL1L home-made antibody overnight at

4°C with gentle rocking. SEL1L IP lysates were incubated with Protein A agarose (Invitrogen; catalog 20333) at 4 °C for 3 hours. The incubated agaroses were washed three times with IP lysis buffer and eluted in SDS sample buffer at 95ºC for 5 min followed by SDS-PAGE and Immunoblot. For denaturing IP to evaluate the ubiquitination, 1% SDS was added to the lysates after protein level measurements and normalization with all other processes remain the same as above.

Cell surface biotinylation and pull-down assay by NeutrAvidin beads. The biotinylation of cell membrane proteins was performed 48 hours after transfection in cells. The whole experiment was performed on ice. Cells were resuspended in ice-cold PBS and transferred into centrifuge tubes, followed by washes with ice-cold PBS (1ml each time, centrifuge at 300g, 3min at 4°C). Sulfo-NHS-SS-Biotin (ThermoFisher; catalog 21331) was dissolved in PBS at 1 mg ml^{-1} and store on ice. Cells were resuspended at a concentration of 1×10^7 cells/mL in freshly made biotin-containing PBS and incubated for 30min on ice with gentle shaking. Non-reacted biotinylation reagent was quenched and removed by 3 washes with ice-cold PBS supplemented with 50mM glycine. Cells were lysed in IP lysis buffer [150 mM NaCl, 0.2% Nonidet P-40 (NP40), 0.1% Triton X-100, 25 mM Tris-HCl pH 7.5] supplemented with protease inhibitors, protein phosphatase inhibitors, and 10 mM N ethylmaleimide and incubated on ice for 30min followed by centrifugation (13,000 g, 10 min at 4 °C). Supernatants were collected and analyzed for protein concentration using Bradford assay (Bio-Rad; catalog 5000006). Neutravidin beads (50µl per sample, ThermoFisher; catalog 29200) were washed 3 times in IP buffer. Incubate equal amount of total protein across all

samples with beads and rotate for 4hrs at 4°C. The beads were spun down at 300g in a 4 °C centrifuge for 3min to remove the supernatant followed by 3 washes with 1 ml IP buffer (with inhibitors) by rotating the mixture for 5 min in the 4 °C room and centrifugation. After the final wash, the supernatant was removed and the beads were incubated in 40µl 2xloading buffer at 65 °C for 10 min to elute and denature samples.

Endoglycosidase H (EndoH) and PNGase F treatment. EndoH and PNGase F treatment were performed as previously described [35]. Briefly, cell lysates were incubated with 1x glycoprotein denaturing buffer (New England BioLabs; catalog B1704S) at 100 °C for 10 min, and then digested with EndoH (New England BioLabs; catalog P0702L) with GlycoBuffer 3 (New England BioLabs; catalog B1720S) or PNGase F (New England BioLabs; catalog P0704L) with GlycoBuffer 2 (New England BioLabs; catalog B3704S) at 37 °C for 1 hr. The reaction was stopped by the addition of 5X denaturing sample buffer and boiled at 95 °C for 5 min.

Statistics. Results are expressed as the mean ± SEM unless otherwise stated. Statistical analyses were performed in GraphPad Prism version 8.0 (GraphPad Software Inc.). Comparisons between the groups were made by unpaired two-tailed Student's t test for two groups, or one-way ANOVA or two-way ANOVA followed by multiple comparisons test for more than two groups. P value < 0.05 was considered as statistically significant. All experiments were repeated at least twice and/or performed with several independent biological samples, and representative data are shown.

Study Approval. All experiments performed with mice were in compliance with University of Michigan (Ann Arbor, MI) Institutional Animal Care and Use Committee (#PRO00006888) guidelines.

Data and material availability. The materials and reagents used are either commercially available or available upon the request, with detailed information included in Methods. The predicted structure of mLepRb is available at AlphaFold ID AF-P48356-F1. All data supporting the findings and materials for the manuscript are available within the article and the Supplementary Information.

Author Contribution

H.M. and G.H.K. designed the most of experiments and H.M., with the help of G.H.K., performed most of the experiments and data analysis. H.M., with the help of G.H.K., wrote the methods and figure legends. L.Q. and H.M. wrote the manuscript. All authors have approved the manuscript.

Acknowledgements

We thank Drs. Richard Wojcikiewicz and Martin Myers for reagents; Drs. Peter Arvan, Carol Elias and Daniel Klionsky for critical comments and suggestions, and members of the Qi and Arvan laboratories for comments and technical assistance. This work was supported by NIH grants 1R01DK11174 (to P.A. and L.Q.), 1R01DK105393, 1R01DK120047, and American Diabetes Association (ADA) 1-19-IBS-235 (to L.Q.).

3.6 References

1. McLean, F.H., et al., *A high-fat diet induces rapid changes in the mouse hypothalamic proteome.* Nutr Metab (Lond), 2019. 16: p. 26.
2. Dalvi, P.S., et al., *High fat induces acute and chronic inflammation in the hypothalamus: effect of high-fat diet, palmitate and TNF-alpha on appetite-regulating NPY neurons.* Int J Obes (Lond), 2017. 41(1): p. 149-158.
3. Beutler, L.R., et al., *Obesity causes selective and long-lasting desensitization of AgRP neurons to dietary fat.* Elife, 2020. 9.
4. Horvath, T.L., et al., *Synaptic input organization of the melanocortin system predicts diet-induced hypothalamic reactive gliosis and obesity.* Proc Natl Acad Sci U S A, 2010. 107(33): p. 14875-80.
5. Souza, G.F., et al., *Defective regulation of POMC precedes hypothalamic inflammation in diet-induced obesity.* Sci Rep, 2016. 6: p. 29290.
6. Poon, K., *Behavioral Feeding Circuit: Dietary Fat-Induced Effects of Inflammatory Mediators in the Hypothalamus.* Front Endocrinol (Lausanne), 2020. 11: p. 591559.
7. Velloso, L.A. and M.W. Schwartz, *Altered hypothalamic function in diet-induced obesity.* Int J Obes (Lond), 2011. 35(12): p. 1455-65.
8. Zhang, K. and R.J. Kaufman, *From endoplasmic-reticulum stress to the inflammatory response.* Nature, 2008. 454(7203): p. 455-62.
9. Chaudhari, N., et al., *A molecular web: endoplasmic reticulum stress, inflammation, and oxidative stress.* Front Cell Neurosci, 2014. 8: p. 213.
10. Zhang, Y., et al., *Synergistic mechanism between the endoplasmic reticulum and mitochondria and their crosstalk with other organelles.* Cell Death Discov, 2023. 9(1): p. 51.
11. Wu, H., P. Carvalho, and G.K. Voeltz, *Here, there, and everywhere: The importance of ER membrane contact sites.* Science, 2018. 361(6401).
12. Kornmann, B., et al., *An ER-mitochondria tethering complex revealed by a synthetic biology screen.* Science, 2009. 325(5939): p. 477-81.
13. Rowland, A.A. and G.K. Voeltz, *Endoplasmic reticulum-mitochondria contacts: function of the junction.* Nat Rev Mol Cell Biol, 2012. 13(10): p. 607-25.
14. Marchi, S., S. Patergnani, and P. Pinton, *The endoplasmic reticulum-mitochondria connection: one touch, multiple functions.* Biochim Biophys Acta, 2014. 1837(4): p. 461-9.
15. Ozcan, L., et al., *Endoplasmic reticulum stress plays a central role in development of leptin resistance.* Cell Metab, 2009. 9(1): p. 35-51.
16. Purkayastha, S., et al., *Neural dysregulation of peripheral insulin action and blood pressure by brain endoplasmic reticulum stress.* Proc Natl Acad Sci U S A, 2011. 108(7): p. 2939-44.
17. Ramirez, S. and M. Claret, *Hypothalamic ER stress: A bridge between leptin resistance and obesity.* FEBS Lett, 2015. 589(14): p. 1678-87.
18. Schneeberger, M., et al., *Mitofusin 2 in POMC neurons connects ER stress with leptin resistance and energy imbalance.* Cell, 2013. 155(1): p. 172-87.
19. Ye, Z., et al., *Hypothalamic endoplasmic reticulum stress as a key mediator of obesity-induced leptin resistance.* Obes Rev, 2018. 19(6): p. 770-785.

20. Zhang, X., et al., *Hypothalamic IKKbeta/NF-kappaB and ER stress link overnutrition to energy imbalance and obesity.* Cell, 2008. 135(1): p. 61-73.
21. Yao, T., et al., *Ire1alpha in Pomc Neurons Is Required for Thermogenesis and Glycemia.* Diabetes, 2017. 66(3): p. 663-673.
22. Xiao, Y., et al., *Knockout of inositol-requiring enzyme 1alpha in pro-opiomelanocortin neurons decreases fat mass via increasing energy expenditure.* Open Biol, 2016. 6(8).
23. Williams, K.W., et al., *Xbp1s in Pomc neurons connects ER stress with energy balance and glucose homeostasis.* Cell Metab, 2014. 20(3): p. 471-82.
24. Friedlander, R., et al., *A regulatory link between ER-associated protein degradation and the unfolded-protein response.* Nat Cell Biol, 2000. 2(7): p. 379-84.
25. Qi, L., B. Tsai, and P. Arvan, *New Insights into the Physiological Role of Endoplasmic Reticulum-Associated Degradation.* Trends Cell Biol, 2017. 27(6): p. 430-440.
26. Travers, K.J., et al., *Functional and genomic analyses reveal an essential coordination between the unfolded protein response and ER-associated degradation.* Cell, 2000. 101(3): p. 249-58.
27. Hwang, J. and L. Qi, *Quality Control in the Endoplasmic Reticulum: Crosstalk between ERAD and UPR pathways.* Trends Biochem Sci, 2018. 43(8): p. 593-605.
28. Carvalho, P., V. Goder, and T.A. Rapoport, *Distinct ubiquitin-ligase complexes define convergent pathways for the degradation of ER proteins.* Cell, 2006. 126(2): p. 361-73.
29. Gardner, R.G., et al., *Endoplasmic reticulum degradation requires lumen to cytosol signaling. Transmembrane control of Hrd1p by Hrd3p.* J Cell Biol, 2000. 151(1): p. 69-82.
30. Hampton, R.Y., R.G. Gardner, and J. Rine, *Role of 26S proteasome and HRD genes in the degradation of 3-hydroxy-3-methylglutaryl-CoA reductase, an integral endoplasmic reticulum membrane protein.* Mol Biol Cell, 1996. 7(12): p. 2029-44.
31. Bhattacharya, A. and L. Qi, *ER-associated degradation in health and disease - from substrate to organism.* J Cell Sci, 2019. 132(23).
32. Vashistha, N., et al., *Direct and essential function for Hrd3 in ER-associated degradation.* Proc Natl Acad Sci U S A, 2016. 113(21): p. 5934-9.
33. Wu, X. and T.A. Rapoport, *Mechanistic insights into ER-associated protein degradation.* Curr Opin Cell Biol, 2018. 53: p. 22-28.
34. Schoebel, S., et al., *Cryo-EM structure of the protein-conducting ERAD channel Hrd1 in complex with Hrd3.* Nature, 2017. 548(7667): p. 352-355.
35. Sha, H., et al., *The ER-associated degradation adaptor protein Sel1L regulates LPL secretion and lipid metabolism.* Cell Metab, 2014. 20(3): p. 458-70.
36. Wu, S.A., et al., *The mechanisms to dispose of misfolded proteins in the endoplasmic reticulum of adipocytes.* Nat Commun, 2023. 14(1): p. 3132.
37. Bhattacharya, A., et al., *Hepatic Sel1L-Hrd1 ER-associated degradation (ERAD) manages FGF21 levels and systemic metabolism via CREBH.* EMBO J, 2018. 37(22).
38. Wei, J., et al., *HRD1-ERAD controls production of the hepatokine FGF21 through CREBH polyubiquitination.* EMBO J, 2018. 37(22).

39. Kim, G.H., et al., *Hypothalamic ER-associated degradation regulates POMC maturation, feeding, and age-associated obesity.* J Clin Invest, 2018. 128(3): p. 1125-1140.
40. Shi, G., et al., *ER-associated degradation is required for vasopressin prohormone processing and systemic water homeostasis.* J Clin Invest, 2017. 127(10): p. 3897-3912.
41. Yoshida, S., et al., *Endoplasmic reticulum-associated degradation is required for nephrin maturation and kidney glomerular filtration function.* J Clin Invest, 2021. 131(7).
42. Shrestha, N., et al., *Sel1L-Hrd1 ER-associated degradation maintains beta cell identity via TGF-beta signaling.* J Clin Invest, 2020. 130(7): p. 3499-3510.
43. Toda, C., et al., *POMC Neurons: From Birth to Death.* Annu Rev Physiol, 2017. 79: p. 209-236.
44. Bumaschny, V.F., et al., *Obesity-programmed mice are rescued by early genetic intervention.* J Clin Invest, 2012. 122(11): p. 4203-12.
45. Munzberg, H., et al., *Role of signal transducer and activator of transcription 3 in regulation of hypothalamic proopiomelanocortin gene expression by leptin.* Endocrinology, 2003. 144(5): p. 2121-31.
46. Liu, H., et al., *STAT3 phosphorylation in central leptin resistance.* Nutr Metab (Lond), 2021. 18(1): p. 39.
47. Baumann, H., et al., *The full-length leptin receptor has signaling capabilities of interleukin 6-type cytokine receptors.* Proc Natl Acad Sci U S A, 1996. 93(16): p. 8374-8.
48. Chen, H., et al., *Evidence that the diabetes gene encodes the leptin receptor: identification of a mutation in the leptin receptor gene in db/db mice.* Cell, 1996. 84(3): p. 491-5.
49. Uotani, S., et al., *Functional properties of leptin receptor isoforms: internalization and degradation of leptin and ligand-induced receptor downregulation.* Diabetes, 1999. 48(2): p. 279-86.
50. Plemper, R.K., et al., *Genetic interactions of Hrd3p and Der3p/Hrd1p with Sec61p suggest a retro-translocation complex mediating protein transport for ER degradation.* J Cell Sci, 1999. 112 (Pt 22): p. 4123-34.
51. Sun, S., et al., *Sel1L is indispensable for mammalian endoplasmic reticulum-associated degradation, endoplasmic reticulum homeostasis, and survival.* Proc Natl Acad Sci U S A, 2014. 111(5): p. E582-91.
52. Cao, L., et al., *Global site-specific analysis of glycoprotein N-glycan processing.* Nat Protoc, 2018. 13(6): p. 1196-1212.
53. Nunziata, A., et al., *Functional and Phenotypic Characteristics of Human Leptin Receptor Mutations.* J Endocr Soc, 2019. 3(1): p. 27-41.
54. Saeed, S., et al., *Genetic variants in LEP, LEPR, and MC4R explain 30% of severe obesity in children from a consanguineous population.* Obesity (Silver Spring), 2015. 23(8): p. 1687-95.
55. Saeed, S., et al., *High morbidity and mortality in children with untreated congenital deficiency of leptin or its receptor.* Cell Rep Med, 2023. 4(9): p. 101187.
56. Peelman, F., et al., *20 years of leptin: insights into signaling assemblies of the leptin receptor.* J Endocrinol, 2014. 223(1): p. T9-23.

57. Moharana, K., et al., *Structural and mechanistic paradigm of leptin receptor activation revealed by complexes with wild-type and antagonist leptins.* Structure, 2014. 22(6): p. 866-77.
58. Tsirigotaki, A., et al., *Mechanism of receptor assembly via the pleiotropic adipokine Leptin.* Nat Struct Mol Biol, 2023. 30(4): p. 551-563.
59. Zhou, Z., et al., *Endoplasmic reticulum-associated degradation regulates mitochondrial dynamics in brown adipocytes.* Science, 2020. 368(6486): p. 54-60.
60. Hosoi, T., et al., *Endoplasmic reticulum stress induces leptin resistance.* Mol Pharmacol, 2008. 74(6): p. 1610-9.
61. Heifetz, A., R.W. Keenan, and A.D. Elbein, *Mechanism of action of tunicamycin on the UDP-GlcNAc:dolichyl-phosphate Glc-NAc-1-phosphate transferase.* Biochemistry, 1979. 18(11): p. 2186-92.
62. Qi, L., L. Yang, and H. Chen, *Detecting and quantitating physiological endoplasmic reticulum stress.* Methods Enzymol, 2011. 490: p. 137-46.
63. Yang, L., et al., *A Phos-tag-based approach reveals the extent of physiological endoplasmic reticulum stress.* PLoS One, 2010. 5(7): p. e11621.
64. Kamran, P., et al., *Parabiosis in mice: a detailed protocol.* J Vis Exp, 2013(80).

3.7 Figures and figure legends

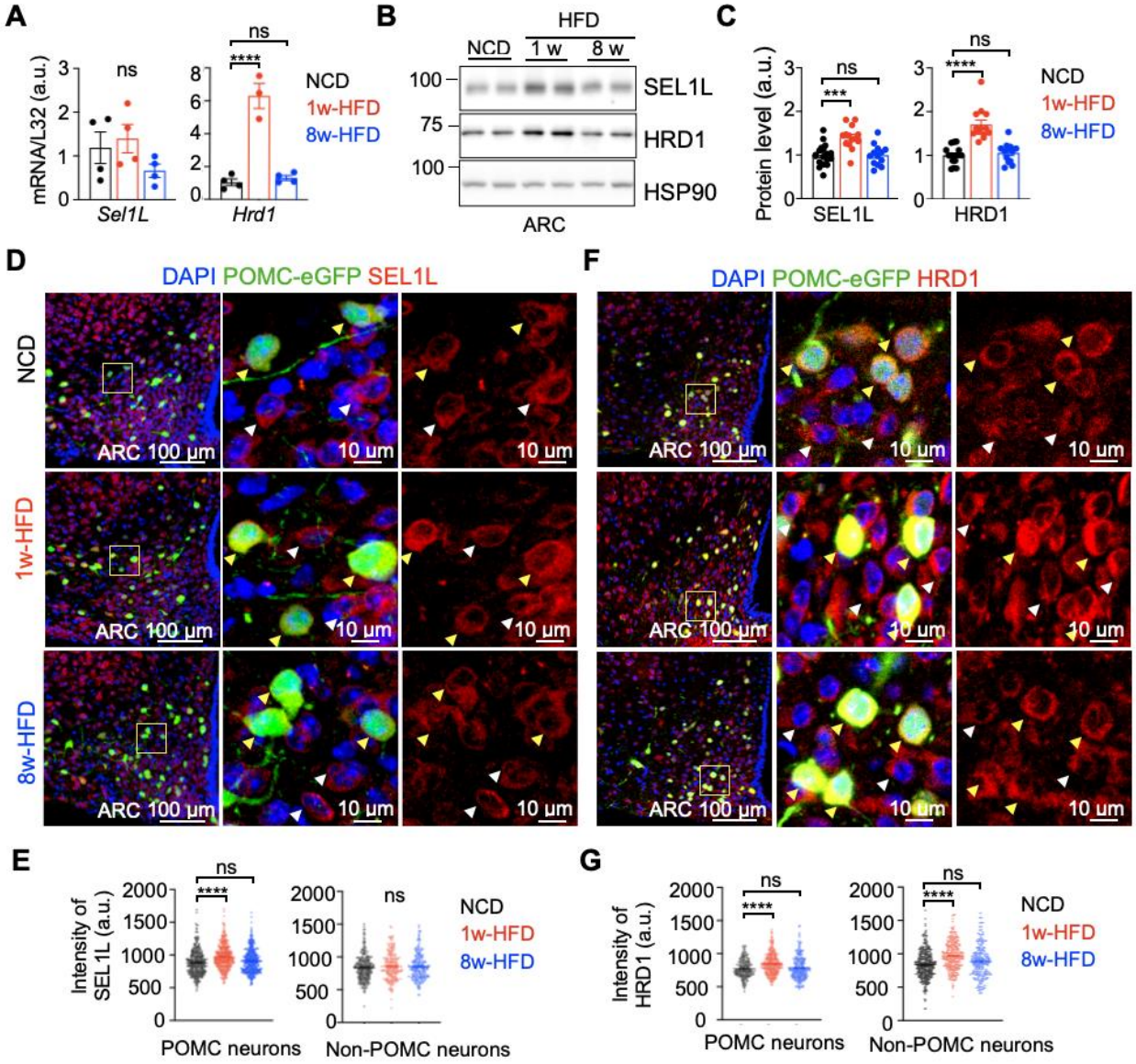

Figure 3.1 Transient upregulation of SEL1L-HRD1 ERAD expression in the hypothalamus in response to high fat diet (HFD) feeding.

(A) Quantitative PCR (qPCR) analysis of *Sel1L* and *Hrd1* mRNA levels in the arcuate nucleus (ARC) of the C57BL/6J male mice fed on normal chow diet (NCD), 1w- and 8w-HFD (n=3-4 mice per group).

(B-C) Representative Western blot of SEL1L and HRD1 in the ARC of the C57BL/6J male mice fed on NCD, 1w- and 8w-HFD, with quantitation shown on the right (n=13-15 mice per group).

(D-E, F-G) Representative images and quantitation of IF staining of SEL1L (D-E) and HRD1 (F-G) in the ARC of POMC-eGFP mice fed NCD, or HFD for 1-week or 8-week (n=3-4 mice per group, 70-100 POMC and non-POMC cells respectively per mice). Yellow arrows, GFP-positive POMC neurons; White arrows, GFP-negative non-POMC neurons.

Values, mean ± SEM. ns., not significant; *p<0.05, **p<0.01, ***p<0.001 and ****p<0.0001 by one-way ANOVA followed by Tukey's multiple comparisons test (A, C, E, G).

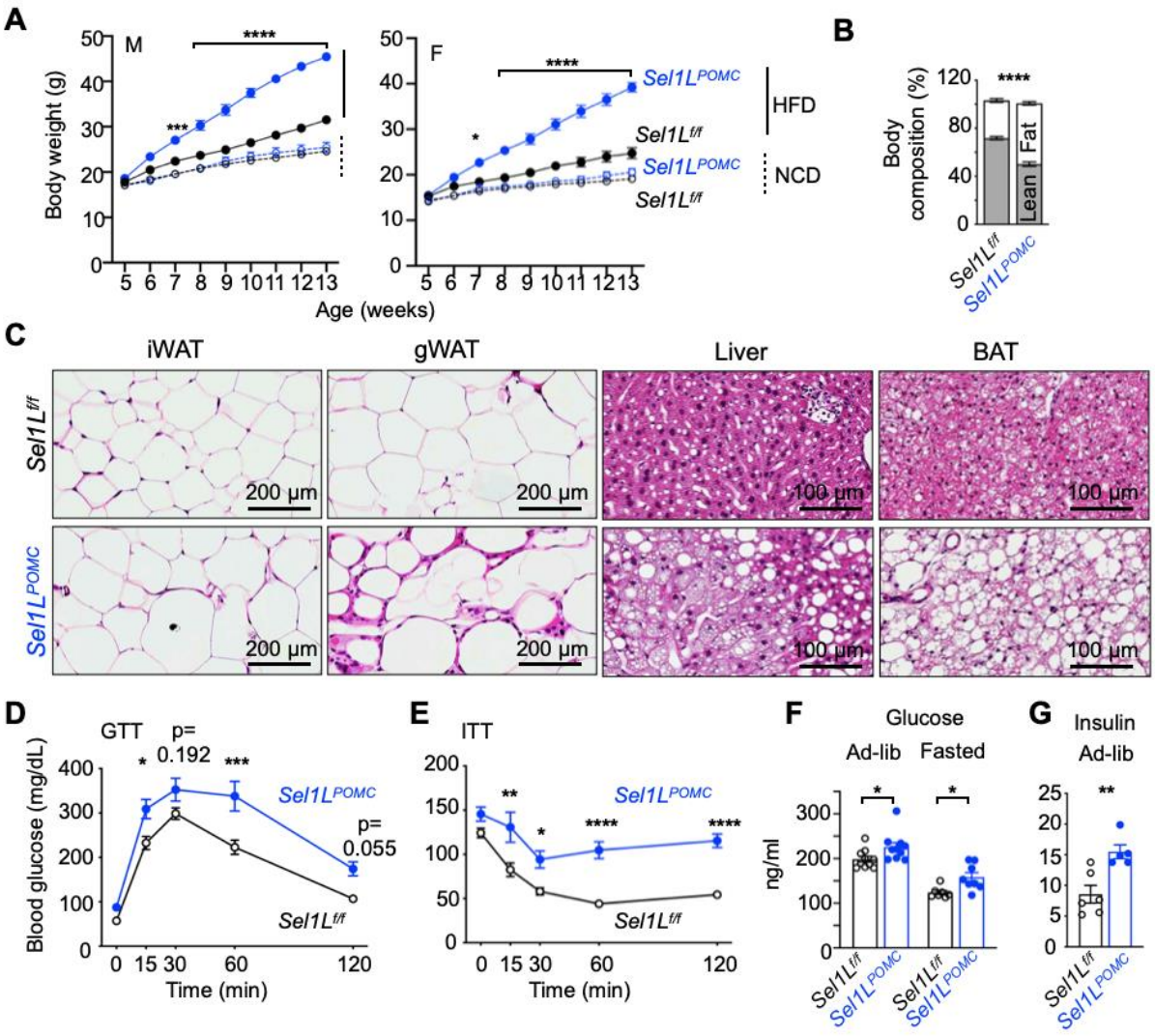

Figure 3.2 Hypothalamic POMC-specific ERAD deficiency leads to early-set DIO and its pathologies.

(A) Growth curve of *Sel1L*$^{f/f}$ and *Sel1L*^{POMC} mice, male (left) and female (right), fed on NCD (open symbols/dotted lines) or HFD (solid symbols/lines) (n=18-24 per group for male mice, n=10-16 per group for female mice).

(B) Body composition of *Sel1L*$^{f/f}$ and *Sel1L*^{POMC} male mice after 8w-HFD (n=4-7 mice per group).

(C) H&E images of peripheral tissues from male mice fed HFD for 8 weeks (n=3 mice per group). iWAT and gWAT, inguinal and gonadal white adipose tissues; BAT, brown adipose tissues.

(D-E) Glucose tolerance (D) and insulin tolerance tests (E) in male mice fed HFD for 8 weeks. Mice were fasted for 16 or 6 hours prior to glucose (2 g/kg body weight) or insulin (1 unit/kg body weight) injection, respectively (n=6 mice per group).

(F) Serum glucose in 8w-HFD male mice, either ad-lib or after 6h-fasting (n=7-10 mice per group).

(G) Insulin levels in 8w-HFD male mice under ad-lib condition (n=5-6 mice per group).

Values, mean ± SEM. ns, not significant; *p<0.05, **p<0.01, ***p<0.001 and ****p<0.0001 by two-way ANOVA followed by multiple comparisons test (A-B, D-F) or two-tailed Student’s t-test (G).

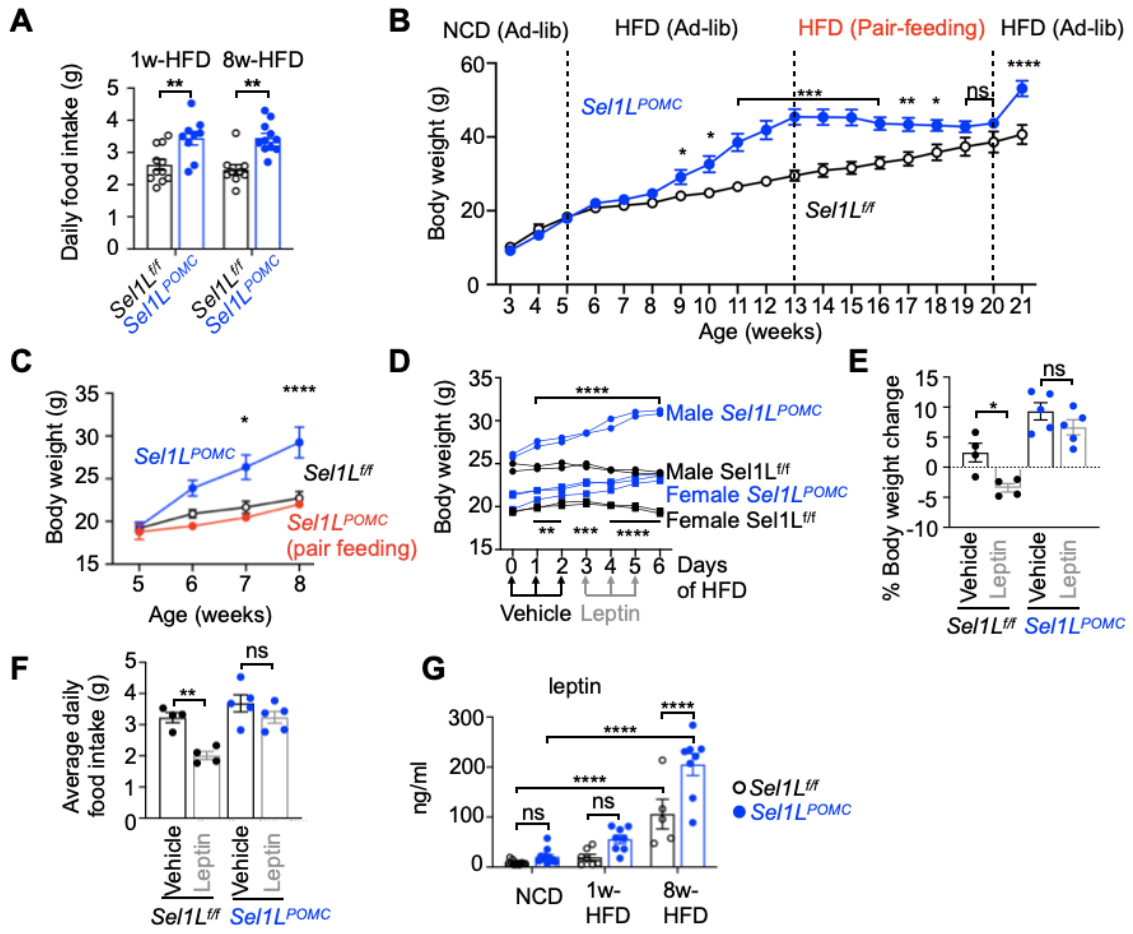

Figure 3.3 Hypothalamic ERAD deficiency triggers hyperphagia and leptin resistance.

(A) Daily food intake of male *Sel1L*$^{f/f}$ and *Sel1L*^{POMC} mice at 1w- and 8w-HFD (n=9-11 mice per group).

(B) Growth curve of male *Sel1L*^{POMC} mice fed with either NCD or HFD under ad libitum or pair feeding as indicated (n=3 mice per group, blue solid circles). Male *Sel1L*$^{f/f}$ mice fed ad libitum with the same diets were included as controls (n=3 mice per group, black open circles)

(C) Growth of *Sel1L*^{POMC} male mice with either ad libitum or pair-feeding of HFD starting at 5 weeks of age (n=3-5 mice per group).

(D) Body weights of 12-week-old mice put on HFD (at day 0) followed by daily i.p. injected with vehicle (PBS) and leptin (2 mg/kg body weight) for 3 days (n=2 per group for male mice, indicated in dots; n=2-3 per group for female mice, indicated in squares).

(E-F) Percentage of body weight change (E), average daily food intake (F) following 3 daily vehicle and leptin injections of the mice (n=2 per group for male mice, indicated in dots; n=2-3 per group for female mice). % Body weight is calculated based on the body weights at the end point over those at the starting point for each treatment.

(G) Serum leptin levels in mice fed on NCD, 1w- and 8w-HFD (n=5-13 mice per group). Values, mean ± SEM. ns, not significant; *p<0.05, **p<0.01, ***p<0.001 and ****p<0.0001 by two-way ANOVA followed by multiple comparisons test (A-G).

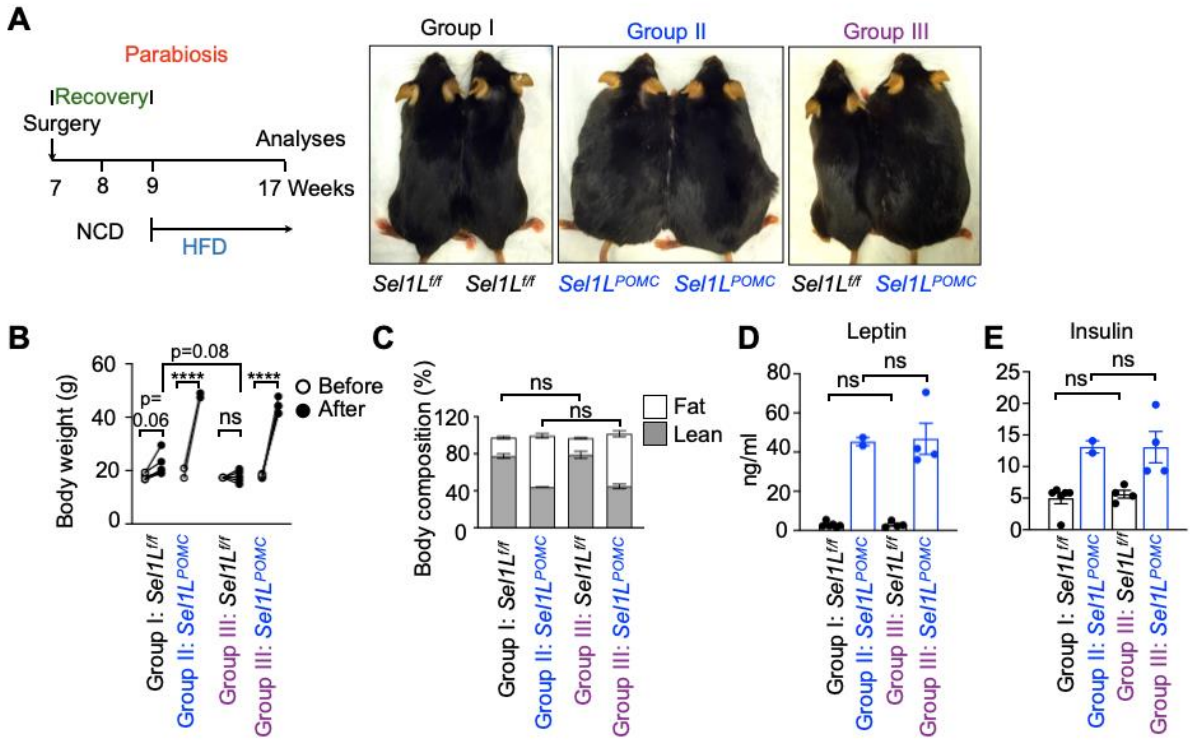

Figure 3.4 Hypothalamic SEL1L-HRD1 deficiency leads to DIO via leptin signaling.
(A) Schematic diagram for parabiosis and pictures (right) of *Sel1L*$^{f/f}$ and *Sel1L*^{POMC} female mice after parabiosis HFD for 8 weeks (n=3 pairs in group I, n=1 pair in group II, n=5 pairs in group III).
(B-C) Body weights (B) of mice before and after parabiosis and body composition (C) after parabiosis following 8-week HFD for 8 weeks (n=6 mice in group I, n=2 mice in group II, n=5 mice per genotype in group III).
(D-E) Serum leptin (D) and insulin (E) levels of mice after parabiosis HFD for 8 weeks (n=6 mice in group I, n=2 mice in group II, n=5 mice per genotype in group III).
Values, mean ± SEM. ns, not significant; *p<0.05, **p<0.01, ***p<0.001 and ****p<0.0001 by two-way ANOVA followed by multiple comparisons test (B-E).

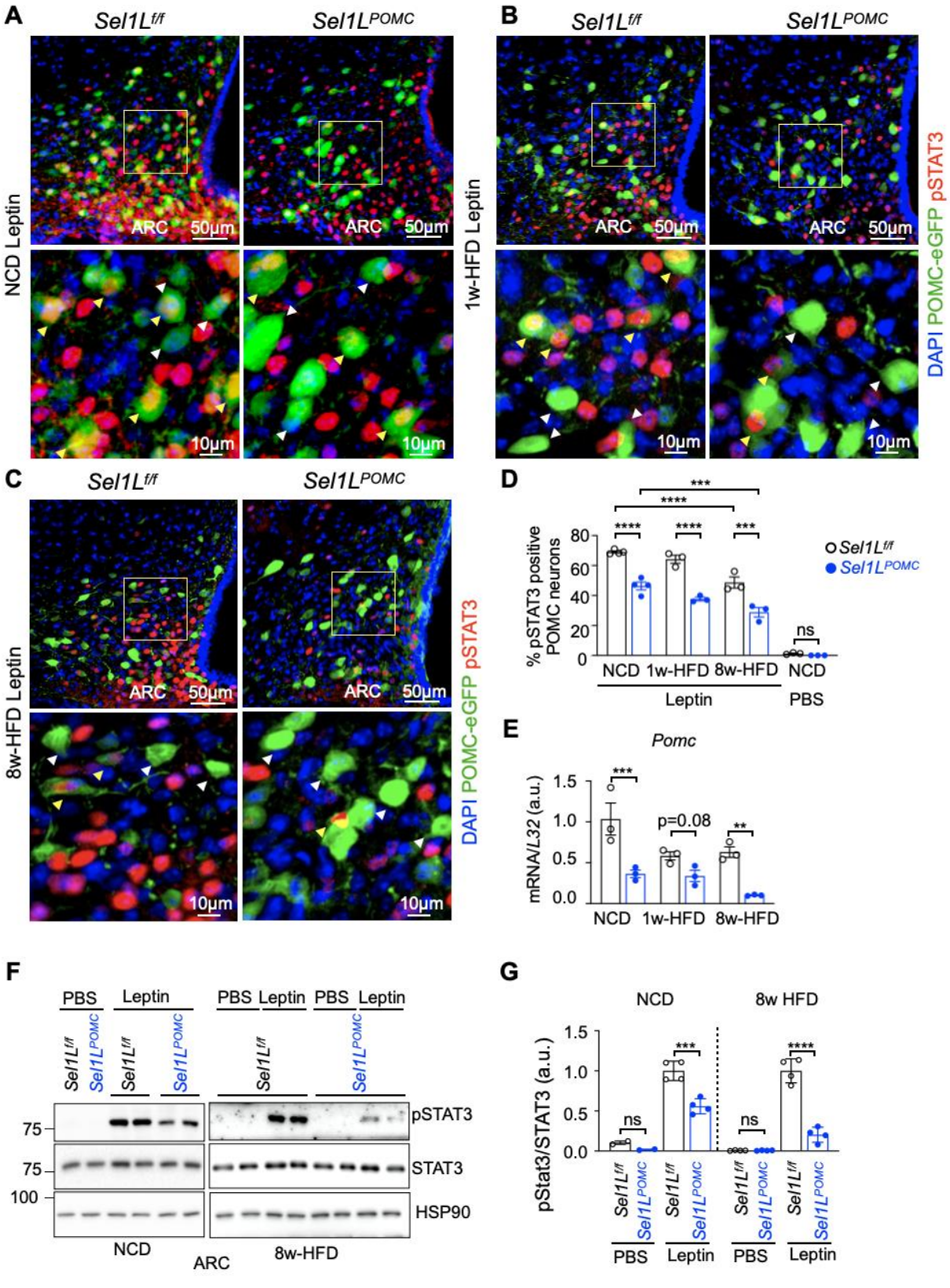
A
Sel1L f/f
Sel1L POMC
NCD Leptin
ARC
50μm
10μm
B
1w-HFD Leptin
DAPI POMC-eGFP pSTAT3
C
8w-HFD Leptin
D
% pSTAT3 positive POMC neurons
Sel1L f/f
Sel1L POMC
NCD 1w-HFD 8w-HFD NCD
Leptin
PBS
ns
E
Pomc
mRNA/L32 (a.u.)
p=0.08
F
PBS Leptin PBS Leptin PBS Leptin
pSTAT3
STAT3
HSP90
75
100
NCD
8w-HFD
ARC
G
NCD
8w HFD
pStat3/STAT3 (a.u.)
PBS Leptin PBS Leptin

Figure 3.5 Hypothalamic SEL1L-HRD1 ERAD deficiency impairs leptin-pSTAT3 signaling.
(A-D) Representative immunofluorescence (IF) staining of pSTAT3 in *Sel1L*$^{f/f}$;POMC-eGFP and *Sel1L*^{POMC};POMC-eGFP mice at NCD (A), 1w-HFD (B) and 8w-HFD (C), with quantitation shown in D. Mice were fasted for overnight (16hrs) and administrated with leptin (i.p., 2 mg/kg body weight) for 30 min (n=3-4 mice per group). Yellow arrows, pSTAT3 positive POMC neurons; White arrows, pSTAT3 negative POMC neurons. PBS-injected mice were included as negative controls and shown in Supplementary Fig. 3.
(E) Quantitative PCR (qPCR) analysis of *Pomc* mRNA expression levels in ARC of *Sel1L*$^{f/f}$ and *Sel1L*^{POMC} mice at 8w-HFD (n=3 mice per group).
(F-G) Representative Western blot for pSTAT3 in ARC of *Sel1L*$^{f/f}$ and *Sel1L*^{POMC} mice at NCD or 8w-HFD, injected with leptin or PBS for 30 min (n=4 male mice per group), with quantitation shown in G.
Values, mean ± SEM. ns, not significant; *p<0.05, **p<0.01, ***p<0.001 and ****p<0.0001 by two-way ANOVA followed by multiple comparisons test (D, E, G).

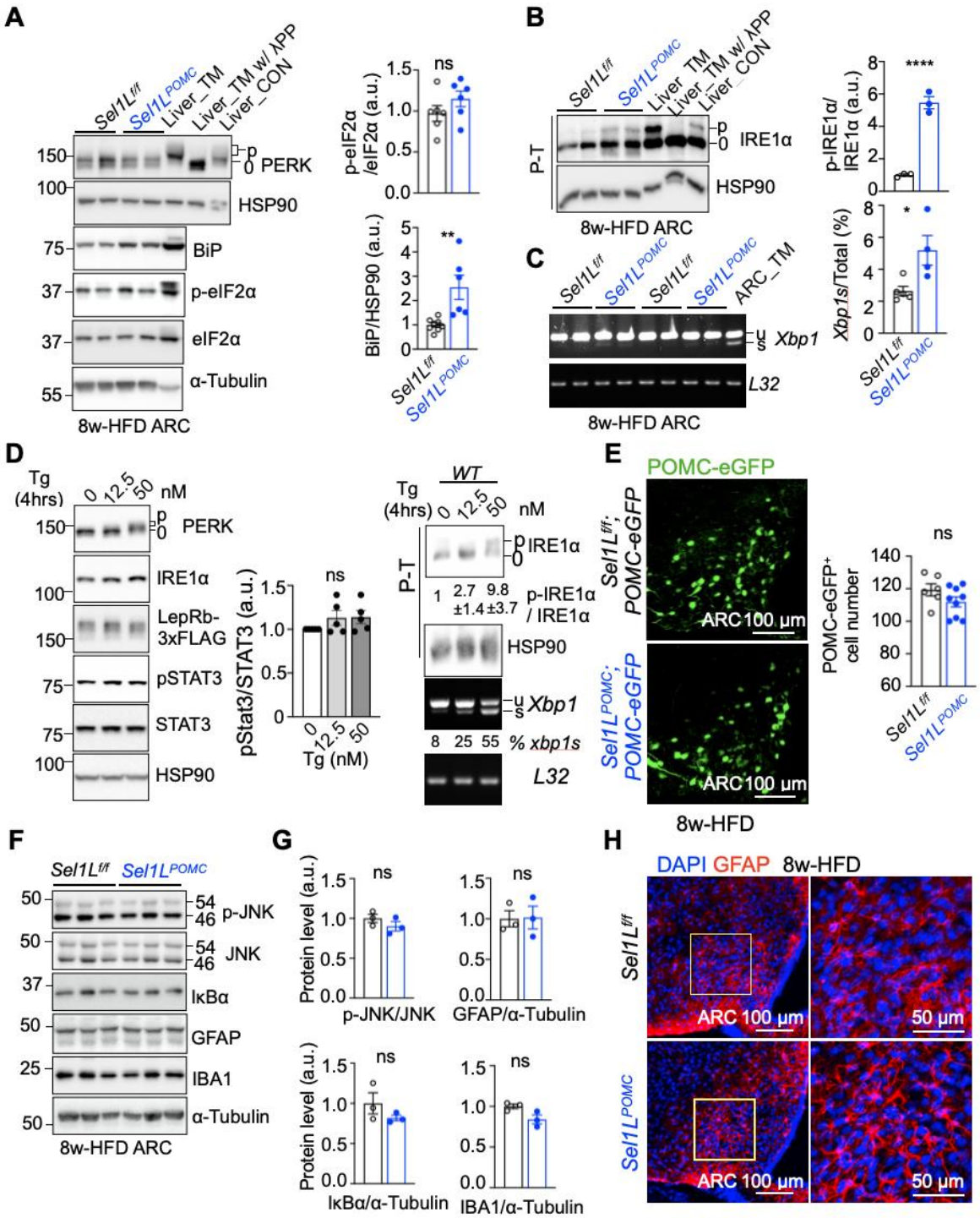

Figure 3.6 The effect of POMC-specific ERAD in DIO is likely uncoupled from UPR and inflammation.

(A) Representative Western blot for the PERK pathway of UPR in the ARC of *Sel1L*$^{f/f}$ and *Sel1L*^{POMC} mice fed on 8w-HFD (n=6 mice per group with 3 male mice and 3 female), with quantitation shown on the right. Livers of mice treated with tunicamycin (TM, 1 mg/kg, i.p.) for 24 hours (Liver_TM) or not (Liver_CON), as well as lysates treated with Lambda protein phosphatase, included as controls.

(B) Phostag gel (P-T)-based Western blot for IRE1α phosphorylation in the ARC of *Sel1L*$^{f/f}$ and *Sel1L*^{POMC} mice fed on 8w-HFD, with quantitation shown on the right (n=3 mice per group with 2 male and 1 female).
(C) Reverse transcriptase PCR (RT-PCR) analysis of *Xbp1* mRNA splicing (u, unspliced; s, spliced) in ARC of *Sel1L*$^{f/f}$ and *Sel1L*^{POMC} mice fed on 8w-HFD (n=2-3 male mice and n=2-3 female mice per group), with quantitation shown on the right. ARC of mice treated with tunicamycin (TM, 1 mg/kg, i.p.) for 24 hours (ARC_TM) included as a positive control.
(D) Representative assays for UPR and pSTAT3 in mLepRb-transfected HEK293T treated with leptin with/without Thapsigargin (Tg) (n=5 independent cell samples for SDS-PAGE gel, n=3 for P-T gel, two independent repeats for RT-PCR).
(E) Representative confocal images of the number of GFP-expressing POMC neurons in *Sel1L*$^{f/f}$;POMC-eGFP and *Sel1L*^{POMC};POMC-eGFP mice after 8w-HFD, with quantitation shown on the right (n=6-9 mice per group).
(F-G) Representative Western blot analysis of inflammatory markers in the ARC of *Sel1L*$^{f/f}$ and *Sel1L*^{POMC} mice fed on 8w-HFD, with quantitation shown in G (n=3 mice per group).
(H) Representative confocal images of GFAP, a marker of astrocytes, in the ARC of male *Sel1L*$^{f/f}$ and *Sel1L*^{POMC} mice fed on 8w-HFD (n=3 mice per group).
Values, mean ± SEM. ns, not significant; *p<0.05, **p<0.01, ***p<0.001 and ****p<0.0001 by two-way ANOVA followed by multiple comparisons test (D) or two-tailed Student's t-test (A-C, E, G).

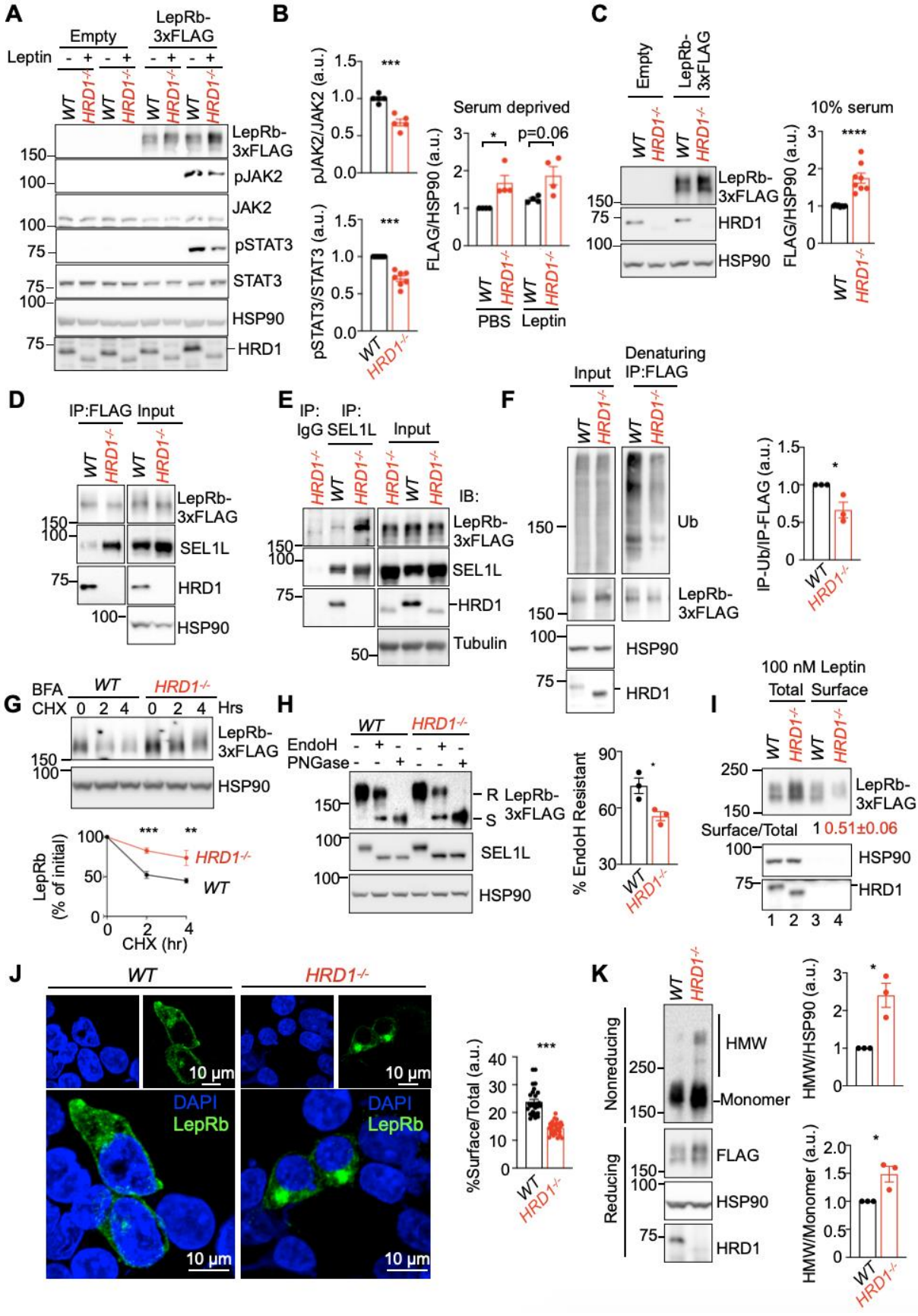
A
Empty
LepRb-3xFLAG
Leptin
WT
HRD1-/-
LepRb-3xFLAG
pJAK2
JAK2
pSTAT3
STAT3
HSP90
HRD1
150
100
75
B
pJAK2/JAK2 (a.u.)
pSTAT3/STAT3 (a.u.)
***
Serum deprived
FLAG/HSP90 (a.u.)
*
p=0.06
PBS
Leptin
C
Empty
LepRb-3xFLAG
HRD1
HSP90
10% serum
****
D
IP:FLAG
Input
SEL1L
E
IP: IgG
IP: SEL1L
IB:
Tubulin
50
F
Denaturing IP:FLAG
Ub
IP-Ub/IP-FLAG (a.u.)
G
BFA
CHX 0 2 4 0 2 4 Hrs
LepRb (% of initial)
CHX (hr)
**
H
EndoH
PNGase
R
S
% EndoH Resistant
I
100 nM Leptin
Total
Surface
Surface/Total
1 0.51±0.06
J
10 μm
DAPI
LepRb
%Surface/Total (a.u.)
K
Nonreducing
Reducing
HMW
Monomer
FLAG
HMW/HSP90 (a.u.)
HMW/Monomer (a.u.)

Figure 3.7 SEL1L-HRD1 is required for the maturation of nascent LepRb.
(A-B) Representative Western blot analysis for pJAK2, pSTAT3 and LepRb in HEK293T transfected with or without mLepR, treated with or without leptin (A), with quantitation shown in (B) (n=4-7 individual cell samples per group).
(C) Representative Western blot analysis of mLepRb protein levels in mLepRb-transfected HEK293T in complete medium (DMEM w/ 10% FBS), with quantitation shown on the right (n=8 individual cell samples per group).
(D-E) Representative Western blot analysis of interaction between SEL1L-HRD and mLepRb following immunoprecipitation (IP) of Flag (D) or SEL1L (E) from lysates of mLepRb-transfected HEK293T (n=2-3 individual cell samples).
(F) Representative Western blot analysis of Ub following denaturing immunoprecipitation (IP) of Flag from lysates of mLepRb-transfected HEK293T, with quantitation shown on the right (n=3 individual cell samples per group).
(G) Representative Western blot analysis of LepRb protein decay in LepRb-transfected HEK293T cells co-treated with protein trafficking inhibitor Brefeldin-A and translation inhibitor cycloheximide (CHX) for the 0, 2 and 4 hours, with quantitation shown below (n=4 individual cell samples per group).
(H) Representative Western blot analysis of LepRb glycosylation in LepRb-transfected HEK293T with EndoH and PNGase treatment, with quantitation shown on the right (n=3 individual cell samples per group).
(I) Representative Western blot analysis of mLepRb membrane display by surface biotinylation and streptavidin-bead pull down assay in mLepRb-transfected HEK293T treated with leptin. T, total lysate; S, surface fraction. (n=2 individual cell samples per group).
(J) Representative IF images of LepRb in mLepRb-transfected HEK293T treated with leptin, with quantitation of %surface signals over total shown on the right (n=28 cells per genotype from 3 independent repeats).
(K) Reducing and non-reducing SDS-PAGE and Western blot analysis of LepRb high molecular-weight aggregates of LepRb in mLepRb-transfected WT and HRD1$^{-/-}$ HEK293T, with quantitation shown on the right (n=3 individual cell samples per group).
Values, mean ± SEM. ns, not significant; *p<0.05, **p<0.01, ***p<0.001 and ****p<0.0001 by two-tailed Student's t-test (A, C, F, H, J, K) or two-way ANOVA followed by multiple comparisons test (B, G).

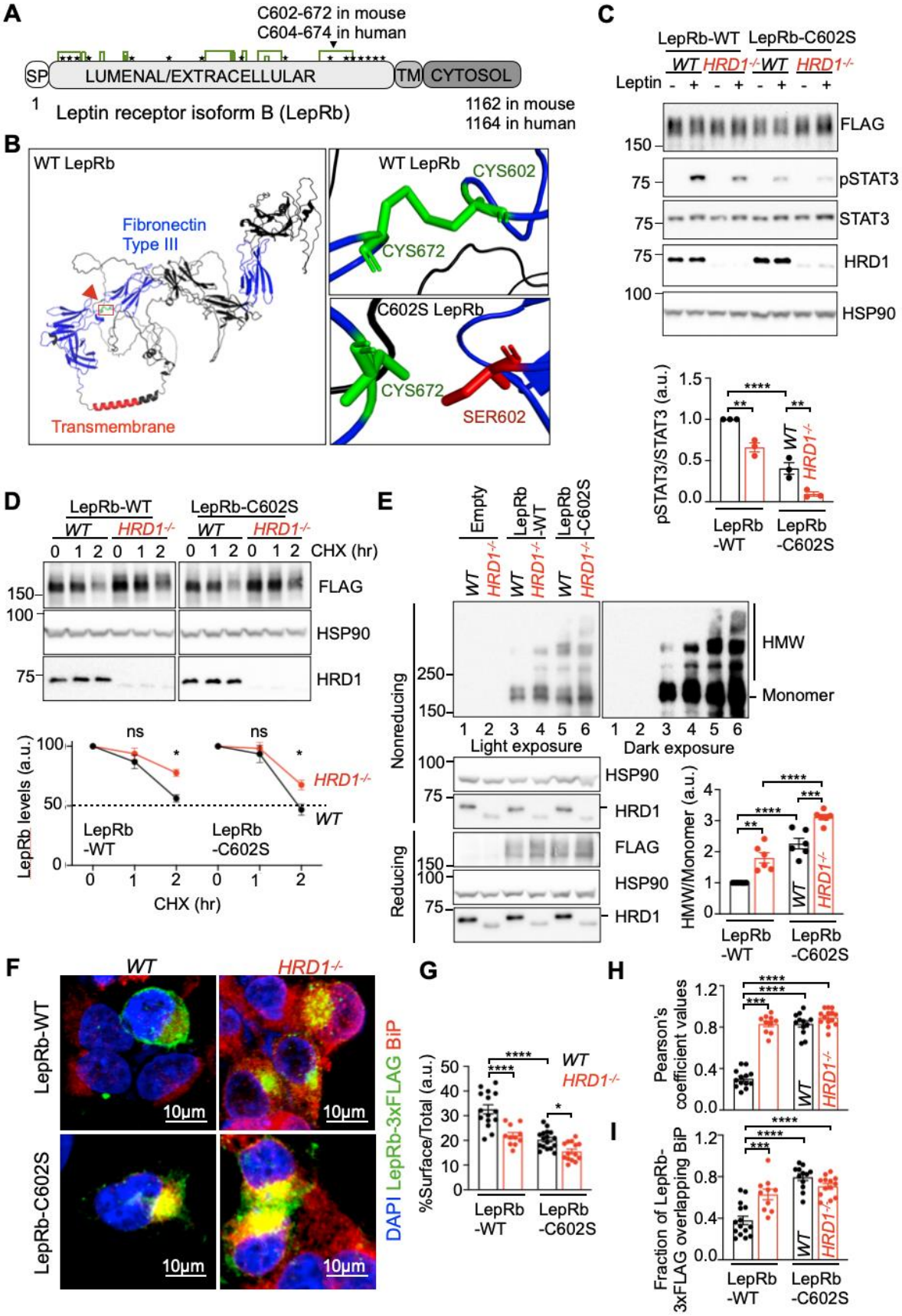
A
C602-672 in mouse
C604-674 in human
SP
LUMENAL/EXTRACELLULAR
TM
CYTOSOL
1
Leptin receptor isoform B (LepRb)
1162 in mouse
1164 in human
B
WT LepRb
Fibronectin
Type III
Transmembrane
WT LepRb
CYS602
CYS672
C602S LepRb
CYS672
SER602
C
LepRb-WT
LepRb-C602S
WT
HRD1-/-
WT
HRD1-/-
Leptin - + - + - + - +
150
75
75
100
FLAG
pSTAT3
STAT3
HRD1
HSP90
pSTAT3/STAT3 (a.u.)
1.5
1.0
0.5
0.0
LepRb -WT
LepRb -C602S
D
LepRb-WT
LepRb-C602S
WT
HRD1-/-
WT
HRD1-/-
0 1 2 0 1 2 0 1 2 0 1 2 CHX (hr)
150
100
75
FLAG
HSP90
HRD1
LepRb levels (a.u.)
100
50
0
ns
ns
*
*
HRD1-/-
WT
LepRb -WT
LepRb -C602S
0 1 2 0 1 2
CHX (hr)
E
Empty
LepRb -WT
LepRb -C602S
WT
HRD1-/-
WT
HRD1-/-
WT
HRD1-/-
Nonreducing
250
150
HMW
Monomer
1 2 3 4 5 6 1 2 3 4 5 6
Light exposure
Dark exposure
Reducing
100
75
HSP90
HRD1
150
100
75
FLAG
HSP90
HRD1
HMW/Monomer (a.u.)
4
3
2
1
0
LepRb -WT
LepRb -C602S
F
WT
HRD1-/-
LepRb-WT
LepRb-C602S
10μm
DAPI LepRb-3xFLAG BiP
G
%Surface/Total (a.u.)
50
40
30
20
10
0
WT
HRD1-/-
LepRb -WT
LepRb -C602S
H
Pearson's coefficient values
1.2
0.8
0.4
0.0
WT
HRD1-/-
I
Fraction of LepRb-3xFLAG overlapping BiP
1.2
0.8
0.4
0.0
LepRb -WT
LepRb -C602S

Figure 3.8 SEL1L-HRD1 ERAD degrades and limits the pathogenicity of LepRb Cys602Ser disease mutant.
(A) Schematic diagram of mouse LepRb. “SP”, Signal Peptide; “TM”, Transmembrane. Star symbols, N-glycosylation sites; Green lines, disulfide bonds.
(B) Structural modeling of mouse LepRb by AlphaFold2. Red arrow, location of human mutation C604S (mouse C602S).
(C) Representative Western blot analysis for pSTAT3 in HEK293T transfected with mLepRb-WT or mLepRb-C602S with or without leptin treatment, with quantitation shown below (n=3 individual cell samples per group).
(D) Representative Western blot analysis of LepRb protein decay in WT and HRD1$^{-/-}$ HEK293T transfected with mLepRb-WT or -C602S, treated with brefeldin-A and cycloheximide (CHX) for the 0, 1 and 2 hours, with quantitation shown below (n=4 individual cell samples per group).
(E) Reducing and non-reducing SDS-PAGE and Western blot analysis of LepRb high molecular-weight (HMW) aggregates of LepRb in WT and HRD1$^{-/-}$ HEK293T transfected with mLepRb-WT or -C602S, with quantitation shown on the right (n=6 individual cell samples per group).
(F-I) Representative IF images of mLepRb-WT and -C602S in transfected WT and HRD1$^{-/-}$ HEK293T cells (F) with quantitation %surface signals over total (G) (n=11-17 cells per group) and analysis of co-localization of LepRb with BiP signals by Pearson correlation coefficient (H) and Manders overlap coefficient (I) (n=10-14 cells per group). Values, mean ± SEM. ns, not significant; *p<0.05, **p<0.01, ***p<0.001 and ****p<0.0001 by two-way ANOVA followed by multiple comparisons test (C, D, E, G, H, I).

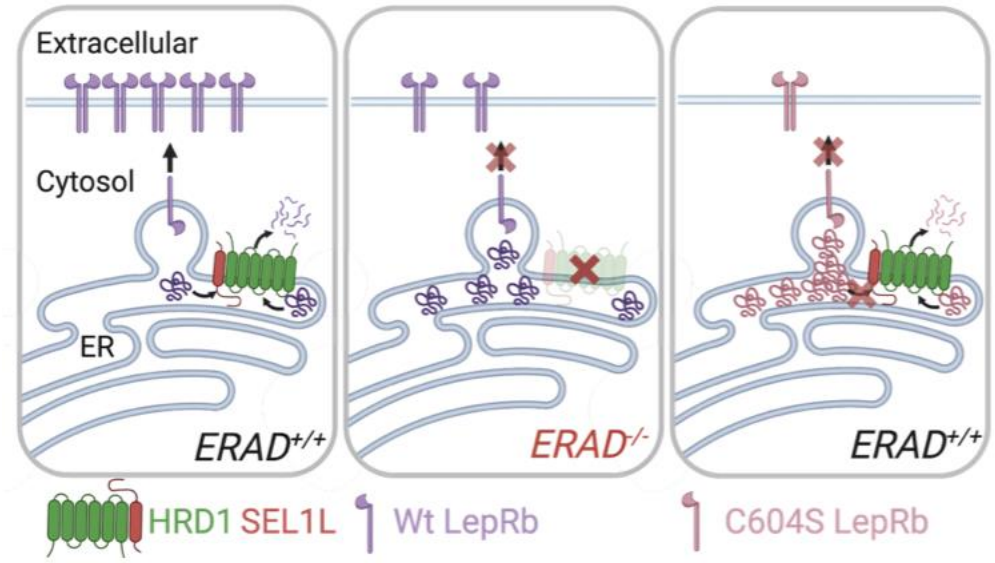

Figure 3.9 Proposed models for SEL1L-HRD1 ERAD degradation of wildtype LepRb and C604S disease mutant.
In the basal conditions, SEL1L-HRD1 ERAD constitutively degrades misfolded LepRb and ensures the proper folding, maturation and surface expression of the LepRb. In the absence of ERAD, the accumulation of misfolded receptors forms aggregates, interferes with the folding and maturation of the nascent LepRb with attenuated surface display. In the context of recessive LepRb C604S mutant, though degraded by SEL1L-HRD1 ERAD, C604S LepRb readily forms aggregates to the extent beyond the capacity of ERAD, resulting in impaired maturation and surface display of the receptors.

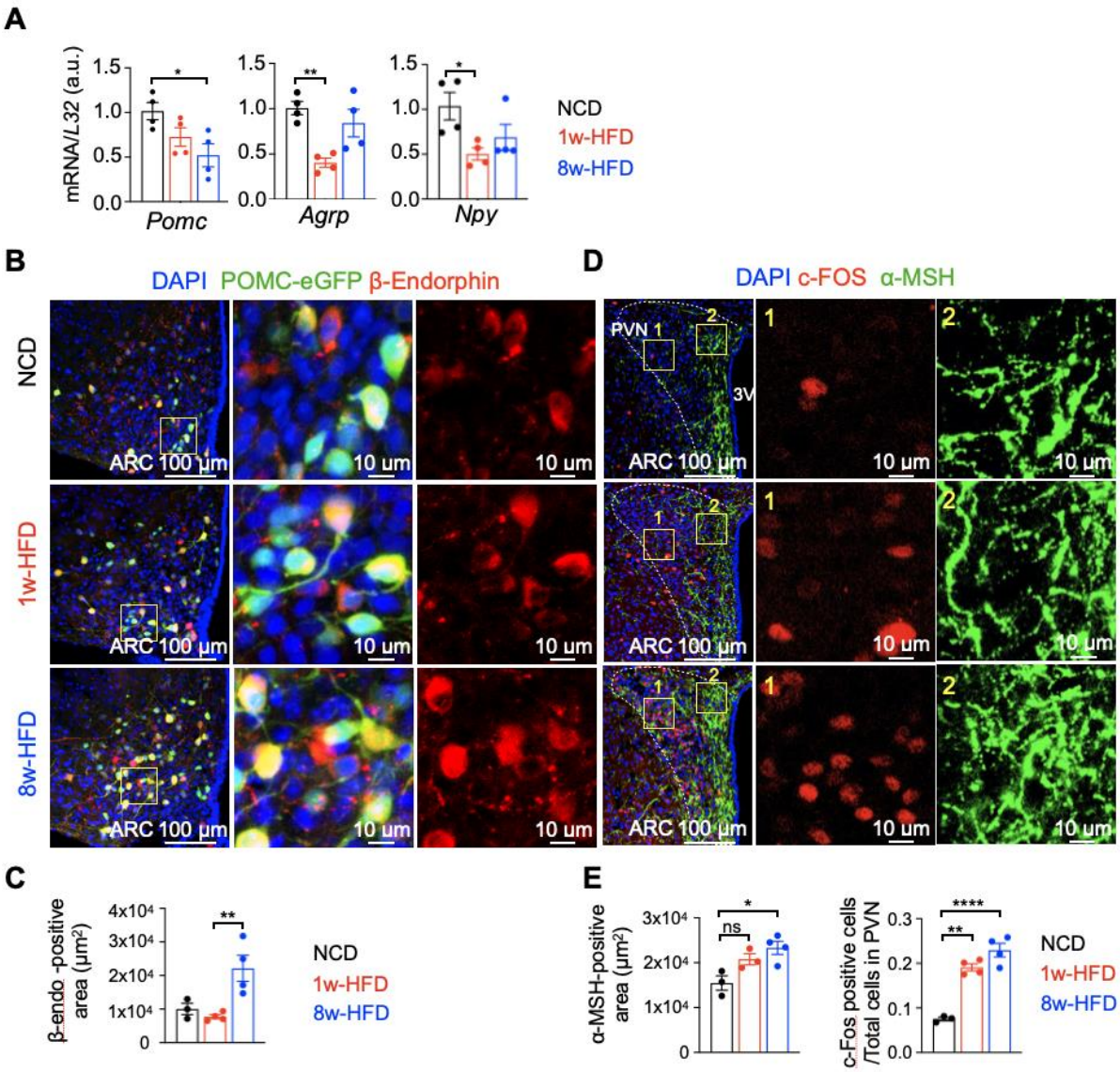

Figure 3.10 Altered hypothalamic proteostasis upon HFD.
(A) Quantitative PCR (qPCR) analysis of hormones and neurotrophins mRNA expression in the arcuate nucleus (ARC) of the C57BL/6J male mice fed on normal chow diet (NCD), 1w- and 8w-HFD (n=3-4 mice per group).
(B-C) IF staining and quantitation of β-endorphin in the ARC of male mice fed on NCD, 1w- and 8w-HFD. (n=3-4 mice per group).
(D-E) Co-IF staining and quantitation of α-MSH (green) and c-Fos (red) in the paraventricular nucleus (PVN) of male mice fed on NCD, 1w- and 8w-HFD (n=3-4 mice per group). 3V, third ventricle.
Values, mean ± SEM. ns, not significant; *p<0.05, **p<0.01, ***p<0.001 and ****p<0.0001 by one-way ANOVA followed by Tukey's multiple comparisons test (A, C, E).

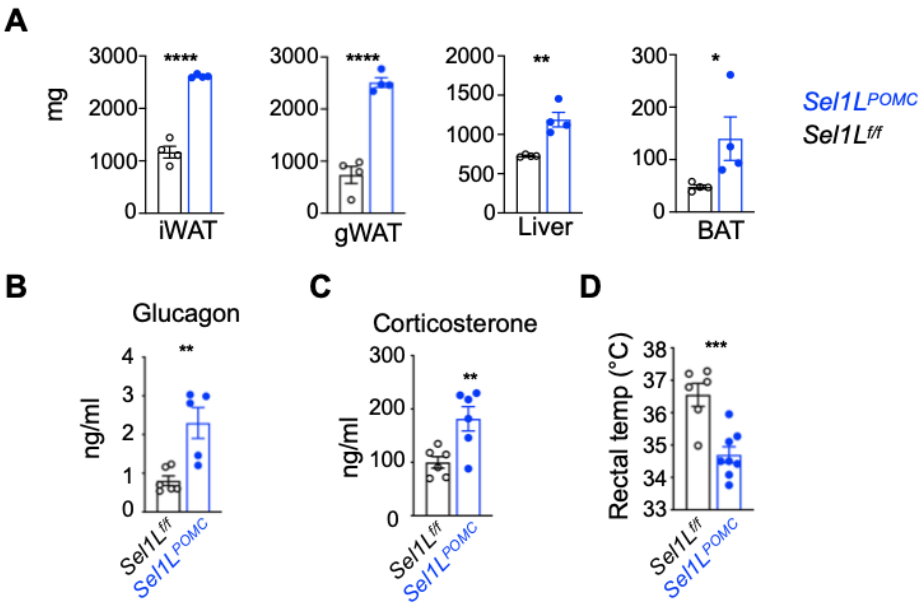

Figure 3.11 Metabolic characterization of *Sel1L$^{f/f}$* and *Sel1L^{POMC}* mice upon HFD.
(A) Tissue weight of *Sel1L$^{f/f}$* and *Sel1L^{POMC}* male mice after 8w-HFD (n=4 mice per group).
(B-C) Glucagon (B) and corticosterone (C) levels in male mice fed HFD for 8 weeks (n=5-6 mice per group).
(D) Rectal temperature of *Sel1L$^{f/f}$* and *Sel1L^{POMC}* male mice after 8w-HFD (n=6-8 mice per group).
Values, mean ± SEM. ns, not significant; *p<0.05, **p<0.01, ***p<0.001 and ****p<0.0001 by two-tailed Student's t-test (A-D).

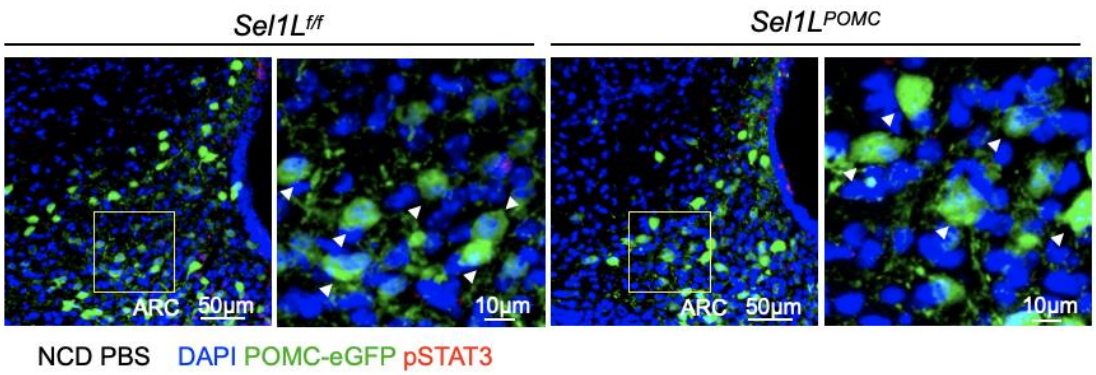

Figure 3.12 Leptin signaling in fasted *Sel1L$^{f/f}$* and *Sel1L^{POMC}* mice.
Representative immunofluorescence (IF) staining of pSTAT3 in *Sel1L$^{f/f}$*;POMC-eGFP and *Sel1L^{POMC}*;POMC-eGFP mice. Mice were fasted for overnight (16hrs) and administrated with PBS for 30 min (n=3 mice per group). White arrows, POMC neurons. Quantitation is shown in Fig. 5.

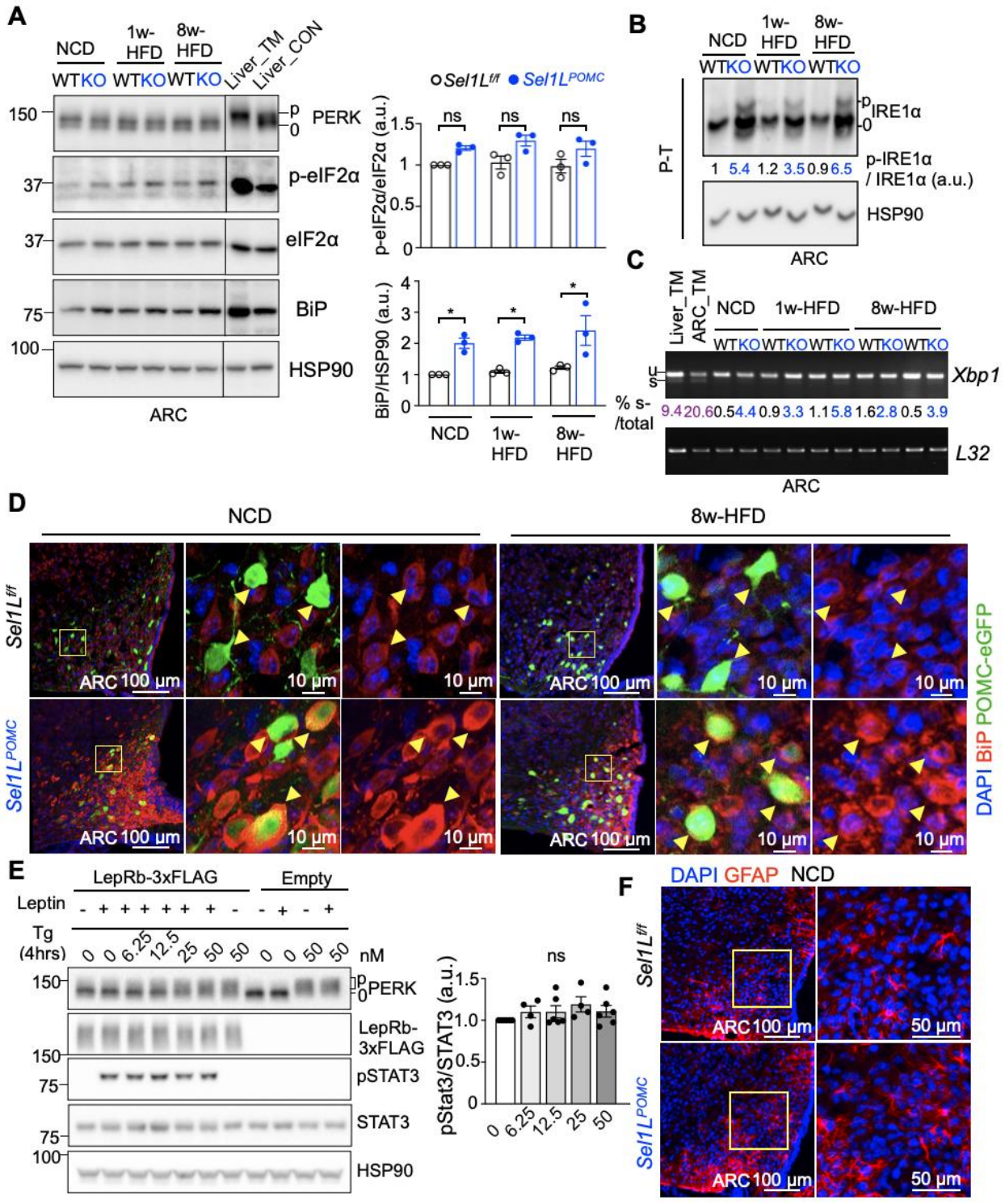

Figure 3.13 Analysis of UPR and inflammation in *Sel1L*$^{f/f}$ and *Sel1L*^{POMC} mice. **(A)** Representative Western blot for the PERK pathway of UPR in the ARC of *Sel1L*$^{f/f}$ and *Sel1L*^{POMC} mice fed on NCD, 1w- and 8w-HFD (n=3 mice per group), with quantitation shown on the right. Livers of mice treated with tunicamycin (TM, 1 mg/kg, i.p.) for 24 hours (Liver_TM) or not (Liver_CON), included as controls.

(B) Phostag-gel (P-T)-based Western blot for IRE1α phosphorylation in the ARC of *Sel1L*$^{f/f}$ (WT) and *Sel1L*^{POMC} (KO) mice fed on on NCD, 1w- and 8w-HFD (n=2 mice per group).
(C) Reverse transcriptase PCR (RT-PCR) analysis of *Xbp1* mRNA splicing (u, unspliced; s, spliced) in ARC of *Sel1L*$^{f/f}$ and *Sel1L*^{POMC} mice fed on NCD, 1w- and 8w-HFD (n=2 mice per group), with quantitation shown on the right. Liver and ARC of mice treated with tunicamycin (TM, 1 mg/kg, i.p.) for 24 hours (LIVER_TM, ARC_TM), included as controls.
(D) Representative confocal images of BiP in the ARC of *Sel1L*$^{f/f}$;POMC-eGFP and *Sel1L*^{POMC};POMC-eGFP mice fed on NCD and 8w-HFD. Yellow arrows, POMC neurons. (n=3 mice per group).
(E) Representative assays for pPERK and pSTAT3 in mLepRb-transfected HEK293T treated with leptin and treated with or without Thapsigargin (Tg), with quantitation shown on the right (n=4-6 independent cell samples).
(F) Representative confocal images of immunostaining of GFAP, a marker of astrocytes, in the ARC of *Sel1L*$^{f/f}$ and *Sel1L*^{POMC} mice fed on NCD (n=3 mice per group). NCD for normal chow diet; HFD for high fat diet. ARC, arcuate nucleus. Values, mean ± SEM. ns, not significant; *p<0.05, **p<0.01, ***p<0.001 and ****p<0.0001 by two-way ANOVA followed by multiple comparisons test (A) or one-way ANOVA followed by Tukey's multiple comparisons test (E).

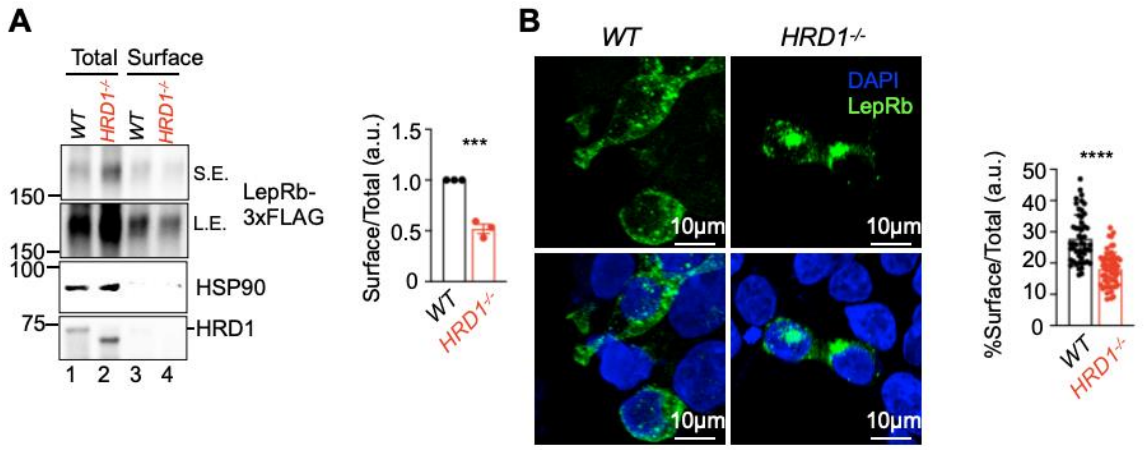

Figure 3.14 SEL1L-HRD1 deficiency reduces display of LepRb for leptin binding.
(A) Representative Western blot analysis of mLepRb membrane display by surface biotinylation and streptavidin-bead pull down assay in mLepRb-transfected HEK293T in complete medium (DMEM w/ 10% FBS), with quantitation shown on the right. T, total lysate; S, surface fraction. (n=3 individual cell samples per group).
(B) Representative IF images of LepRb in mLepRb-transfected HEK293T in compete medium, with quantitation of %surface signals over total shown on the right. (n=52-57 cells per group)
Values, mean ± SEM. ns, not significant; *p<0.05, **p<0.01, ***p<0.001 and ****p<0.0001 by two-tailed Student's t-test (A, B).

Chapter 4 The Role of SEL1L-HRD1 ERAD in Neuron-Astroglia Communication - An Insight from Astrotactin-1

Hancheng Mao[1], Liangguang Leo Lin[1,2], Ling Qi[2*]

[1]Department of Molecular & Integrative Physiology, University of Michigan Medical School, Ann Arbor, MI 48105, USA

[2] Department of Molecular Physiology and Biological Physics, University of Virginia, School of Medicine, Charlottesville, VA 22903, USA

Correspondence: xvr2hm@virginia.edu

The authors have declared that no conflict of interest exists.

Short title: Regulation of ASTN1 by SEL1L-HRD1 ERAD

Summary: Here we report that SEL1L-HRD1 ER-associated degradation is indispensable for ASTN1 protein quality control and functionality in mediating neuron-glia contacts by regulating the turnover and maturation of nascent leptin receptor in the ER.

Keywords: SEL1L-HRD1 ERAD, ASTN1, neuron-glia interaction

4.1 Abstract

To date, despite various studies investigating the unfolded protein response (UPR) and autophagy regulation in neurons and glia, the investigation of potential roles of endoplasmic reticulum-associated degradation (ERAD) in the central nervous system (CNS) is still very limited. Interestingly, our recent exploration of endogenous SEL1L-HRD1 ERAD substrates in different tissues and cell lines provided a variety of putative endogenous substrates in a cell type-specific manner. Particularly, astrotactin-1 (ASTN1) was identified as a neuron-specific target among the top hits from a proteomic screen in neuroblastoma cells (N2a), which engages in contacts between neuron and astrocytes. Here, we show comprehensive *in vitro* demonstration of ASTN1 as an endogenous substrate of SEL1L-HRD1 ERAD followed by *in vivo* characterization. This evidence, for the first time, sheds light on the potential role of SEL1L-HRD1 ERAD in regulating neuron-glia crosstalk.

4.2 Introduction

Approximately one third of proteins, particularly membrane and secretory proteins, pass through the endoplasmic reticulum (ER) during their maturation. Misfolding of these proteins occasionally occurs that, if not resolved efficiently and effectively, may result in protein aggregation and even accumulation of aggregates, leading to concomitant pathogenic consequences. To cope with the folding challenge, eukaryotic cells have evolved ER protein quality control systems including unfolded protein response (UPR), ER-associated degradation (ERAD) and autophagy (ER-phagy), In particular, ERAD is a constitutively active machinery maintaining both protein quantity and quality control. SEL1L-HRD1 ERAD, as the most conserved ERAD across mammals, has been reported to play vital patho-physiological roles in a cell type- and substrate-specific manner. Moreover, recent identification of human patients carrying SEL1L and HRD1 variants with ERAD-associated neurodevelopmental disorders with onset infancy syndrome (ENDI) further emphasize the importance of SEL1L-HRD1 in central nervous system (CNS)[1, 2]. We recently deciphered several proteome-wide endogenous SEL1L-HRD1 substrates in vitro (HEK293T cells) and in vivo (mouse brown adipose tissue) using SEL1L-IP based mass spectrometry (IP-MS)[3]. Despite recent advances in understanding the SEL1L-HRD1 complex, a lot remains unknown including how SEL1L-HRD1 regulates neuronal health and diseases potentially in a substrate specific manner in CNS.

Here, we identified a bona fide neuron-specific substrate of SEL1L-HRD1 ERAD, Astrotactin-1 (ASTN1), from SEL1L-IP based IP-MS in mouse neuroblastoma cell line (N2a). Both in vitro and in vivo characterization demonstrated that the quantity as well

as maturation of ASTN1 highly relies on SEL1L-HRD1 degradative activity. ASTN1 has been reported as a fundamental factor involved in gial-guided neuronal migration and synaptic plasticity via mediating neuron-glia physical contact[4-9]. Further, chromosomal mapping of astrotactin localizes the gene to human chromosome region associated with micrencephaly, the smaller brain size attributed to a variety of neurodevelopmental disorders in human patients exhibiting cerebral malformation and cerebellar hypoplasia[10, 11]. Consistently, mice lack of astrotactin exhibited slower granule cell migration, defective cerebellar cortical development and impaired coordinated balance and movement[12]. Hence, our study, for the first time, shines a light on the potential role of SEL1L-HRD1 in regulating neuron-glia contacts and communication, directly via substrate mediation, which is indispensable for proper neurodevelopment and function.

4.3 Results

Identification of ASTN1 as endogenous SEL1L-HRD1 ERAD substrate in N2a

We performed proteomics screen of the SEL1L interactome to identify ERAD substrates in N2a cells with or without SEL1L or HRD1, based on the notion that in the absence of HRD1 degradative activity, the interactions between SEL1L and substrates will be prolonged and more substrates can be pulled down by SEL1L IP (Figure 4.5A). Several protein candidates are selected with stringent cut-off criteria with higher signal detected only in *HRD1*$^{-/-}$ cells, and no or very low signal in WT and *SEL1L*$^{-/-}$ cells. Notably, ASTN1 showed up as one of the top hits (Figure 4.5B). The interaction between endogenous ASTN1 and endogenous SEL1L was confirmed (Figure 4.1A) along with detection of significantly increased ASTN1 protein abundance in *SEL1L*$^{-/-}$ and *HRD1*$^{-/-}$

cells (Figure 4.1B). Further, reciprocal immunoprecipitation of transfected ASTN1 also validated the interaction (Figure 4.1C). Moreover, the induction of ASTN1 protein levels in SEL1L-HRD1 deficient cells are independent of mRNA regulation (Figure 4.5C), suggesting post-translational regulation as major contributor to the altered protein turnover. Indeed, ASTN1 has several post-translational modifications, including six glycosylation sites and multiple intramolecular disulfide bonds (Figure 4.1D), requiring high demand in quality control for correct folding. ASTN1 is cleaved at the second transmembrane domain between Ser401 and Ser402, resulting two fragments that remain connected with a disulfide bond [13-15] (Figure 4.1D). Therefore, the major band of ASTN1 detected and shown using the available ASTN1 antibody will be around 130kDa (Figure 4.5D).

ASTN1 is a bona fide endogenous substrate of SEL1L-HRD1

To further demonstrate whether SEL1L-HRD1 indeed regulates post-translational turnover of the ASTN1, we performed cycloheximide (CHX) chase, which suggested that ASTN1 protein was unstable in WT N2a cells with a half-life less than 6 hours, but was completely stabilized in *SEL1L*$^{-/-}$ or *HRD1*$^{-/-}$ cells (Figure 4.2A). Further in *SEL1L*$^{-/-}$ or *HRD1*$^{-/-}$ N2a cells, ASTN1 accumulated and formed high molecular weight (HMW) aggregates mediated by disulfide bonds (Figure 4.2B), which decayed significantly slower in the absence of SEL1L or HRD1 (Figure 4.6A and B). The deficiency of SEL1L or HRD1 resulted in reduced polyubiquitination of ASTN1 (Figure 4.2C). Further investigation of cellular location of the accumulated ASTN1 aggregation in *SEL1L*$^{-/-}$ or *HRD1*$^{-/-}$ N2a cells using EndoH and PNGase treatment indicated that the majority, if not

all, of the ASTN1 increment was retained inside of the ER (Figure 4.6C). To our surprise, in the absence of glial cells, there was no evident EndoH resistant fraction of ASTN1 even in *WT* N2a (Figure 4.6C).

ASTN1 maturation is regulated by SEL1L-HRD1 in CNS

We then wondered whether ASTN1 was regulated by SEL1L-HRD1 ERAD in vivo. We first evaluated the protein level of ASTN1 widely across various tissues of peripheral and CNS, and detected high level of ASTN1 protein expression in CNS tissues, but relatively low, if not absent, in peripheral tissues (Figure 4.7A), though various brain regions express different levels and distinct forms of ASTN1 (Figure 4.7A and C). Thus, we focused on characterization of ASTN1 in mouse models with SEL1L deficiency in different neuron populations. We included mice with hypothalamic POMC neuron-specific SEL1L knockout (*SEL1L*^{POMC}) as well as mice deficient in SEL1L in CamKII-expressing neurons (*SEL1L*^{CamKII}). Strikingly, compared to control littermates (*SEL1L*$^{f/f}$) there are significant increase of ASTN1 only in regions with SEL1L deficient cell populations, including the ARC in *SEL1L*^{POMC} mice (Figure 4.3A) as well as the hippocampus and cortex in *SEL1L*^{CamK} mice (Figure 4.3D), but not in the unaffected regions such as the cerebellum in *SEL1L*^{CamK} mice (Figure 4.3D). Moreover, the increase of ASTN1 in the KO tissues were attributed to additional band with lower molecular weight (Figure 4.3A and D). Further EndoH digestion indicated that this extra smaller band is immature ASTN1 retained inside of the ER (Figure 4.3B, E and Figure 4.7B). Further the ER retention of the immature ASTN1 in SEL1L deficient neurons tended to form HMW aggregates (Figure 4.3C), consistent with the observation in vitro.

Hence, ASTN1 is a bona fide substrate of SEL1L-HRD1 ERAD, which accumulates and is retained if ERAD function is impaired in vitro and in vivo.

SEL1L-HRD1 deficiency in neurons alters neuron-glia plasticity with impaired neuronal activity

Considering the function of ASTN1 in mediating neuron-glia contacts, we then wonder whether the SEL1L deficiency in specific neurons may alter their contact with astrocytes. Immunofluorescent staining for GFAP as biomarker of astrocytes indicated increased astrogliosis in SEL1L deficient POMC neuron-enriched ARC region but not in other neighboring areas (Figure 4.4A and Figure 4.8A). There was putative increased coverage of SEL1L deficient POMC neurons by surrounding astrocytes (Figure 4.4A and Figure 4.8A). The glial coverage of POMC neurons is negatively correlated with neuronal firing and activity[16]. Therefore, we tested whether increased astroglial ensheathing would interfere with neuronal activity. Immunofluorescent staining and immunoblotting of cFOS as readout of neuronal firing activities suggested reduced neuronal activation in ARC regions in response to fasting-refeeding stimulus (Figure 4.4B, C and D), which is mainly attributed to the impaired neuronal activities in SEL1L-deficient POMC neurons (Figure 4.4B and C). Hence, in vivo evidence suggested alteration of neuron-glia plasticity upon neuronal SEL1L deficiency with defective neuronal activities.

4.4 Discussion

In this study our data identified ASTN1 as an endogenous SEL1L-HRD1 ERAD substrate that is highly dependent on the activity of SEL1L-HRD1 for proper folding, maturation and trafficking. The deficiency of SEL1L-HRD1 both in vitro and in vivo renders impaired maturation of ASTN1 with ER retention and accumulation. However, it still remains unclear how ASTN1 may link SEL1L-HRD1 regulation to neuron-glial crosstalk and plasticity as well as neuronal activity and function. The SEL1L deficiency in POMC neurons induced astrogliosis with increased contacts between neurons and astrocytes. The increase of ASTN1 protein levels has previously been correlated with increase in Bergmann glia[17]. Considering the intrinsic feature of neuronal adhesion protein ASTN1, one potential mechanism underlying induced physical neuron-astroglia contacts may be attributed to the overall ASTN1 gain-of-function due to lack of quantity control upon ERAD deficiency, despite that a fraction of ASTN1 increment is immature. However, it cannot be ruled out the possibility that astrogliosis is merely a secondary effect.

Further, both family members of ASTN, ASTN1 and ASTN2, involve regulating neuronal migration, morphogenesis and synaptic strengths[9, 12-14, 17-22], and human genetic defects in ASTN have been linked to neurodevelopmental symptoms such as developmental delay and intellectual disability [10, 22-26]. Hence, it’s tempting to speculate that impaired function of specific SEL1L-HRD1 ERAD substrate(s) such as ASTN1 may underlie neurological defects in ENDI patients with genetic SEL1L or HRD1 mutations. Future studies are required to identify and validate more such substrates and to delineate importance of SEL1L-HRD1 in health and disease of CNS.

4.5 Methods

Mice. As described previously [27], POMC-specific *Sel1L*-deficient mice (*Sel1L*^{POMC}) and control littermates (*Sel1L*$^{f/f}$) were generated. To generate CaMKII expressing neuron-specific *Sel1L*-deficient mice (*Sel1L*^{CaMKII}), *Sel1L*$^{f/f}$ mice[28] on the C57BL/6J background were crossed with CaMKIIα-Cre line (B6.Cg-Tg(Camk2a-cre)T29-1Stl/J**, JAX 005359**). C57BL/6J mice were purchased from JAX and bred in our mouse facility. Mice were fed a chow diet (13% fat, 57% carbohydrate and 30% protein, PicoLab Rodent Diet 5L0D). All mice were housed in a temperature-controlled room with a 12-hour light/12-hour dark cycle.

Cell culture, CRISPR/Cas9-based knockout in HEK293T and N2a cells. HEK293T and N2a cells were cultured at 37°C with 5% CO_2 in DMEM with 10% fetal bovine serum (Fisher Scientific). To generate SEL1L- or HRD1-deficient HEK293T and N2a cells, sgRNA oligonucleotides designed for human *SEL1L* (5'-GGCTGAACAGGGCTATGAAG-3'), mouse *SEL1L* (5'-GAGCATAGGACACTCTCTCC-3'), human *HRD1* (5'- GGACAAAGGCCTGGATGTAC-3') or mouse *HRD1* (5'-GTACGCCATTCTGATGACCA-3') were inserted into lentiCRISPR v2 (plasmid 52961, Addgene). To generate ASTN1-deficient N2a cells, mouse ASTN1 (5'-AGGAGCTGGAGTGCAAGCTC-3', Crispr1) and (5'- GCGGGCCCTGGGCCATGGAC-3', Crispr2) were inserted lentiCRISPR v2. Cells transfected with empty plasmids without sgRNA were used as wild type control. Cells grown in 10 cm petri dishes were transfected with indicated plasmids using 5μl 1 mg/ml polyethylenimine (PEI, Sigma)

per 1μg of plasmids for HEK293T cells. Cells were cultured 24 hours after transfection in medium containing 2 μg/ml puromycin for 48 hours and then in normal growth media.

SEL1L IP-based mass spectrometry in N2a cells. N2a cells were collected and pooled from 4x10cm petri dishes for each group. For SEL1L-IP, immunoprecipitation of endogenous SEL1L in WT, *SEL1L*$^{-/-}$ or *HRD1*$^{-/-}$ N2a cells were performed using 5 mg proteins from each sample lysed with the ice-cold NP-40 lysis buffer [150 mM NaCl, 0.2% Nonidet P-40 (NP40), 0.1% Triton X-100, 25 mM Tris–HCl pH 7.5] supplemented with protease inhibitors (Sigma-Aldrich, P8340), protein phosphatase inhibitors (Sigma-Aldrich, P5726), and 10 mM N- ethylmaleimide. The cell lysates were first incubated anti-SEL1L (home-made, 1:10,000) at 4°C overnight, followed by incubating with Protein A Agarose (Invitrogen, 20333) at 4°C for 2 hours. An IP reaction with IgG using cell lysate of HRD1-deficient N2a cells was included as a negative control.
Samples were resuspended in 50 μl of 0.1M ammonium bicarbonate buffer (pH~8). Disulfide bonds were reduced by adding 50 μl of 10 mM DTT and incubating at 45°C for 30 min. Samples were cooled to room temperature and alkylation of cysteines was achieved by incubating with 65 mM 2-Chloroacetamide, under darkness, for 30 min at room temperature. An overnight digestion with 1 μg sequencing-grade modified trypsin was carried out at 37°C with constant shaking in a Thermomixer. Digestion was stopped by acidification and peptides were desalted using SepPak C18 cartridges using manufacturer's protocol (Waters). Samples were completely dried using vacufuge and were proceeded to mass spectrometry signal acquisition and database searching following the same procedure described above.

For the mass spectrometry of SEL1L-IP, the protein hits from mass spectrometry were first filtered by restricting peptide-spectrum match (PSM) counts to be zero in both IgG and wildtype samples, not greater than 1 in the *SEL1L*$^{-/-}$ sample and greater than 1 in the *HRD1*$^{-/-}$ sample. The remaining hits meeting at least one of the following criteria were kept: contains a signal peptide, contains transmembrane domain(s), is N-glycosylated, contains disulfide bond(s), or is not a nuclear, ribosomal or keratin-derived protein. The hits identified from both two independent IP- MS experiments were considered as final SEL1L-interacting candidates. Detailed criteria were the same as previously described[3].

Plasmid. Plasmid pcDNA3-mASTN1-FLAG (ASTN1-FLAG) was generated where mouse ASTN1 cDNA was cloned from N2a cell cDNA and inserted into the pcDNA3. The primers

Cycloheximide (CHX) treatment in vitro. To study protein degradation, cycloheximide (CHX) chase experiments were performed where N2a or (transfected) HEK293T cells were cultured in DMEM w/ 10%FBS with CHX (50 μg/ml) treatment for the indicated times and harvested by snap-frozen in liquid nitrogen.

EndoH and PNGase treatment. EndoH and PNGase F treatment were performed as previously described [29]. Briefly, cell lysates were incubated with 1x glycoprotein denaturing buffer (New England BioLabs; catalog B1704S) at 100 °C for 10 min, and then digested with EndoH (New England BioLabs; catalog P0702L) with GlycoBuffer 3

(New England BioLabs; catalog B1720S) or PNGase F (New England BioLabs; catalog P0704L) with GlycoBuffer 2 (New England BioLabs; catalog B3704S) at 37 °C for 1 hr. The reaction was stopped by the addition of 5X denaturing sample buffer and boiled at 95 °C for 5 min.

Fasting-refeeding. The mice were fasted for 16 hours and refed for 2 hours on chow diet before fix perfusion or tissue collection.

Tissue collection. These procedures were carried out as previously described[27]. For brain microdissection, Adult Mouse Brain Slicer Matrix (BSMAA001-1, Zivic Instruments) was used to collect coronal brain slices containing ARC region with further microdissection to obtain ARC-enriched region. All tissues were snap-frozen in liquid nitrogen and stored at -80°C before use.

Preparation of brain sections. Mice were anesthetized with isoflurane, perfused with PBS followed by 4% paraformaldehyde (PFA) (Electron Microscopy Sciences; catalog 19210) for fixation. Brains were then postfixed in 4% PFA for overnight at 4°C, dehydrated in 15% sucrose and then 30% sucrose consecutively overnights at 4°C, and sectioned (30 μm) on a cryostat (Microm HM550 Cryostat, Thermo Fisher Scientific). The sections were stored in DEPC-containing anti-freezing media (50% 0.05 M sodium phosphate pH 7.3, 30% ethylene glycol, 20% glycerol) at −20°C. Different brain regions were identified using the Paxinos and Franklin atlas. Counted as distance from bregma, the following coordinates were used: PVN (–0.82 mm to –0.94 mm) and ARC (–1.58

mm to –1.7 mm).

RNA isolation, RT-PCR and qRCR. Microdissected brain tissues were homogenized in Trizol reagent (Invitrogen; catalog 15596-018). The RNA was further extracted using BCP phase separation reagent (Molecular Research Center; catalog TR 118) and isopropanol precipitation. cDNA was synthesized with SuperScript™ III Reverse Transcriptase (Invitrogen; catalog 18080044).

For RT-PCR analysis the following primer sequences were used:

mASTN1-F: CAATCTCTTCAATGGCTACAC R: TCAGATCTCCAAGCTGGGAAAGGAT

Western blot and antibodies. Frozen tissue or cells were homogenized by sonication in lysis buffer [150mM NaCl, 50mM Tris pH 7.5, 10 mM EDTA, 1% Triton X-100] with freshly added protease inhibitors (Sigma; catalog P8340), phosphatase inhibitors (Sigma; catalog P5726) and 10 mM N-ethylmaleimide (Thermo Scientific; catalog 23030). Lysates were incubated on ice for 30 min followed by centrifugation (13,000 g, 10 min at 4 °C). Supernatants were collected and analyzed for protein concentration using Bradford assay (Bio-Rad; catalog 5000006). For non-reducing SDA-PAGE, samples were prepared in 5x non-denaturing sample buffer (250 mM Tris-HCl pH 6.8, 10% sodium dodecyl sulfate, 0.05% bromophenol blue, 50% glycerol). For phostag gel analysis based on phos-tag system as described[30, 31], SDS-PAGE gel was supplemented by 50μM MnCl2 (Sigma) and 25μM phostag reagent (NARD Institute; catalog AAL-107) and must be protected from light until finishing running. Protein isolated from the liver of mice treated with tunicamycin (TM, 1 mg/kg, i.p.) for 24 hours

was used as a positive control to indicate the position of phosphorylated PERK and IRE1a. For phosphatase treatment, 100 µg tissue lysates were incubated with 1 µl lambda phosphatase (λPPase, New England BioLabs; catalog P0753S) in 1× PMP buffer (New England BioLabs; catalog B0761S) with 1 mM $MnCl_2$ (New England BioLabs; catalog B1761S) at 30°C for 30 min. Reaction was stopped by adding 5× SDS sample buffer and incubated at 90°C for 5 min.

All samples were incubated in 65°C for 10min and run with 15-30 µg total lysate on SDS-PAGE gel for separation followed by electrophoretic transfer to PVDF membrane (0.45µm, Millipore; catalog IPFL00010). The blots were incubated in 2% BSA/Tri-buffered saline tween-20 (TBST) with primary antibodies overnight at 4°C, washed with TBST followed by 1hr incubation with goat anti-rabbit or mouse IgG HRP at room temperature. Band density was quantitated using the Image Lab software on the ChemiDOC XRS+ system (Bio-Rad).

Antibodies for Western blot were as follows: SEL1L (rabbit, 1:8000, Abclonal; catalog E112049), HRD1 (rabbit, 1:2000, ABclonal; catalog E15102), GRP78 BiP (rabbit, 1:5000, Abcam; catalog ab21685), HSP90 (rabbit, 1:5,000, Santa Cruz Biotechnology Inc.; catalog sc-7947), FLAG (mouse, 1:2000, Sigma-Aldrich; catalog F-1804), IRE1α (rabbit, 1:2,000, Cell Signaling Technology; catalog 3294), OS9 (Abcam, ab109510), ASTN1 (Santa Cruz, sc-514299)

Secondary antibodies for Western blot were goat anti-rabbit IgG HRP and goat anti-mouse IgG HRP at 1:5,000, both from Bio-Rad.

Immunoprecipitation (IP). Cells were lysed in IP lysis buffer [150 mM NaCl, 0.2%

Nonidet P-40 (NP40), 0.1% Triton X-100, 25 mM Tris-HCl pH 7.5] supplemented with protease inhibitors, protein phosphatase inhibitors, and 10 mM N ethylmaleimide for anti-LepRb-FLAG and SEL1L IP. A total of 2 mg protein lysate was incubated with 20 µl anti-FLAG agarose (Sigma; catalog A2220), or 1µl anti-SEL1L home-made antibody overnight at 4°C with gentle rocking. SEL1L IP lysates were incubated with Protein A agarose (Invitrogen; catalog 20333) at 4 °C for 3 hours. The incubated agaroses were washed three times with IP lysis buffer and eluted in SDS sample buffer at 95^{o}C for 5 min followed by SDS-PAGE and Immunoblot.

Denaturing IP. HEK293T cells transfected with the indicated plasmids were snap-frozen in liquid nitrogen and whole cell lysate was prepared in the NP-40 lysis buffer [50 mM Tris-HCl at pH7.5, 150 mM NaCl, 1% NP-40, 1 mM EDTA] at 4°C supplemented with 10 mM N-ethylmaleimide, 1% SDS and 5 mM DTT, and denatured at 95°C for 10 min. The lysates were diluted 1:10 with the NP-40 lysis buffer and a total of 2mg protein lysate incubated with 20 µl anti-FLAG agarose (Sigma; catalog A2220) overnight at 4°C with gentle rocking. The incubated agaroses were washed three times with the NP-40 IP lysis buffer and eluted in the SDS sample buffer at 95°C for 5 min followed by SDS-PAGE and Immunoblot.

Immunostaining and antibodies. For fluorescent immunostaining in free-floating brain sections, samples were picked out of anti-freezing buffer followed by 3 washes with PBS. Free-floating sections were simultaneously incubated with primary antibodies in blocking buffer (0.3% donkey serum and 0.25% Triton X-100 in 0.1 M PBS) overnight at

4°C. Following 3 washes with PBS, sections were incubated with secondary antibodies for 2 hours at room temperature. Brain sections were then mounted on gelatin-coated slides (Southern Biotech; catalog SLD01-CS). Counterstaining and mounting were performed with mounting medium containing DAPI (Vector Laboratories; catalog H-1200) and Fisherfinest Premium Cover Glasses (Fisher Scientific; catalog 12-548-5P). For immunostaining in cells, 24 hours after transfection of LepRb-3xFLAG constructs, cells were placed on Poly-L-Lysine (Advanced Biomatrix; catalog 5048) coated Millicell EZ SLIDE 8-well glasses (Millipore; catalog PEZGS0816) for 24 hours before treatment and fixation. For staining surface bound leptin, samples were washed by ice cold PBS for 5 times and fixed by 4% formaldehyde (VWR; catalog 89370-094) for 15 minutes on ice followed by 3 washes with PBS. No permeabilization reagents were involved. For staining other markers, permeabilization was included and the overall process were the same as described above. To quantify immunoreactivity, identical acquisition settings were used for imaging each brain section from all groups within an experiment. The numbers of immunoreactivity-positive soma analysis and intensity of immunoreaction were quantified in 3D stack volumes after uniform background subtraction using the NIS Elements AR software (Nikon) and FIJI (National Institute of Health, USA).

Antibodies for immunostaining were as follows: GFP (chicken IgY, 1:300, Abcam; catalog ab13970), GFAP (rabbit, 1:500, Agilent; Z033429-2), cFOS (rabbit, 1:500, Cell Signaling Technology; catalog 2250)

Secondary antibodies for fluorescent immunostaining (all 1:500) were as follows: Anti-rabbit IgG Alexa Fluor 647 was from Jackson ImmunoResearch. Donkey anti-mouse IgG Alexa flour 555 was from Invitrogen (catalog A32773) and goat anti-chicken IgY

FITC was from Aves Labs (catalog F-1005).

Statistics. Results are expressed as the mean ± SEM unless otherwise stated. Statistical analyses were performed in GraphPad Prism version 8.0 (GraphPad Software Inc.). Comparisons between the groups were made by unpaired two-tailed Student's t test for two groups, or one-way ANOVA or two-way ANOVA followed by multiple comparisons test for more than two groups. P value < 0.05 was considered as statistically significant. All experiments were repeated at least twice and/or performed with several independent biological samples, and representative data are shown.

Study Approval. All experiments performed with mice were in compliance with University of Michigan (Ann Arbor, MI) Institutional Animal Care and Use Committee (#PRO00006888) guidelines.

4.6 References

1. Wang, H.H., et al., *Hypomorphic variants of SEL1L-HRD1 ER-associated degradation are associated with neurodevelopmental disorders.* J Clin Invest, 2024. 134(2).
2. Weis, D., et al., *Biallelic Cys141Tyr variant of SEL1L is associated with neurodevelopmental disorders, agammaglobulinemia, and premature death.* J Clin Invest, 2024. 134(2).
3. Wei, X., et al., *Proteomic screens of SEL1L-HRD1 ER-associated degradation substrates reveal its role in glycosylphosphatidylinositol-anchored protein biogenesis.* Nat Commun, 2024. 15(1): p. 659.
4. Edmondson, J.C., et al., *Astrotactin: a novel neuronal cell surface antigen that mediates neuron-astroglial interactions in cerebellar microcultures.* J Cell Biol, 1988. 106(2): p. 505-17.
5. Fishell, G. and M.E. Hatten, *Astrotactin provides a receptor system for CNS neuronal migration.* Development, 1991. 113(3): p. 755-65.
6. Zheng, C., N. Heintz, and M.E. Hatten, *CNS gene encoding astrotactin, which supports neuronal migration along glial fibers.* Science, 1996. 272(5260): p. 417-9.
7. Stitt, T.N. and M.E. Hatten, *Antibodies that recognize astrotactin block granule neuron binding to astroglia.* Neuron, 1990. 5(5): p. 639-49.
8. Hatten, M.E. and C.A. Mason, *Mechanisms of glial-guided neuronal migration in vitro and in vivo.* Experientia, 1990. 46(9): p. 907-16.
9. Horn, Z., H. Behesti, and M.E. Hatten, *N-cadherin provides a cis and trans ligand for astrotactin that functions in glial-guided neuronal migration.* Proc Natl Acad Sci U S A, 2018. 115(42): p. 10556-10563.
10. Fink, J.M., et al., *Astrotactin (ASTN), a gene for glial-guided neuronal migration, maps to human chromosome 1q25.2.* Genomics, 1997. 40(1): p. 202-5.
11. Hatten, M.E., *Central nervous system neuronal migration.* Annu Rev Neurosci, 1999. 22: p. 511-39.
12. Adams, N.C., et al., *Mice that lack astrotactin have slowed neuronal migration.* Development, 2002. 129(4): p. 965-72.
13. Lara, P., et al., *Murine astrotactins 1 and 2 have a similar membrane topology and mature via endoproteolytic cleavage catalyzed by a signal peptidase.* J Biol Chem, 2019. 294(12): p. 4538-4545.
14. Chang, H., *Cleave but not leave: Astrotactin proteins in development and disease.* IUBMB Life, 2017. 69(8): p. 572-577.
15. Chang, H., et al., *Intramembrane Proteolysis of Astrotactins.* J Biol Chem, 2017. 292(8): p. 3506-3516.
16. Nuzzaci, D., et al., *Postprandial Hyperglycemia Stimulates Neuroglial Plasticity in Hypothalamic POMC Neurons after a Balanced Meal.* Cell Rep, 2020. 30(9): p. 3067-3078 e5.
17. Hanzel, M., et al., *Mice lacking Astn2 have ASD-like behaviors and altered cerebellar circuit properties.* bioRxiv, 2024.
18. Ito, T., et al., *Astrotactin 2 (ASTN2) regulates emotional and cognitive functions by affecting neuronal morphogenesis and monoaminergic systems.* J Neurochem, 2023. 165(2): p. 211-229.

19. Wilson, P.M., et al., *Astn2, a novel member of the astrotactin gene family, regulates the trafficking of ASTN1 during glial-guided neuronal migration.* J Neurosci, 2010. 30(25): p. 8529-40.
20. Ni, T., K. Harlos, and R. Gilbert, *Structure of astrotactin-2: a conserved vertebrate-specific and perforin-like membrane protein involved in neuronal development.* Open Biol, 2016. 6(5).
21. Behesti, H., et al., *ASTN2 modulates synaptic strength by trafficking and degradation of surface proteins.* Proc Natl Acad Sci U S A, 2018. 115(41): p. E9717-E9726.
22. Reiner, O., et al., *Regulation of neuronal migration, an emerging topic in autism spectrum disorders.* J Neurochem, 2016. 136(3): p. 440-56.
23. Lionel, A.C., et al., *Disruption of the ASTN2/TRIM32 locus at 9q33.1 is a risk factor in males for autism spectrum disorders, ADHD and other neurodevelopmental phenotypes.* Hum Mol Genet, 2014. 23(10): p. 2752-68.
24. Arioka, Y., et al., *Induced pluripotent stem cells derived from a schizophrenia patient with ASTN2 deletion.* Stem Cell Res, 2018. 30: p. 81-84.
25. Wang, K.S., et al., *Polymorphisms within ASTN2 gene are associated with age at onset of Alzheimer's disease.* J Neural Transm (Vienna), 2015. 122(5): p. 701-8.
26. Freitag, C.M., et al., *The role of ASTN2 variants in childhood and adult ADHD, comorbid disorders and associated personality traits.* J Neural Transm (Vienna), 2016. 123(8): p. 849-58.
27. Kim, G.H., et al., *Hypothalamic ER-associated degradation regulates POMC maturation, feeding, and age-associated obesity.* J Clin Invest, 2018. 128(3): p. 1125-1140.
28. Sun, S., et al., *Sel1L is indispensable for mammalian endoplasmic reticulum-associated degradation, endoplasmic reticulum homeostasis, and survival.* Proc Natl Acad Sci U S A, 2014. 111(5): p. E582-91.
29. Sha, H., et al., *The ER-associated degradation adaptor protein Sel1L regulates LPL secretion and lipid metabolism.* Cell Metab, 2014. 20(3): p. 458-70.
30. Qi, L., L. Yang, and H. Chen, *Detecting and quantitating physiological endoplasmic reticulum stress.* Methods Enzymol, 2011. 490: p. 137-46.
31. Yang, L., et al., *A Phos-tag-based approach reveals the extent of physiological endoplasmic reticulum stress.* PLoS One, 2010. 5(7): p. e11621.

4.7 Figures and figure legends

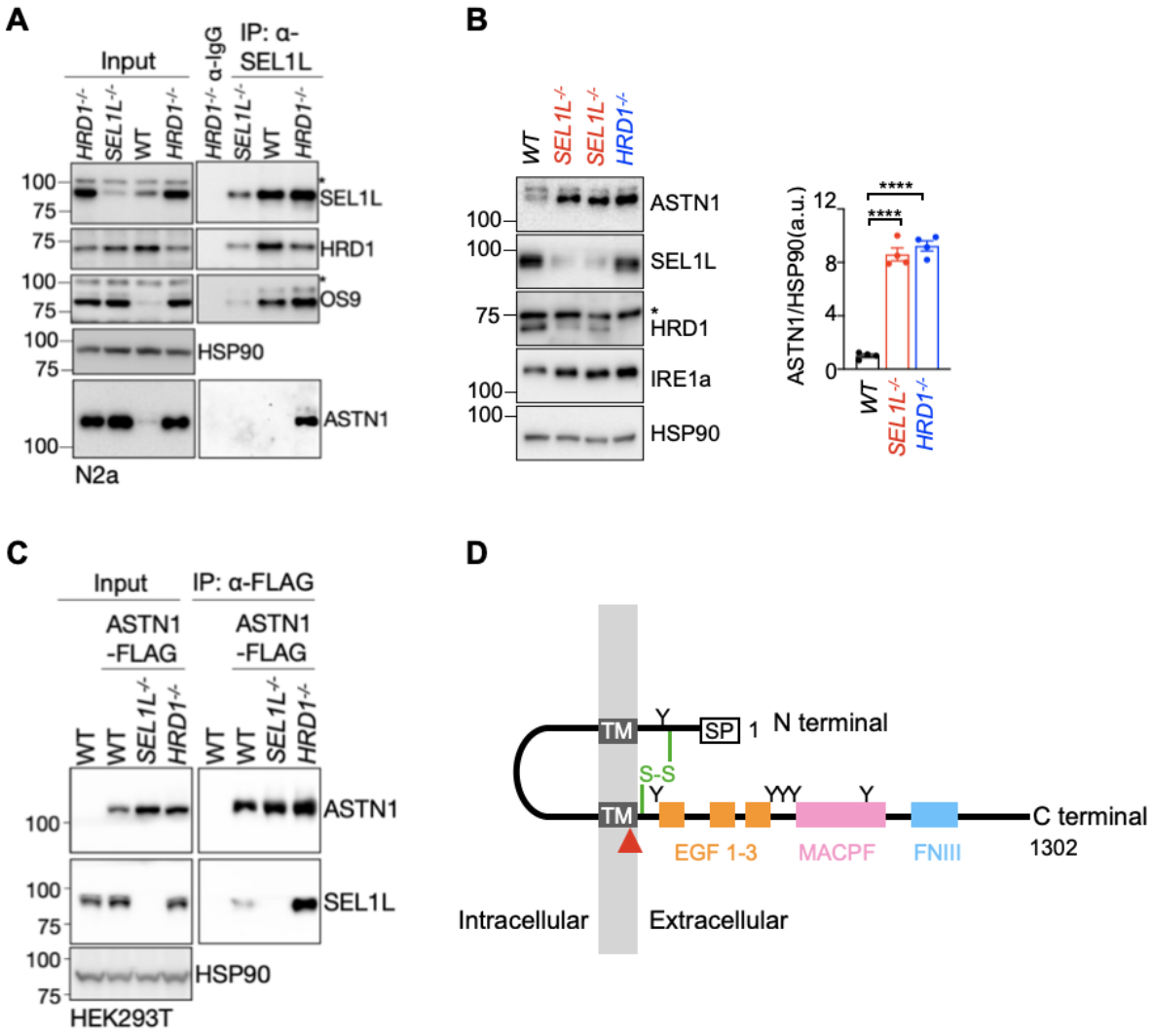

Figure 4.1 ASTN1 as putative SEL1L-HRD1 ERAD substrates from IP-MS analysis in N2a cells.
(A) Immunoprecipitation of SEL1L in *WT, SEL1L*$^{-/-}$ *or HRD1*$^{-/-}$ N2a cells to evaluate the interaction between SEL1L and ASTN1. *, non-specific bands.
(B) Representative images and quantitation of ASTN1 protein abundance in *WT, SEL1L*$^{-/-}$ *or HRD1*$^{-/-}$ N2a cells. *, non-specific bands.
(C) Immunoprecipitation analysis by FLAG-agarose pull-down in WT, SEL1L$^{-/-}$ or HRD1$^{-/-}$ HEK293T cells to evaluate the interaction between SEL1L and ASTN1.
(D) Domain structure of mouse ASTN1 protein. SP, signal peptide; TM, transmembrane domain; EGF, epidermal growth factor domain; MACPF, MAC/Perforin domain; FNIII, fibronectin III domain; "Y", N-glycosylation; red arrow head, cleavage site; green line, disulfide bond that keeps the two proteolytic fragments together.

Values, mean ± SEM. ns, not significant; *p<0.05, **p<0.01, ***p<0.001 and ****p<0.0001 by one-way ANOVA followed by multiple comparisons test (B).

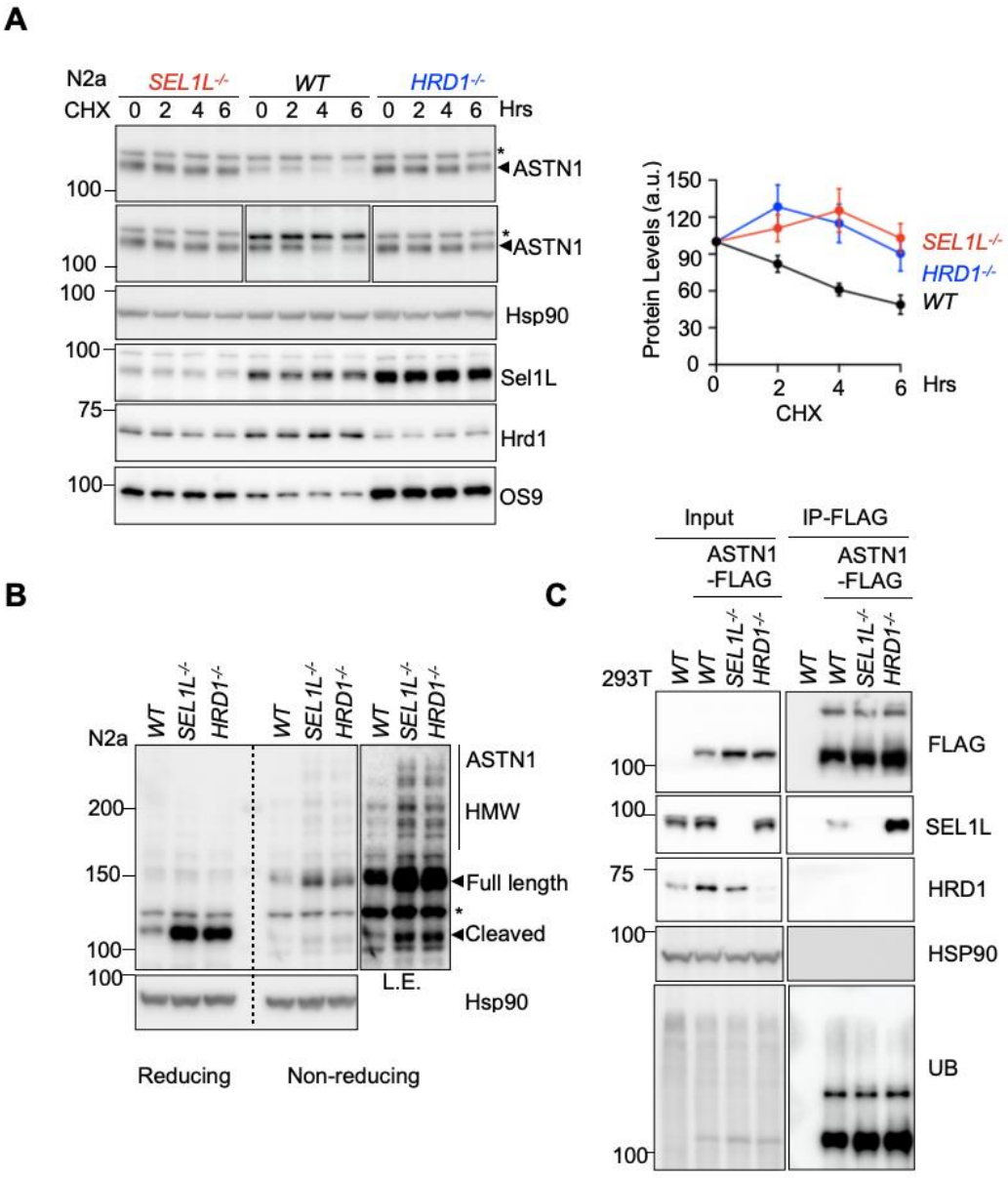

Figure 4.2 Identification of ASTN1 as an endogenous SEL1L-HRD1 ERAD substrate.

(A) Cycloheximide (CHX) chase analysis and quantitation of ASTN1 protein in *WT, SEL1L*$^{-/-}$ *or HRD1*$^{-/-}$ N2a cells. *, non-specific bands. (n=3 independent biological repeats)

(B) Reducing and non-reducing SDS-PAGE and western blot analyses of ASTN1 high molecular-weight (HMW) aggregates in *WT, SEL1L*$^{-/-}$ *or HRD1*$^{-/-}$ N2a cells. *, non-specific bands.

(C) Immunoblot analysis of Ub following denaturing immunoprecipitation (IP) of FLAG from lysates of HEK293T transfected with ASTN1-FLAG.

Values, mean ± SEM. ns, not significant; *p<0.05, **p<0.01, ***p<0.001 and ****p<0.0001 by two-way ANOVA followed by multiple comparisons test (A).

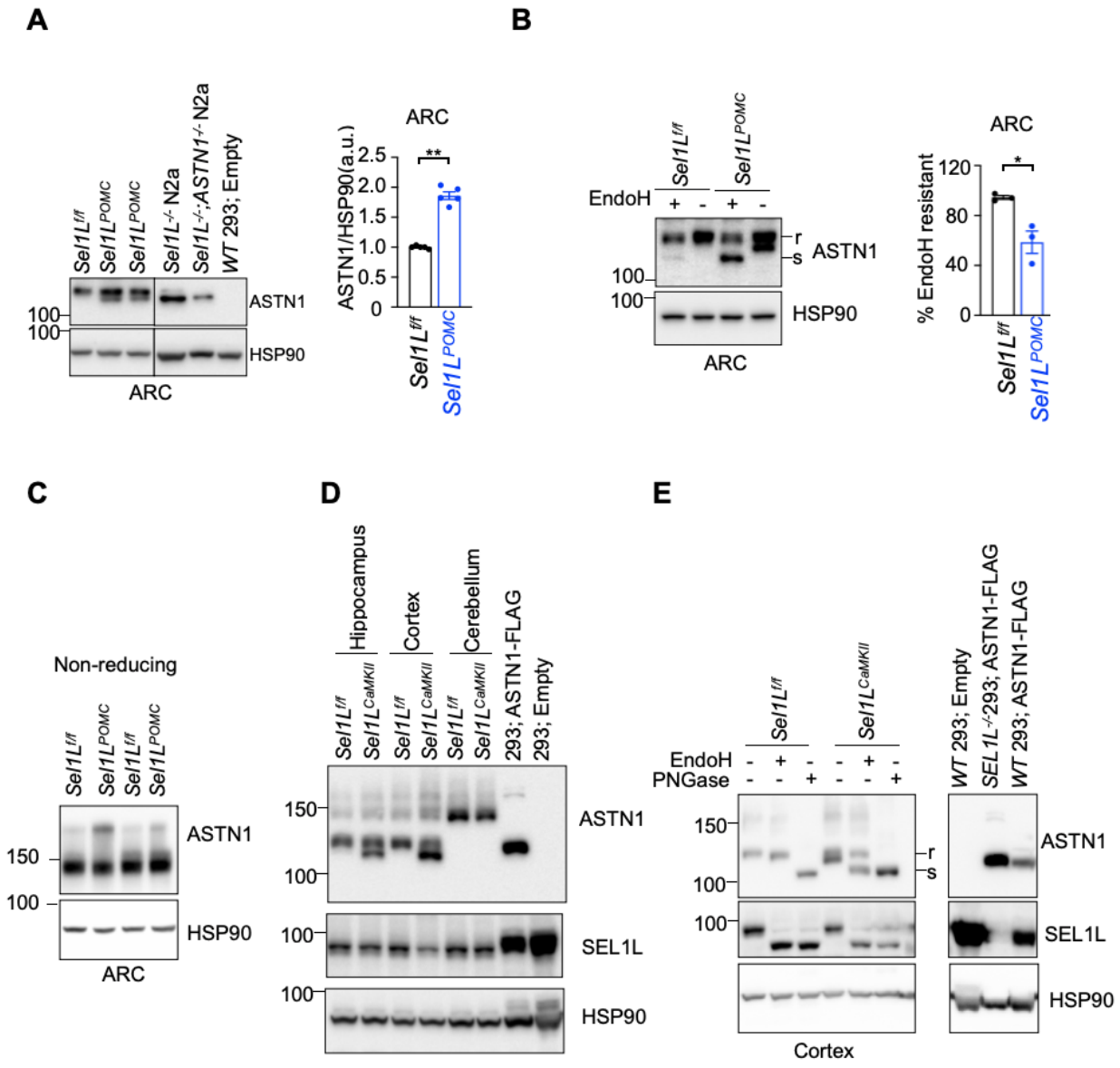

Figure 4.3 Characterization of ASTN1 in various neuronal regions with SEL1L-HRD1 deficiency.

(A) Immunoblot analysis of ASTN1 in ARC of the mice deficient in SEL1L in POMC neurons (*Sel1L*^{POMC}) and littermate control (*Sel1L*$^{f/f}$). (n=3 mice each group)

(B) EndoH treatment analysis of ASTN1 in *Sel1L*^{POMC} and *Sel1L*$^{f/f}$ mice. (n=3 mice each group)

(C) Non-reducing SDS-PAGE and western blot analyses of ASTN1 high molecular-weight (HMW) aggregates in *Sel1L*^{POMC} and *Sel1L*$^{f/f}$.

(D) Immunoblot analysis of ASTN1 in hippocampus, cortex and cerebellum of the mice deficient in SEL1L in CaMKII-expressing neurons (*Sel1L*^{CaMKII}) and littermate control (*Sel1L*$^{f/f}$).

(E) Representative images of western blot for ASTN1 in cortex of *Sel1L*^{CaMKII} and *Sel1L*$^{f/f}$ ice with EndoH and PNGase treatment.
Values, mean ± SEM. ns, not significant; *p<0.05, **p<0.01, ***p<0.001 and ****p<0.0001 by two-tailed Student's t-test (A, B).

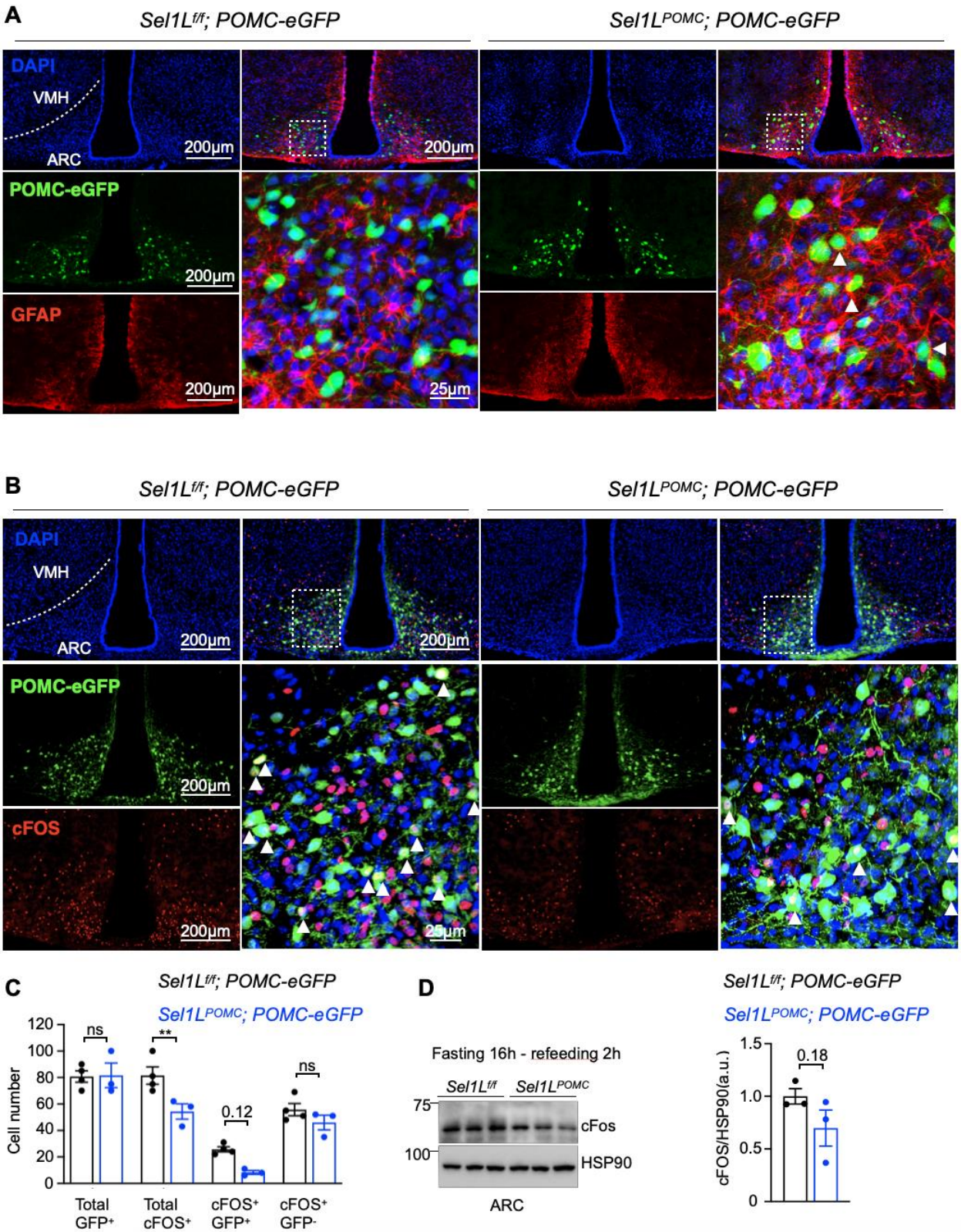
A
Sel1L f/f; POMC-eGFP
Sel1L POMC; POMC-eGFP
DAPI
VMH
ARC
200μm
POMC-eGFP
GFAP
25μm
B
cFOS
C
Cell number
ns
**
0.12
Total GFP+
Total cFOS+
cFOS+ GFP+
cFOS+ GFP-
D
Fasting 16h - refeeding 2h
75
100
cFos
HSP90
cFOS/HSP90(a.u.)
0.18

Figure 4.4 Alteration of neuron-glia contacts and neuronal activity
(A) Representative immunofluorescence (IF) staining of GFAP in the ARC of *Sel1L*$^{f/f}$ and *Sel1L*^{POMC} mice. Putative contacts between POMC neuron and astrocytes are indicated by white arrows. (n=3 mice each group)
(B-C) Representative immunofluorescence (IF) staining(B) and quantitation(C) of cFOS in the ARC of *Sel1L*$^{f/f}$ and *Sel1L*^{POMC} mice. Mice were fasted for overnight (16hrs), followed by 2h refeeding before harvested. cFOS positive POMC neurons are indicated by white arrows. (n=3 mice each group)
(D) Immunoblot analysis of cFOS in the ARC of *Sel1L*$^{f/f}$ and *Sel1L*^{POMC} mice. Mice were fasted for overnight (16hrs), followed by 2h refeeding before harvested. (n=3 mice each group)
VMH, ventromedial nucleus of hypothalamus; ARC, arcuate nucleus. Values, mean ± SEM. ns, not significant; *p<0.05, **p<0.01, ***p<0.001 and ****p<0.0001 by two-way ANOVA followed by multiple comparisons test (C) or two-tailed Student's t-test (D).

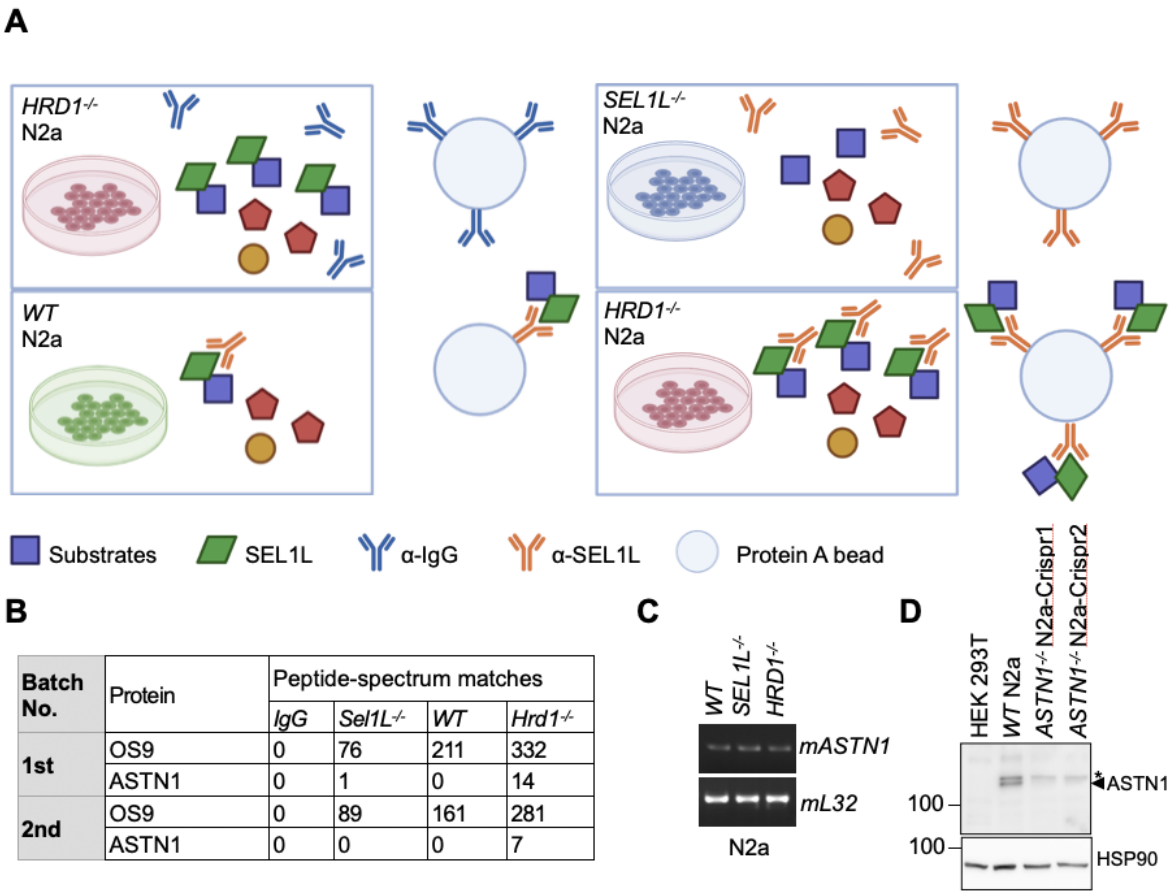

Batch No.	Protein	Peptide-spectrum matches			
		IgG	*Sel1L*$^{-/-}$	*WT*	*Hrd1*$^{-/-}$
1st	OS9	0	76	211	332
	ASTN1	0	1	0	14
2nd	OS9	0	89	161	281
	ASTN1	0	0	0	7

Figure 4.5 ASTN1 as putative SEL1L-HRD1 ERAD substrates from IP-MS analysis in N2a cells.
(A) The diagram of immunoprecipitation and mass spectrometric (IP-MS) analyses of SEL1L interactome in *WT, SEL1L*$^{-/-}$ *or HRD1*$^{-/-}$ N2a cells
(B) Identification of ASTN1 from two independent batches of IP-MS top hits. OS9 is a positive control as a highly abundant SEL1L-HRD1 substrates.
(C) Reverse transcriptase PCR (RT-PCR) analysis of ASTN1 mRNA levels in *WT, SEL1L*$^{-/-}$ *or HRD1*$^{-/-}$ N2a cells.
(D) Validation of ASTN1 antibody by Crispr KO ASTN1 in N2a cells. *, non-specific bands.

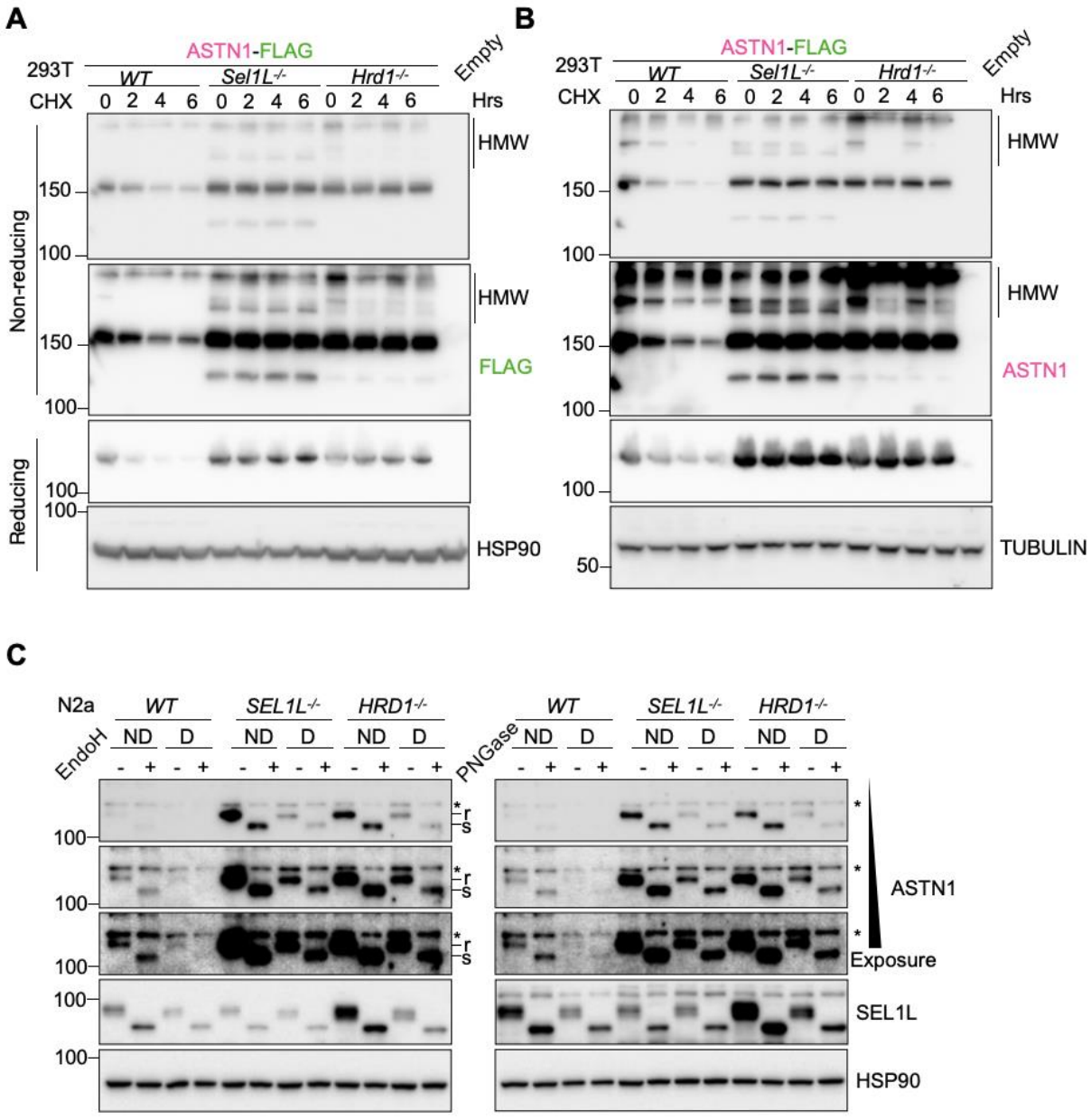

Figure 4.6 ASTN1 is degraded by SEL1L-HRD1 ERAD and retained inside ER accumulatively upon ERAD deficiency.
(A-B) Non-reducing and reducing SDS-PAGE western blot of CHX chase analysis of ASTN1 protein in *WT, SEL1L*$^{-/-}$ *or HRD1*$^{-/-}$ HEK293T transfected with ASTN1-FLAG.
(C) EndoH and PNGase treatment analysis of ASTN1 in *WT, SEL1L*$^{-/-}$ *or HRD1*$^{-/-}$ N2a cells. *, non-specific bands.

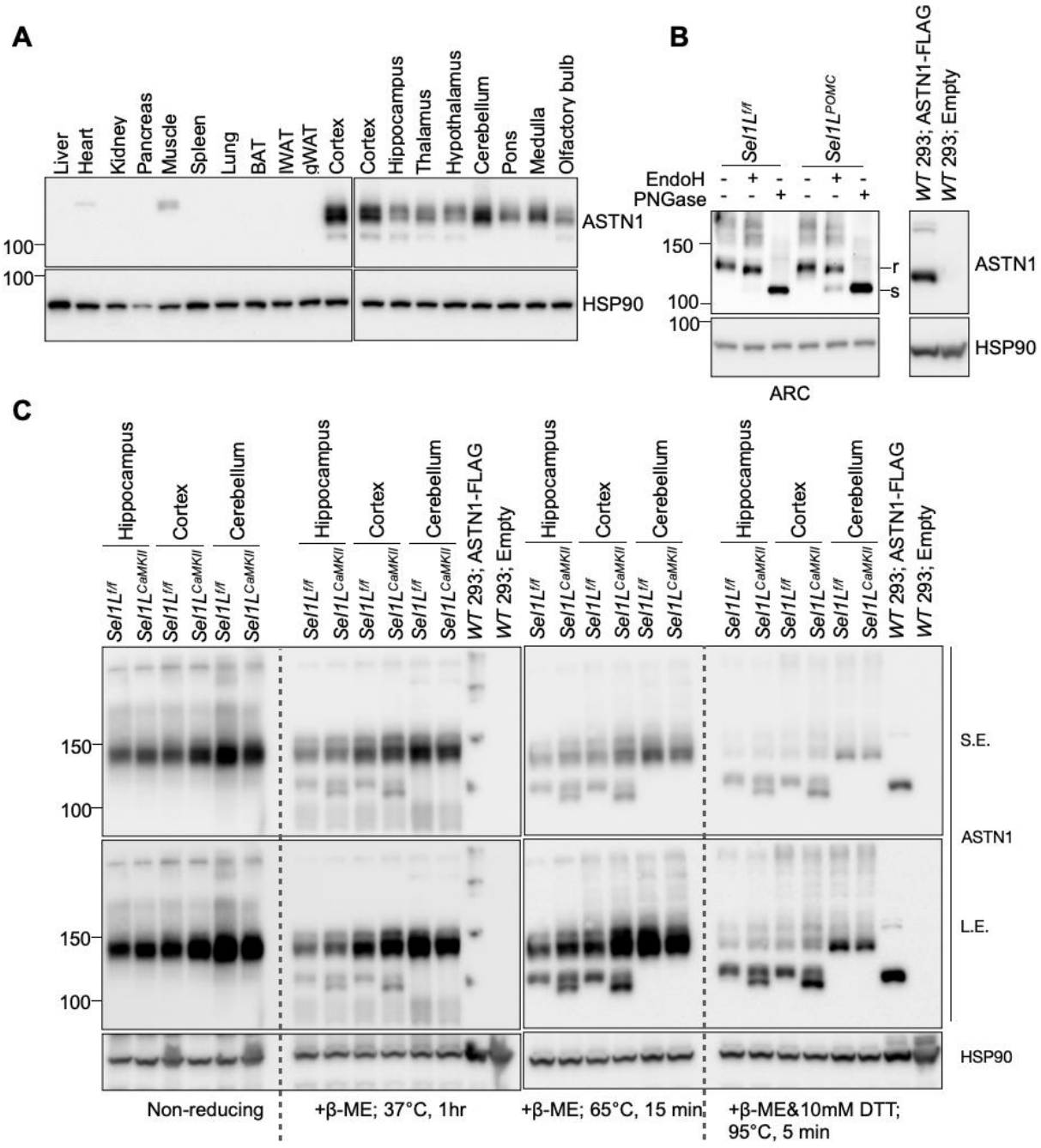

Figure 4.7 Characterization of ASTN1 in various neuronal regions with SEL1L-HRD1 deficiency.

(A) Immunoblot analysis of ASTN1 in various tissues of the wildtype mice. (n=2 mice)
(B) EndoH and PNGase treatment analysis of ASTN1 in *Sel1L*^{POMC} and *Sel1L*$^{f/f}$ mice.
(C) Immunoblot analysis of ASTN1 in hippocampus, cortex and cerebellum of the mice deficient in SEL1L in CaMKII-expressing neurons (*Sel1L*^{CaMKII}) and littermate control (*Sel1L*$^{f/f}$), with different denaturing conditions.

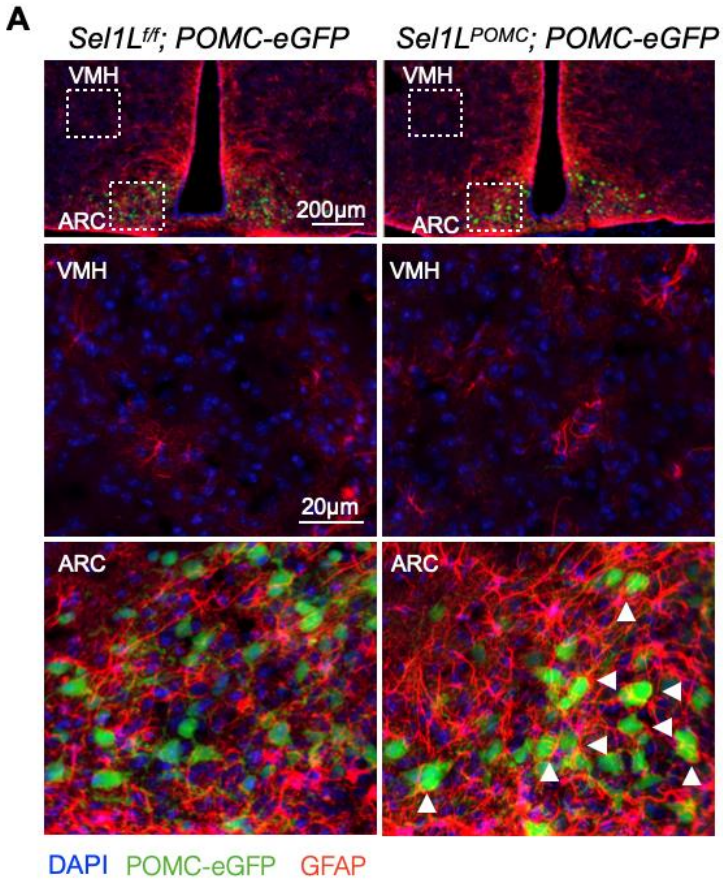

Figure 4.8 Alteration of neuron-glia contacts and neuronal activity.
(A) Representative immunofluorescence (IF) staining of GFAP in the ARC of *Sel1L*$^{f/f}$ and *Sel1L*^{POMC} mice. Putative contacts between POMC neuron and astrocytes are indicated by white arrows. (n=3 mice each group)
VMH, ventromedial nucleus of hypothalamus; ARC, arcuate nucleus.

Chapter 5 Conclusion, Perspectives and Future Directions

5.1 Overview

With high demand in production and trafficking of secretory proteins including neurotransmitters and neuropeptides, ER homeostasis is of vital importance in maintaining neuronal activities and functions. To date, various studies have demonstrated the role of neuronal ER proteostasis in different contexts of health and diseases dominated by regulation of CNS. This dissertation starts from revisiting ER proteostasis in peripheral tissues and CNS upon over nutritional status in Chapter 1, where we provide evidence indicating potential uncoupling of ER stress/UPR from diet-associated pathogenesis including hypothalamic leptin resistance. Further in Chapter 3, we explore the potential role of SEL1L-HRD1 ERAD in maintaining POMC neuronal function mediating organismal adaptive response to nutritional overload. SEL1L-HRD1 ERAD was found indispensable for maintaining leptin sensitivity in POMC neurons to control energy balance by regulating food intake and energy expenditure. Apart from elucidating significance of SEL1L-HRD1 ERAD in hypothalamic regulation of energy homeostasis, we further unravel the concept of neuron-glia crosstalk mediated by SEL1L-HRD1 in Chapter 4. Analysis from recent IP-MS data in neuronblastoma cell lines provide a variety of putative neuronal specific SEL1L-HRD1 ERAD substrate.

From the candidates of top hits, we identified and demonstrated ASTN1 as a genuine endogenous SEL1L-HRD1 ERAD substrate and brought up its potential role, thought remains to elucidate, linking SEL1L-HRD1 to neuron-glia connection. That said, much remains to be investigated in CNS ER proteostasis considering heterogeneity of cell populations within the CNS including complex types of neurons and glia with distinct functionality in different regions of brain responsible for specific physiological and cognitive functions. This chapter will provide several more comprehensive perspectives of proteostasis in the CNS, stepping outside of hypothalamic ER homeostasis for energy regulation, into the broader field of neuronal health and diseases. Future directions are proposed with summary, discussion of previous findings of by us and others, as well as relevant preliminary data that help establish the foundation for upcoming endeavors.

5.2 ER Proteostasis in neuronal health and diseases

5.2.1 ERAD

Neuronal ER homeostasis is indispensable for healthy brain development and aging. Studies have revealed that several neurodevelopmental and neurodegenerative diseases are closely related to the dysfunction of ER proteostasis in neurons.
Of note, recent identification and characterization of hypomorphic human SEL1L and HRD1 variants shines light on importance of SEL1L-HRD1 ERAD in neuronal development[1, 2]. Further, such studies provide insights into the dramatic variance in different tissues in terms of their tolerance to disturbed ER homeostasis due to partial loss-of-function of SEL1L-HRD1 ERAD. As one of the most severe symptoms is

neurodevelopment disorder[1, 2], this implies at neurons in the brain, may be one of the most susceptible systems upon reduced capacity of ERAD. Of note, there's only very mild, if any, constant ER stress or UPR activation upon partial deficiency of the SEL1L-HRD1 ERAD, indicated by non-detectable phosphorylation of the UPR sensors, IRE1α and PERK, as well as downstream effectors, phosphorylation of eIF2α and XBP1 splicing. However, the ER chaperones including BiP and PDI were significantly accumulated in the SEL1L-HRD1 mutant KI cells, suggesting cellular adaptation in disease variants-expressing cells[1, 2].

Previous research identified a specific SEL1L missense mutation (Ser658Pro) in Finnish hounds that developed progressive cerebellar ataxia, gait irregularities with Purkinje cell depletion[3]. More recent study investigating this recessive hypomorphic *SEL1L*^{S658P} mutation characterized partial embryonic lethality in homozygous mice carrying the bi-allelic variant with early-onset cerebellar ataxia[4]. Mechanistically, the study demonstrated how *SEL1L*^{S658P} may attenuate SEL1L-HRD1 interaction and activity. Another early study indicated the decreased HRD1 levels in the cerebral cortex may contribute to pathogenesis of AD[5]. The study further demonstrated that amyloid precursor protein (APP) ubiquitination and degradation is mediated by HRD1, the deficiency of which would sufficiently induce APP accumulation and concomitant production of amyloid-beta (Aβ)[5]. All the aforementioned studies underscore the pathophysiological importance and disease relevance of ERAD, particularly SEL1L-HRD1, in neurodevelopment and degenerative diseases. Further studies are needed to elucidate and unravel more comprehensive roles of ERAD in neuronal health and diseases.

5.2.2 UPR

The organismal adaptive responses can be mediated by a variety of signaling cascades and UPR is one of the most powerful machineries for balancing ER homeostasis upon stress. Indeed, the pathogenesis of age-related neurodegenerative diseases have been closely related to the UPR pathways. Activation of UPR is observed from early onset throughout the entire pathogenesis of several age-related neurodegenerative diseases including Alzheimer's disease (AD), Parkinson's disease (PD), and Huntingdon's diseases (HD). Such close correlation is highly likely due to the accumulation of misfolded proteins, aggregation and inclusion bodies in the pathologies of the diseases. The autopsy samples from AD patients exhibited evident phosphorylation of PERK, IRE1α and eIF2α as well as upregulation of BiP[6-12]. As the featured pathologies of AD, the accumulation of tau proteins may stimulate PERK, IRE1α and ATF6 and trigger a concomitant inflammatory cascade[13, 14]. Evidence found from studies in AD, PD and HD suggested that activation of IRE1α-XBP1s and ATF6 pathways are likely to be neuroprotective by exerting pro-adaptive downstream effectors including upregulation of chaperones BiP and ERAD components[15-21], while PERK- eIF2α cascades may be more neurotoxic via proapoptotic CHOP signaling[22]. However, observations in other neuronal disease models such as amyotrophic lateral sclerosis (ALS) suggesting an opposing interpretation where inhibition of XBP1[23] and activation of PERK-eIF2 α are beneficial[24, 25].

5.2.3 ER-phagy

One protective role of UPR in the pathogenesis of neurodegenerative diseases is via induction of autophagy[15, 26], while basal autophagy levels are critical for maintaining the health of neurons and the decline of autophagy flux has been closely related to neurodegenerative diseases during aging. On the other hand, the dramatic accumulation of aberrant protein aggregates may disrupt autophagy. Particularly, neuronal autophagic activities are essential for axonal and synaptic plasticity which is the fundament of cognitive function and memory. Of note, a more recent study unraveled the role of ER-phagy in axonal ER remodeling during neurogenesis mediated by ER-phagy receptors FAM134 and CCPG1[27].

5.3 Crosstalk between hypothalamic SEL1L-HRD1 ERAD and autophagy

Previous in vivo and in vitro studies have observed a significant increase of autophagy flux in the absence of SEL1L-HRD1 ERAD in a various tissues including pancreatic beta cells[28], adipose tissues[29], and skeletal muscles[30]. Though not validated by experimental evidence, it is likely that autophagy may be upregulated in neurons with SEL1L-HRD1 deficiency as well in order to maintain the proteostasis, prevent proteotoxicity and promote survival of neurons by clearing accumulation of protein aggregates. This is supported by the observation of further increased HMW aggregation of LepRb in HRD1-/- cells upon lysosomal inhibition with bafilomycin A treatment (Figure 5.1A and B).

5.3.1 Investigation of ERAD and autophagy crosstalk in POMC neurons

To this end, we are further interested in the potential interplays between SEL1L-HRD1 ERAD and autophagy in the hypothalamic neuronal proteostasis and function in regulating energy homeostasis. We thus crossed and bred mice with single Sel1L knockout (*Sel1L*^{POMC}), single Atg7 knockout (*Atg7*^{POMC}) and Sel1L, Atg7 double knockout (*DKO*) specifically in POMC neurons. From the preliminary data of bodyweight, the *DKO* mice started to gain significantly higher body weight at younger age than other cohorts in both sexes (Figure 5.2 A and B). In terms of cellular proteostasis, compared to WT control littermates (Figure 5.3A and Figure 5.4A and B), *Sel1L*^{POMC} indicated strong induction of KDEL and IRE1α in the ARC (Figure 5.3C and Figure 5.4A), indicating alteration of ER homeostasis that is absent in *Atg7*^{POMC} mice (Figure 5.3B and Figure 5.4A). On the other hand, *Atg7*^{POMC} mice exhibited a significantly increase of p62 (Figure 5.3B and Figure 5.4A), colocalized with Lamp1 in not only POMC neurons, but also across the entire ARC with a potential trend of projection towards regions outside the ARC (Figure 5.3B and Figure 5.4C). Notably, levels of KDEL and IRE1α as well as p62 in the ARC of DKO mice are evidently higher than control littermates but significantly dampened compared to each single KO counterpart(Figure 5.3D and Figure 5.4A and D). This could be attributed to a dramatic reduction in the number of neurons expressing eGFP reporter according to the IF staining (Figure 5.3D and Figure 5.4D). The remaining detectable POMC-eGFP neurons in DKO mice expressed both KDEL and p62 with a comparably strong signal intensity to that of *Sel1L*^{POMC} and *Atg7*^{POMC} respectively (Figure 5.3D and Figure 5.4D). However, it was the reduction of cell number that dampened the signaling observed in

WB (Figure 5.4A). The underlying mechanisms of why less neurons expressed POMC driven eGFP upon SEL1L and ATG7 double deficiency remains to be determined.

5.3.2 Future directions for understanding interplay between ERAD and autophagy

Three potential hypotheses may explain the cellular phenotype we observed that can be tested. First, the number of mature POMC neurons wasn't significantly affected in single mouse models *Sel1L*^{POMC} and *Atg7*^{POMC}, despite that deficiency of ATG7 in POMC neurons could impair axonal growth. The question is then, whether ERAD and autophagy double deficiency may severely disrupt the differentiation of the POMC-promoter expressing progenitors. To address this, much earlier mice need to be examined at different timepoints of embryonic stages as well as early postnatal days, thus capturing potential neurodevelopment alteration and defects in DKO mice.
Another possibility is the loss of POMC neurons due to neurodegeneration and apoptotic cell death.
Moreover, as in many cases, pos-mitotic neurons may try to avoid direct cell death and instead, undergo senescence to protect against unbearable stress. In this case, we can evaluate the biomarkers of neuronal senescence distinct from apoptosis.
Another interesting point is that, regardless of potential death or senescence at later stage of the adulthood in 30-week-old mice, there were still POMC neurons remaining still and active despite significantly altered ER homeostasis and autophagic flux indicated by KDEL and p62. How those neurons survive and remain responsive is intriguing. Referring to the insights from recent discovery in how adipose tissues dispose of misfolded proteins upon lack of degradation systems, it will be intriguing to

investigate whether those living DKO neurons may also rely on another mechanism to dispose of misfolded proteins and aggregates to cope with the proteotoxicity.

5.4 Proteostasis in glia populations of the CNS

Of note, the majority of the cell populations in CNS are non-neuronal cells named glia. Increasing evidence suggest the significance of ER homeostasis and quality control in CNS glia cells, including oligodendrocytes, microglia and astrocytes, in pathogenesis of a variety of neuronal diseases.

5.4.1 Oligodendrocytes

The role of SEL1L in oligodendrocytes has been explored and reported to be vital for maintaining the myelination of neuronal axons[31, 32]. SEL1L deficiency in oligodendrocytes doesn't necessarily affect development of myelin despite adult-onset, progressive myelin thinning in the CNS[31, 32]. Further inactivation of PERK restored CNS myelin thickness upon loss of SEL1L in oligodendrocytes, suggesting activated PERK signaling links oligodendrocyte-specific SEL1L deficiency to myelin thinning in adult CNS[31].

ER stress/UPR activation in CNS myelinating glia, oligodendrocytes, has also been closely correlated to neurological diseases such as multiple sclerosis (MS). MS is an autoimmune disease that the CNS is attacked by self-immune systems, resulting in inflammation, demyelination with loss of oligodendrocytes and eventually the axonal damage[33]. In MS patients, ATF4 and CHOP mRNA have been observed to be increased in demyelinating lesions in multiple cell types including oligodendrocytes[34].

Further studies using mouse models of autoimmune encephalomyelitis combined with genetic modification investigated the correlation and potential causal relationship underlying UPR in oligodendrocytes and demyelination upon pathogenesis, with comprehensive summary in previous reviews[34-36]. Notably, the PERK signaling cascades in oligodendrocytes are protective against demyelination induced by inflammatory cytokine[37-39]. The loss of PERK in oligodendrocytes rendered increased severity of the disease pathogenesis[38, 40] while oligodendrocyte-specific activation of PERK protected remyelinating during recovery phase of the disease[41]. Apart from the UPR, several CNS myelin disorders have been related to abnormal autophagy flux. LC3B are highly expressed in demyelinated lesions in various types of dysmyelinating disorders. A recent review summarized findings of autophagy in myelinating glia and highlighted its pathophysiological importance[42].

5.4.2 Astrocytes and microglia

Moreover, the UPR and autophagy in another glia populations named astrocytes also plays an essential role in neurological survival and function[43, 44]. In brief, astrocytes not only provide structural support for neuronal synapses and blood vessels, but also mediate synaptic formation, plasticity and nutrient sensing and exchange between neurons and circulating factors, as part of the blood brain barrier (BBB), via electrical and chemical transmission[45]. On the other hand, astrocytes may also mediate inflammation in response, namely astrogliosis, to several stresses including neuronal injury, promoting neurotoxicity by secreting proinflammatory cytokines, closely associated with several neurological diseases[45-49]. Therefore, proteostasis and ER

homeostasis are of equal importance in astrocytes to that in neurons. Recent single cell RNA sequencing revealed the heterogeneity of the astrocytes where subpopulations were identified with increased UPR signaling pathways in mouse models for MS[50]. UPR in astrocytes has been associated with AD and MS that has been reviewed and summarized[6, 26, 43]. Of note, the deficiency of IRE1α signaling significantly improved the memory and learning in AD mice with alleviated astrogliosis[51]. Knockdown of IRE1 specifically in astrocytes reduced the inflammation and severity of the pathogenesis in MS mice[52]. The activation of PERK signaling in astrocytes has been identified in several neurological disease models including AD and PD[6, 26]. Moreover, ATF6 is suggested to involve astrocyte development[53] and, unlike IRE1 and PERK, may be protective in astrocytes during ischemia[54] while studies on its role in other neurological disorders are still limited. Autophagy in astrocytes is not only vital for astrocyte development and differentiation, but also controls age-related senescence and neurodegenerative disorders via regulating neuroinflammation and oxidative stress response[44].

Microglia, as the “macrophages” of the CNS, mediate inflammation and clearance of the apoptotic cells and myelin debris as well as synaptic pruning via phagocytosis. Autophagic activity is indispensable for maintaining the function of the microglia particularly the phagocytosis efficiency, and the deficiency of autophagy in microglia links neuroinflammation-induced exacerbation in age-associated neurological pathogenesis, including AD, PD, HD, MS[55, 56].

5.5 Cell autonomous and non-autonomous regulation of SEL1L-HRD1 in CNS

A closer analysis of evidence from previous chapters not only demonstrated cell autonomous regulation of SEL1L-HRD1 in chapter 3, but also suggested that this complex may control systemic metabolism in a cell nonautonomous manner including signaling between CNS (hypothalamus) and peripheral (liver) in chapter 2; and within CNS among different cell populations such as between neurons and astrocytes in chapter 4. However, a lot remains to explore and validate before any solid conclusion can be made.

5.5.1 Future directions in demonstrating importance of SEL1L-HRD1 in the CNS in a substrate-dependent manner

As such a fundamental protein quality control machinery, SEL1L-HRD1 is expected to regulate an enormous number of protein substrates. Indeed, proteome-wide screening of endogenous substrates via SEL1L-IP based immunoprecipitation provided informative dataset of hundreds of substrate candidates that remain for further validation and characterization of physiological relevance. Additionally, human patients carrying SEL1L and HRD1 mutations exhibit neurodevelopmental disorders as one of the severest symptoms, implying higher vulnerability of the CNS upon SEL1L-HRD1 deficiency. Now that we have obtained a proteomic screen in N2a cells, we can start deciphering the neuronal importance of SEL1L-HRD1 linked by neuron-specific substrates. Meanwhile, as N2a is a tumor cell line unrepresentative of physiological features and functions of CNS, further proteomic screening can be performed in primary neurons, neurons derived from patient-derived iPSC, and brain tissues from genetic mouse models.

5.5.2 Future directions in studying potential cell non-autonomous regulation of SEL1L-HRD1 ERAD

In chapter 2, the project revisiting UPR during DIO, we discovered an acute induction of SEL1L-HRD1 in the hypothalamus, liver and gWAT independent of UPR at the transcriptional level. This finding implied the regulation of SEL1L-HRD1 by other pathways that deserves further exploration. Further, as previous studies demonstrated cell nonautonomous signaling of proteostasis alteration from CNS to peripheral systems, we are curious about whether such signaling may also exist for SEL1L-HRD1 levels. To test potential cell nonautonomous signaling of SEL1L-HRD1 among various tissues, we can overexpress SEL1L-HRD1 in different central and peripheral tissues, one at a time via tissue-specific AAV overexpression, and evaluate the SEL1L-HRD1 in other tissues. Further, it is worthwhile to investigate whether increase of SEL1L-HRD1 activity may help the organism better adapt to nutritional overload. To address this, we can boost ERAD activity within the physiological range either via AAV overexpression or small molecule activator, and evaluate whether and how the treatment may protect mice against DIO and pathogenesis. Lastly, diets with different components and female mice can be included to better understand effect of nutrition ingredients on proteostasis and sexual dimorphism.

In chapter 4, we provided characterization of ASTN1 in vitro and in vivo as a bona fide SEL1L-HRD1 substrate, but it remains uncertain whether ASTN1 exhibits gain or loss of function upon SEL1L-HRD1 deficiency, which can be tested by evaluating interactions between primary neurons or iPSC organoids and astrocytes via co-culture systems. Moreover, the abundance and isoforms of ASTN1 can vary at different developmental

stages across various brain regions, potentially linking SEL1L-HRD1 to distinct physiological relevance in the CNS. Apart from ASTN1, ASTN2 as another family member of astrotactins with similar topology as ASTN1, has been associated with more neurodevelopmental disorders and intellectual disability upon loss of function. It would be worth investigating whether ASTN2 is also substrate of SEL1L-HRD1 ERAD, which will provide comprehensive perspectives on role of SEL1L-HRD1 in neurological disorders via astrotactins.

5.6 Concluding remarks

ER proteostasis in the CNS has been closely related to neuronal function and regulation of systemic metabolism in association with environmental stress and aging. Despite of numerous studies on ER quality control machineries including UPR and ER-phagy, the investigation of ERAD in the CNS is still very limited. One major part of this work demonstrated the vital role of SEL1L-HRD1 in hypothalamic leptin signaling and its importance for central regulation of energy homeostasis in response to nutritional overload. Further, we provided more evidence indicating the great potential of the SEL1L-HRD1 complex in regulating neuronal activity, plasticity and communication between heterogenous cell populations in CNS. I hope that this work can be a great inspiration for future insights, comprehensive exploration and investigation in how ERAD contributes to proteostasis and function in CNS-mediated systemic metabolism.

5.7 References

1. Wang, H.H., et al., *Hypomorphic variants of SEL1L-HRD1 ER-associated degradation are associated with neurodevelopmental disorders.* J Clin Invest, 2024. 134(2).
2. Weis, D., et al., *Biallelic Cys141Tyr variant of SEL1L is associated with neurodevelopmental disorders, agammaglobulinemia, and premature death.* J Clin Invest, 2024. 134(2).
3. Kyostila, K., et al., *A SEL1L mutation links a canine progressive early-onset cerebellar ataxia to the endoplasmic reticulum-associated protein degradation (ERAD) machinery.* PLoS Genet, 2012. 8(6): p. e1002759.
4. Lin, L.L., et al., *SEL1L-HRD1 interaction is required to form a functional HRD1 ERAD complex.* Nat Commun, 2024. 15(1): p. 1440.
5. Kaneko, M., et al., *Loss of HRD1-mediated protein degradation causes amyloid precursor protein accumulation and amyloid-beta generation.* J Neurosci, 2010. 30(11): p. 3924-32.
6. Hoozemans, J.J., et al., *Activation of the unfolded protein response is an early event in Alzheimer's and Parkinson's disease.* Neurodegener Dis, 2012. 10(1-4): p. 212-5.
7. Unterberger, U., et al., *Endoplasmic reticulum stress features are prominent in Alzheimer disease but not in prion diseases in vivo.* J Neuropathol Exp Neurol, 2006. 65(4): p. 348-57.
8. Hoozemans, J.J., et al., *The unfolded protein response is activated in Alzheimer's disease.* Acta Neuropathol, 2005. 110(2): p. 165-72.
9. Hamos, J.E., et al., *Expression of heat shock proteins in Alzheimer's disease.* Neurology, 1991. 41(3): p. 345-50.
10. Hoozemans, J.J., et al., *The unfolded protein response is activated in pretangle neurons in Alzheimer's disease hippocampus.* Am J Pathol, 2009. 174(4): p. 1241-51.
11. Chang, R.C., et al., *Phosphorylation of eukaryotic initiation factor-2alpha (eIF2alpha) is associated with neuronal degeneration in Alzheimer's disease.* Neuroreport, 2002. 13(18): p. 2429-32.
12. O'Connor, T., et al., *Phosphorylation of the translation initiation factor eIF2alpha increases BACE1 levels and promotes amyloidogenesis.* Neuron, 2008. 60(6): p. 988-1009.
13. Salminen, A., et al., *ER stress in Alzheimer's disease: a novel neuronal trigger for inflammation and Alzheimer's pathology.* J Neuroinflammation, 2009. 6: p. 41.
14. Ajoolabady, A., et al., *ER stress and UPR in Alzheimer's disease: mechanisms, pathogenesis, treatments.* Cell Death Dis, 2022. 13(8): p. 706.
15. Fouillet, A., et al., *ER stress inhibits neuronal death by promoting autophagy.* Autophagy, 2012. 8(6): p. 915-26.
16. Egawa, N., et al., *The endoplasmic reticulum stress sensor, ATF6alpha, protects against neurotoxin-induced dopaminergic neuronal death.* J Biol Chem, 2011. 286(10): p. 7947-7957.
17. Hashida, K., et al., *ATF6alpha promotes astroglial activation and neuronal survival in a chronic mouse model of Parkinson's disease.* PLoS One, 2012. 7(10): p. e47950.

18. Silva, R.M., et al., *CHOP/GADD153 is a mediator of apoptotic death in substantia nigra dopamine neurons in an in vivo neurotoxin model of parkinsonism.* J Neurochem, 2005. 95(4): p. 974-86.
19. Valdes, P., et al., *Control of dopaminergic neuron survival by the unfolded protein response transcription factor XBP1.* Proc Natl Acad Sci U S A, 2014. 111(18): p. 6804-9.
20. Casas-Tinto, S., et al., *The ER stress factor XBP1s prevents amyloid-beta neurotoxicity.* Hum Mol Genet, 2011. 20(11): p. 2144-60.
21. Zuleta, A., et al., *AAV-mediated delivery of the transcription factor XBP1s into the striatum reduces mutant Huntingtin aggregation in a mouse model of Huntington's disease.* Biochem Biophys Res Commun, 2012. 420(3): p. 558-63.
22. Moreno, J.A., et al., *Oral treatment targeting the unfolded protein response prevents neurodegeneration and clinical disease in prion-infected mice.* Sci Transl Med, 2013. 5(206): p. 206ra138.
23. Hetz, C., et al., *XBP-1 deficiency in the nervous system protects against amyotrophic lateral sclerosis by increasing autophagy.* Genes Dev, 2009. 23(19): p. 2294-306.
24. Boyce, M., et al., *A selective inhibitor of eIF2alpha dephosphorylation protects cells from ER stress.* Science, 2005. 307(5711): p. 935-9.
25. Saxena, S., E. Cabuy, and P. Caroni, *A role for motoneuron subtype-selective ER stress in disease manifestations of FALS mice.* Nat Neurosci, 2009. 12(5): p. 627-36.
26. Nijholt, D.A., et al., *Endoplasmic reticulum stress activates autophagy but not the proteasome in neuronal cells: implications for Alzheimer's disease.* Cell Death Differ, 2011. 18(6): p. 1071-81.
27. Hoyer, M.J., et al., *Combinatorial selective ER-phagy remodels the ER during neurogenesis.* Nat Cell Biol, 2024.
28. Shrestha, N., et al., *Integration of ER protein quality control mechanisms defines beta cell function and ER architecture.* J Clin Invest, 2023. 133(1).
29. Wu, S.A., et al., *The mechanisms to dispose of misfolded proteins in the endoplasmic reticulum of adipocytes.* Nat Commun, 2023. 14(1): p. 3132.
30. Abdon, B., et al., *Muscle-specific ER-associated degradation maintains postnatal muscle hypertrophy and systemic energy metabolism.* JCI Insight, 2023. 8(17).
31. Wu, S., et al., *The Integrated UPR and ERAD in Oligodendrocytes Maintain Myelin Thickness in Adults by Regulating Myelin Protein Translation.* J Neurosci, 2020. 40(43): p. 8214-8232.
32. Wu, S. and W. Lin, *Endoplasmic reticulum associated degradation is essential for maintaining the viability or function of mature myelinating cells in adults.* Glia, 2023. 71(5): p. 1360-1376.
33. Dobson, R. and G. Giovannoni, *Multiple sclerosis - a review.* Eur J Neurol, 2019. 26(1): p. 27-40.
34. Stone, S. and W. Lin, *The unfolded protein response in multiple sclerosis.* Front Neurosci, 2015. 9: p. 264.
35. Lin, W. and B. Popko, *Endoplasmic reticulum stress in disorders of myelinating cells.* Nat Neurosci, 2009. 12(4): p. 379-85.

36. Clayton, B.L.L. and B. Popko, *Endoplasmic reticulum stress and the unfolded protein response in disorders of myelinating glia.* Brain Res, 2016. 1648(Pt B): p. 594-602.
37. Lin, W., et al., *Endoplasmic reticulum stress modulates the response of myelinating oligodendrocytes to the immune cytokine interferon-gamma.* J Cell Biol, 2005. 169(4): p. 603-12.
38. Lin, W., et al., *Interferon-gamma inhibits central nervous system remyelination through a process modulated by endoplasmic reticulum stress.* Brain, 2006. 129(Pt 5): p. 1306-18.
39. Lin, W., et al., *The integrated stress response prevents demyelination by protecting oligodendrocytes against immune-mediated damage.* J Clin Invest, 2007. 117(2): p. 448-56.
40. Hussien, Y., D.R. Cavener, and B. Popko, *Genetic inactivation of PERK signaling in mouse oligodendrocytes: normal developmental myelination with increased susceptibility to inflammatory demyelination.* Glia, 2014. 62(5): p. 680-91.
41. Lin, W., et al., *Oligodendrocyte-specific activation of PERK signaling protects mice against experimental autoimmune encephalomyelitis.* J Neurosci, 2013. 33(14): p. 5980-91.
42. Belgrad, J., R. De Pace, and R.D. Fields, *Autophagy in Myelinating Glia.* J Neurosci, 2020. 40(2): p. 256-266.
43. Sims, S.G., et al., *The role of endoplasmic reticulum stress in astrocytes.* Glia, 2022. 70(1): p. 5-19.
44. Wang, J.L. and C.J. Xu, *Astrocytes autophagy in aging and neurodegenerative disorders.* Biomed Pharmacother, 2020. 122: p. 109691.
45. Sofroniew, M.V. and H.V. Vinters, *Astrocytes: biology and pathology.* Acta Neuropathol, 2010. 119(1): p. 7-35.
46. Sofroniew, M.V., *Astrogliosis.* Cold Spring Harb Perspect Biol, 2014. 7(2): p. a020420.
47. Eng, L.F. and R.S. Ghirnikar, *GFAP and astrogliosis.* Brain Pathol, 1994. 4(3): p. 229-37.
48. Pekny, M. and M. Pekna, *Astrocyte reactivity and reactive astrogliosis: costs and benefits.* Physiol Rev, 2014. 94(4): p. 1077-98.
49. Pekny, M., et al., *Astrocytes: a central element in neurological diseases.* Acta Neuropathol, 2016. 131(3): p. 323-45.
50. Wheeler, M.A., et al., *MAFG-driven astrocytes promote CNS inflammation.* Nature, 2020. 578(7796): p. 593-599.
51. Duran-Aniotz, C., et al., *IRE1 signaling exacerbates Alzheimer's disease pathogenesis.* Acta Neuropathol, 2017. 134(3): p. 489-506.
52. Wheeler, M.A., et al., *Environmental Control of Astrocyte Pathogenic Activities in CNS Inflammation.* Cell, 2019. 176(3): p. 581-596 e18.
53. Saito, A., et al., *Unfolded protein response, activated by OASIS family transcription factors, promotes astrocyte differentiation.* Nat Commun, 2012. 3: p. 967.
54. Yoshikawa, A., et al., *Deletion of Atf6alpha impairs astroglial activation and enhances neuronal death following brain ischemia in mice.* J Neurochem, 2015. 132(3): p. 342-53.

55. Plaza-Zabala, A., V. Sierra-Torre, and A. Sierra, *Autophagy and Microglia: Novel Partners in Neurodegeneration and Aging.* Int J Mol Sci, 2017. 18(3).
56. Su, P., et al., *The role of autophagy in modulation of neuroinflammation in microglia.* Neuroscience, 2016. 319: p. 155-67.

5.8 Figures and figure legends

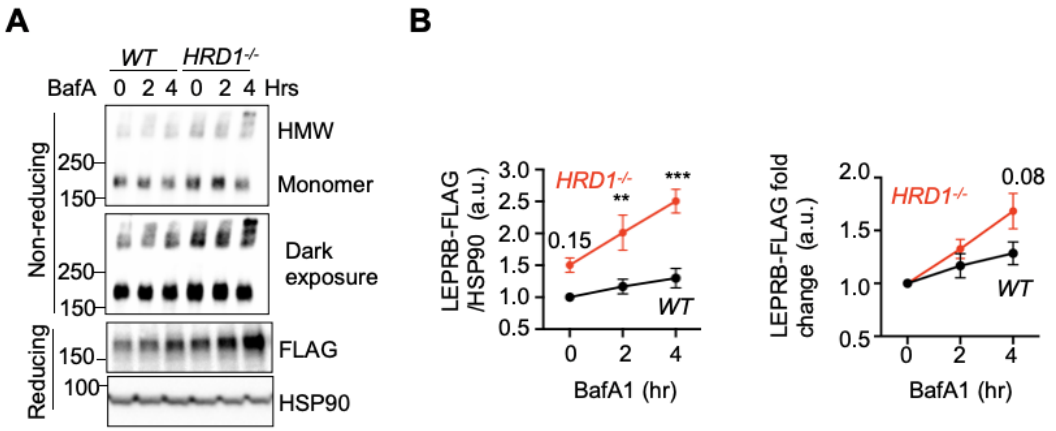

Figure 5.1 The turnover of LepRb is regulated by both SEL1L-HRD1 and lysosomal degradation.
(A-B) Non-reducing and reducing western blot analysis (A) and quantitation(B) of mLepRb-3xFlag in transfected HEK293T cells with Baflomycin A (BafA) for indicated time. (n=3 independent repeats)
Values, mean ± SEM. ns, not significant; *p<0.05, **p<0.01, ***p<0.001 and ****p<0.0001 by two-way ANOVA followed by Sidak's multiple comparisons test (B).

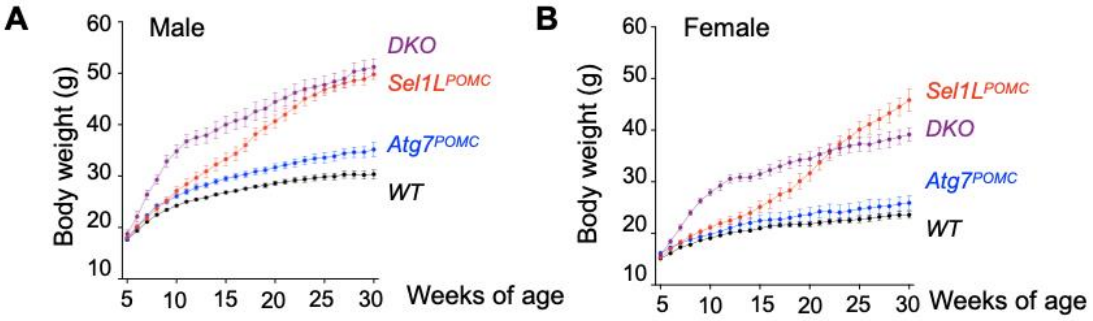

C

Male/Female

Sig. Weeks	*DKO* vs. *Sel1L*^{POMC}	*DKO* vs. *Atg7*^{POMC}	*DKO* vs. *WT*	*Sel1L*^{POMC} vs. *Atg7*^{POMC}	*Sel1L*^{POMC} vs. *WT*	*Atg7*^{POMC} vs. *WT*
5	ns/ns	ns/ns	ns/ns	ns/ns	ns/ns	ns/ns
6	ns/ns	ns/ns	ns/ns	ns/ns	ns/ns	ns/ns
7	**/ns	*/ns	***/*	ns/ns	ns/ns	ns/ns
8	***/**	**/**	****/****	ns/ns	ns/ns	ns/ns
9	****/****	****/****	****/****	ns/ns	ns/ns	ns/ns
10	****/****	****/****	****/****	ns/ns	*/ns	ns/ns
11	****/****	****/****	****/****	ns/ns	**/ns	ns/ns
12	****/****	****/****	****/****	ns/ns	***/ns	ns/ns
13	****/****	****/****	****/****	ns/ns	****/ns	ns/ns
14	****/****	****/****	****/****	*/ns	****/*	ns/ns
15	****/****	****/****	****/****	**/ns	****/*	ns/ns
16	****/****	****/****	****/****	**/ns	****/**	ns/ns
17	***/***	****/****	****/****	****/*	****/****	ns/ns
18	**/***	****/****	****/****	****/*	****/****	*/ns
19	*/*	****/****	****/****	****/**	****/****	*/ns
20	*/ns	****/****	****/****	****/****	****/****	*/ns
21	ns/ns	****/****	****/****	****/****	****/****	*/ns
22	ns/ns	****/****	****/****	****/****	****/****	*/ns
23	ns/ns	****/****	****/****	****/****	****/****	**/ns
24	ns/ns	****/****	****/****	****/****	****/****	**/ns
25	ns/ns	****/****	****/****	****/****	****/****	**/ns
26	ns/*	****/****	****/****	****/****	****/****	**/ns
27	ns/*	****/****	****/****	****/****	****/****	**/ns
28	ns/**	****/****	****/****	****/****	****/****	**/ns
29	ns/***	****/****	****/****	****/****	****/****	**/ns
30	ns/***	****/****	****/****	****/****	****/****	*/ns

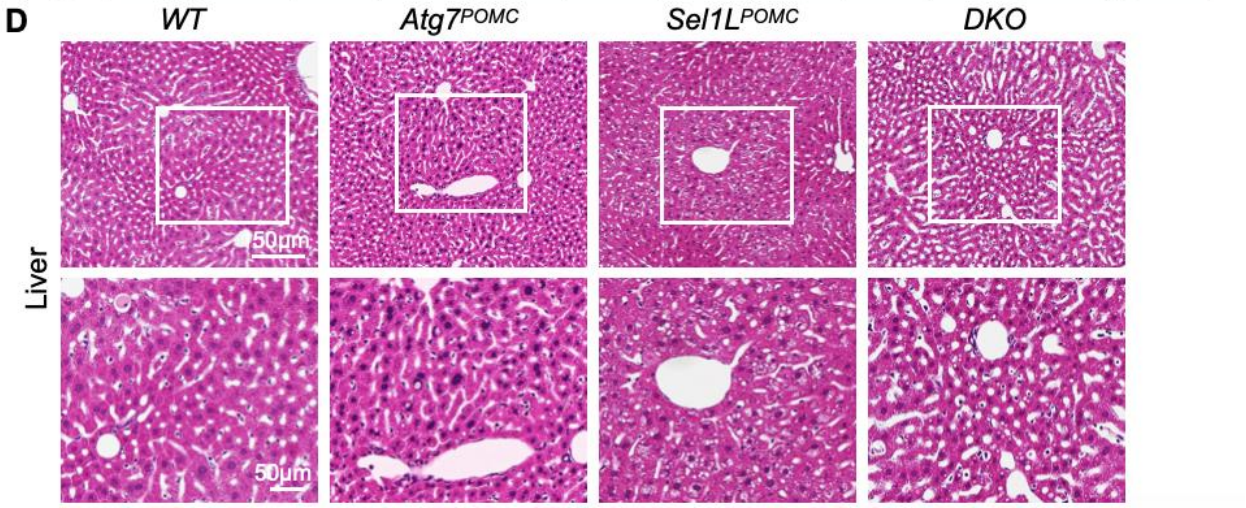

Figure 5.2 High fat diet-associated pathogenesis in peripheral tissues.
(A-B) Growth curve of *WT* (combining *WT* and *Sel1L*$^{POMC/+}$*;Atg7*$^{POMC/+}$), *Sel1L*^{POMC} (combining *Sel1L*^{POMC}*;Atg7*$^{+/+}$ and *Sel1L*^{POMC}*;Atg7*$^{POMC/+}$), *Atg7*^{POMC} (*Atg7*^{POMC}*;Sel1L*$^{+/+}$ and *Atg7*^{POMC}*;Sel1L*$^{POMC/+}$) and *DKO* mice on normal chow diet (NCD) for both sexes. (n=15-20 in each group).
(C) Significance between bodyweights of various cohorts at indicated weeks of age by by two-way ANOVA followed by Tukey's multiple comparisons test shown in (A) and (B)
(D) Representative images of H&E staining in the liver of the *WT, Sel1L*^{POMC}*, Atg7*^{POMC} and *DKO* male mice fed on NCD. (n=3 mice per group)
Values, mean ± SEM. ns, not significant; *p<0.05, **p<0.01, ***p<0.001 and ****p<0.0001 by two-way ANOVA followed by Tukey's multiple comparisons test (C).

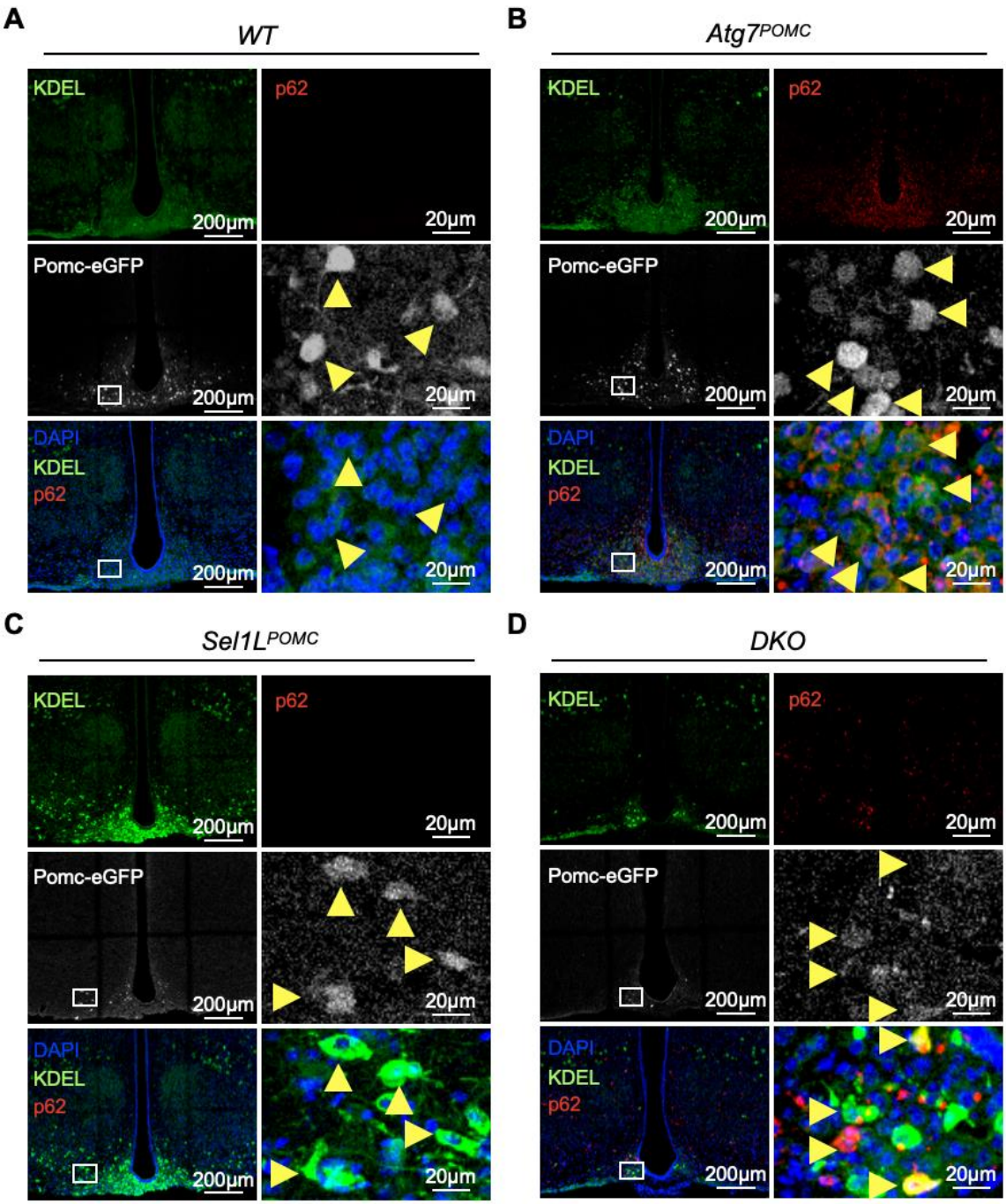

Figure 5.3 Characterization of ER homeostasis and autophagy in ARC of mice.
(A-D) Representative immunofluorescence (IF) staining of KDEL (ER maker) and P62 (autophagy substrate) in the ARC of *WT* (A), *Atg7*^{POMC} (B), *Sel1L*^{POMC} (C) and *DKO* (D) male mice at 25 weeks of age. (n=2 mice each group)
ARC, arcuate nucleus.

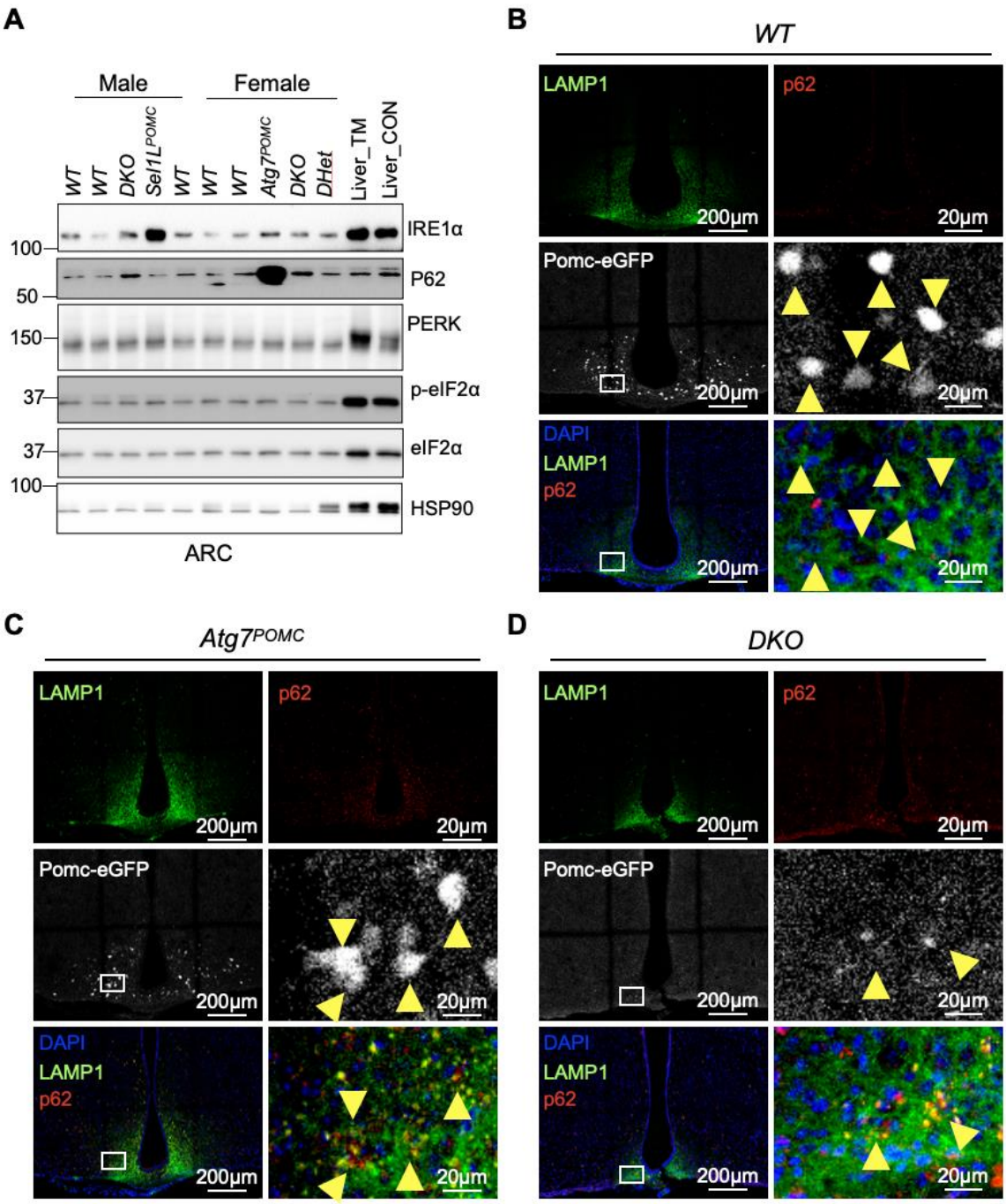

Figure 5.4 Evaluation of UPR and autophagy in ARC of mice.
(A) Western blotting of *WT*, *Atg7*^{POMC}, *Sel1L*^{POMC} and *DKO* mice at 30 weeks of age. **(B-D)** Representative immunofluorescence (IF) staining of LAMP1 (lysosome maker) and P62 (autophagy substrate) in the ARC of *WT* (B), *Atg7*^{POMC} (C) and *DKO* (D) male mice at 25 weeks of age. (n=1 mice each group)
ARC, arcuate nucleus.